UNIVERSITÀ
DEGLI STUDI
DI PADOVA

Sede Amministrativa: **UNIVERSITÀ DEGLI STUDI DI PADOVA**

DIPARTIMENTO DI INGEGNERIA INDUSTRIALE

SCUOLA DI DOTTORATO DI RICERCA IN INGEGNERIA INDUSTRIALE
INDIRIZZO INGEGNERIA DELLA PRODUZIONE INDUSTRIALE

CICLO XXV

SOLID STATE PHASE TRANSFORMATIONS IN ADVANCED STEELS

Direttore della scuola: ***Ch.mo Prof. Andrea Stella***
Coordinatore d'indirizzo**: *Prof. Enrico Savio***
Supervisore :***Prof.ssa Irene Calliari***

Dottoranda : ***Argelia Fabiola Miranda Pérez***

PREFACE

The fulfillment of the research project presented in this Thesis has involved the financial and intellectual support of many people, to whom the author is most grateful. Most of the research and experimental part of the work was carried out in the Industrial Engineering Department of the University of Padova (Italy), under the main supervision of Professor Irene Calliari. Part of the work has been carried out at the Materials Science and Engineering Department of the Royal Institute of Technology, Stockholm, (Sweden) under the supervision of Professor Rolf Sandström.

The list of publications drawn from this research project is reported below.

Publications in Journals

- A.F. Miranda Pérez, I. Calliari, K. Brunelli, F.A. Reyes Valdés and G. Y Pérez Medina (2012). ANALYSIS OF THE MICROSTRUCTURE AND MECHANICAL PROPERTIES OF DUAL PHASE STEEL UNDER THE EFFECTS OF DIFFERENT BRAZING RATES. MRS Proceedings, 1381, imrc11-1381-S22-013 doi:10.1557/opl.2012.380.

- A.F. Miranda Pérez, I. Calliari, E. Ramous, M. Breda (2012). TRATTAMENTI DI RICOTTURA DELL'ACCIAIO INOSSIDABILE DUPLEX 2205 DOPO DEFORMAZIONE PLASTICA. METALLURGIA ITALIANA, vol. 5; p. 13-17, ISSN: 0026-0843

Publications in Conference Proceedings

- I. Rampin, M. Piazza, S. Baldo, A.F. Miranda Pérez, K. Brunelli, I. Calliari, F.A. Reyes Valdés. (2010). THE EFFECT OF BRAZE-WELDING SPEED ON THE MICROSTRUCTURE AND MECHANICAL PROPERTIES OF DUAL PHASE STEEL. In: 2nd International Conference Super High Strength Steels, Peschiera del Garda (Italy), 17-19 October

- A.F. Miranda Pérez, I. Calliari, E. Ramous, M. Breda. (2011). TRATTAMENTI DI RICOTTURA D'ACCIAI INOSSIDABILE DUPLEX 2205 DOPO DEFORMAZIONE PLASTICA. In: 23 Convegno Nazionale Trattamenti Termici. Verona, 19-20-21 October

- P. Bassani, F. Passaretti, I. Calliari, A.F. Miranda Pérez. (2011). PHASE ANALYSES OF A THERMALLY TREATED 2507 DUPLEX STEEL THROUGH EBSD. In: Proceedings 7th European Stainless Steel Conference. Como (Italy), 21-23 September

- I. Calliari, S. Baldo, A.F. Miranda Pérez, G. Tortoreto, I. Mészaros. (2011). MAGNETIC AND METALLOGRAPHIC INVESTIGATION OF PHASE TRANSFORMATIONS IN DUPLEX STAINLESS STEELS. In: Proceedings 8th

International Workshop on Progress in Analytical Chemistry & Materials Characterisation in the Steel and Metal Industries. Luxembourg, 17-19 May

- E. Ramous, M. Breda, A.F. Miranda Pérez, J.C. Cárdenas, R. Bertelli. (2012). GLI AZOTURI NEGLI ACCIAI INOSSIDABILI DUPLEX. In: ATTI DEL 34° CONVEGNO NAZIONALE AIM. Trento, 7- 9 November

- I. Calliari, M. Breda, A.F. Miranda Pérez, E. Ramous, R. Bertelli. (2012). PHASE TRANSFORMATION INDUCED BY HEAT TREATMENT IN COLD ROLLED DUPLEX STAINLESS STEELS. In: Proceedings of the International Conference & Exhibition on Analysis & Testing of Metallurgical Process & Materials. Beijing, China, Oct. 31 – Nov. 3

The following theses performed at the Industrial Engineering Department of the University of Padova (Italy) were supervised.

- M. Bianchi, *Complex magnetic and microstructural investigation of duplex stainless steels*, A.A. 2011
- E. Manfrin, *Heat treatment and deformation of super duplex stainless steels*, A.A. 2011
- M. Ganzina, *Study of crack propagation in 2205 DSS using low cycle fatigue*, A.A. 2011

Other activities not included in the Thesis

In the past, it was customary to use out-of-circulation coins as pendants by brazing a peg or ring on the edge of the coin in order to transform it into a devotional or decorative object; this practice was very common for specimens of the Papal States, especially for silver coins. A metallurgical investigation of a 19th century Scudo was performed, in order to provide information on the solidification microstructure arising from a strongly nonequilibrium process such as brazing.

- I. Calliari, M. Breda, C. Canovaro, A.F. Miranda Pérez. (2012). FROM COINS TO MEDAL: A METALLURGICAL STUDY OF THE BRAZING DROP ON A XIX CENTURY SCUDO. JOM, vol. 64; p. 1350-1354, ISSN: 1047-4838, doi: 10.1007/s11837-012-0455-5

- C. Canovaro, M. Breda, A.F. Miranda Pérez, I. Calliari *(in press).* CARATTERIZZAZIONE METALLOGRAFICA DI UNO SCUDO ROMANO DEL XIX SECOLO: LA MONETA DIVENTA MEDAGLIA. METALLURGIA ITALIANA

SUMMARY

In order to achieve progress in Advanced Steels development came more emphasis in solid state phase transformations are received. For achieving the desired mechanical and corrosion resistance properties in Duplex Stainless Steels (DSS), a precise knowledge of the precipitation kinetics of secondary phases, the morphology of the precipitates and effects of the alloying elements on different properties is needed. A complicated chemical composition and the production technology route make each grade of DSS a unique object for a study. Besides, when the market needs to reduce weight and increase product durability by utilizing Advance Strength Steels, a deeper understanding of their transformations is required.

The aim of the present work was to study the main features of phase precipitation in diverse Duplex Stainless Steels grades, including Lean Duplex, Standard and Superduplex. Beside analyze the effects of metallurgical features on the properties of DSS and Advanced High Strength Dual Phase (DP) steels. One of the tasks was to study the effects plastic deformation after heat treatment in diverse duplex grades.

In the first part of the research, which is Chapter 4, is focused on the influence of microstructure on the mechanical properties and weldability of Advanced High Strength Steels. Fatigue behavior and weldability are considered as indispensable factors especially in the design for structural automotive applications. Hence, the influence of braze-welding parameters on microstructural and mechanical properties was highlighted in DP steel.

On Chapter 5, diverse Duplex Stainless Steels grades were selected for the study in order to establish the main features of the nitride precipitation behavior. Besides, analysis of the morphology of sigma phase in welded standard duplex stainless steels. The metallurgical features and phase transformations in the microstructure due to diverse heating cycles is studied.

Furthermore, Chapter 6 deals with an investigation about the effect in the microstructure of diverse DSS performing cold working after isothermal heat. Consequently a deeper investigation on lower alloyed Lean DSS, and their behavior was analyzed. To reduce the costs, strong austenite phase stabilizers such as Ni are substituted with less stabilizing element as Mn, leading to a certain austenite phase (γ) instability which eventually transforms into ferromagnetic lath martensite (α') during plastic deformation. This phase transformation can potentially affect the properties of the material. Therefore the possible $\gamma \rightarrow \alpha'$ evolution during cold rolling was evaluated mainly through magnetic and X-ray diffraction techniques.

CONTENT

ACRONYMS

AHSS	Advanced High Strength Steels
AISI	American Iron and Steel Institute
AOD	Argon Oxygen Decarburization
AWS	American Welding Society
Bcc	Body-centered cubic
Bct	Body centered tetragonal
BH	Bake Hardening
BIW	Body in White
C	Carbon
C	Carbon
CALPHAD	Computer Coupling of Phase Diagrams and Thermochemistry
CIP	Cold Isostatic Pressing
CO_2	Carbon dioxide
CP	Complex phase
Cr	Chromium
Cr_2N	Chromium nitride
CrN	Chromium nitride
Cu	Cooper
$CuSi_3$	Copper-Silicon Mig Welding Wire
DP	Dual phase
DSS	Duplex Stainless steels
DSS	Duplex Stainless Steels
EDAX	Energy Dispersive Analysis of X-Rays
EDS	Energy-dispersive X-ray spectroscopy
EN	European Standard
ER 2209	Welding wire alloy
FB	Ferritic-bainitic
Fcc	Face-centered cubic
Fe	Iron
HDSS	Hyper Duplex Stainless Steels

HF	Hot Formed Steels
HIP	Hot Isostatic Pressing
HSLA	High Strength Low Alloy
HSS	High Strength Steels
IF	Interstitial free
IMA	International Molybdenum Association
ISO	International Organization for Standardization
kV	Kilovolts
LDX	Lean Duplex
Mn	Manganese
Mo	Molybdenum
MS	Martensitic
N	Nitrogen
Nb	Niobium
Ni	Nickel
OM	Optical Microscope
PRE	Pitting Resistance Equivalent
PREN	Pitting Resistance Equivalent + Nitrogen
PREW	Pitting Resistance Equivalent + Tungsten
PSD	Particle size distribution
RT cold	
SAF	Sandvik Austenite Ferrite
SAW	Submerged Arc Welding
SCC	Stress Corrosion Cracking
SCC	Stress corrosion cracking
SEM	Scanning Electron Microscope
SF	Stretch-flangeable
Si	Silicon
SIP	Strain Induced Precipitation
TC	Thermo-Calc
TEM	Transmission Electron Microscope
Ti	Titanium
TMCP	Thermomechanical Controlling Process
TR	Thickness reduction
TRIP	Transformation Induced Plasticity
TTT	Time-Temperature Transformation

TWIP	Twinning Induced Plasticity
ULSAB	UltraLigth Steel Auto Body
UNI	Italian Organization for Standardization
UNS	*Unified Numbering System*
UR 50	Uranus 50
V	Vanadium
VOD	Vacuum Oxygen Decarburization
W	Tungsten
ZAF	Correction for atomic number effects (Z), absorption (A) and fluorescence (F)
γ	Austenite
γ_2	Secondary austenite
δ-ferrite	Delta ferrite
η_m	Efficiency of junction
π-phase	Pi phase
σ-phase	Sigma phase
σ_R	Fracture strength calculated
σ_{RM}	Fracture strength medium
χ-phase	Chi phase

Chapter 1

1

General Introduction

CHAPTER 1

General Introduction

At present, Advanced Steels are the most common materials widely used in the world, both for structural and functional applications. These steels have been widely using for construction, automobile, machinery, energy and transportation. They can be infinitely recycled, allowing the creation of new products out of old products without any loss of strength, formability or any other important measure of performance. More advanced steel products with the characteristics of high performance, low cost, easy fabrication, low tolerance and environment benign have been elaborated to fulfill the demands from both market and environment protection.

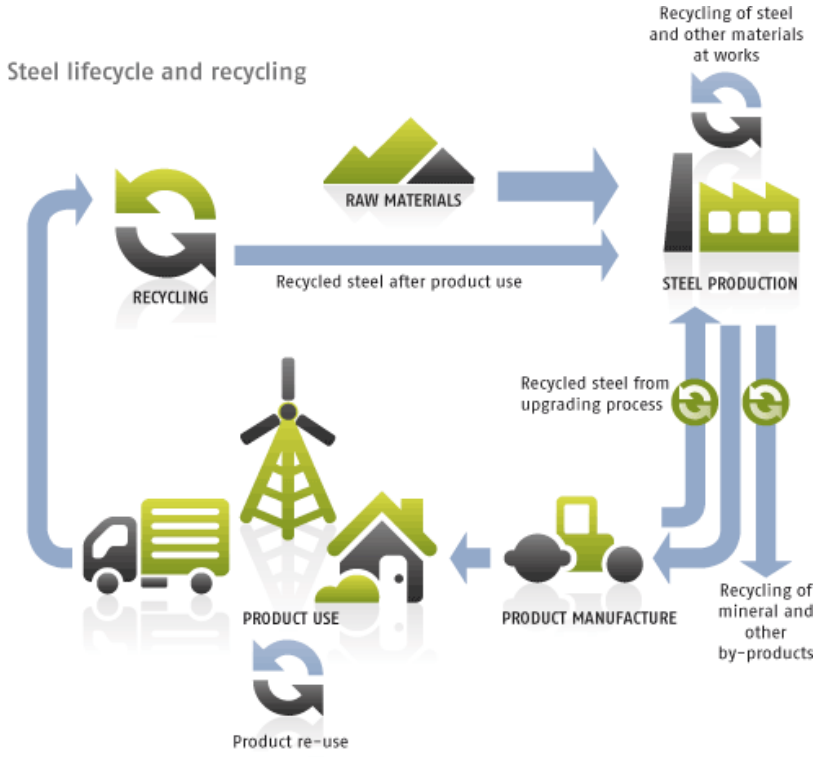

Figure 1.1 *Steel lifecycle and recycling (Rautaruukki Corp., 2012)*

The development of advanced steels is focused on cost reduction in terms of quantity of employed material, chemical composition and life cycle of the product.

The never-ending demand of materials that allows increased fuel efficiency, easy manufacturability and performance make the usage of Advanced High Strength steels (AHSS) increased, while Duplex Stainless Steels (DSS) in applications where corrosion resistance, good weldability and high strength is required, induced scientific and technological researchers towards a deeper investigation to innovate these classes of steels. Both Advanced High Strength and Duplex Stainless Steels despite their each other differences are examples of technological innovation which takes in account the applications previously mentioned.

The production and applications of such alloys are on constantly increment, the interest in solid state phase changes is often under study due to the numerous technological benefits that results from such transformations. Description, interpretation and prediction of phases changes are constantly the focus of interest of both materials science and engineering. The behavior of microstructural and function materials exposed to various external conditions is indeed the main focus of this work.

CHAPTER 2

2

Motivations and Objectives

CHAPTER 2

Motivations and Objectives

The processing microstructure, property and relationships in these materials continue to present challenges to researchers because of the complexity of phase transformation reactions and the wide spectrum of microstructures and properties achievable. The present work started at University of Padova in 2010. All the main features of the behavior of Advanced High Strength Steels (specifically Dual Phase grades) and Duplex Stainless Steels had been well established by that time. However, these advanced grades are very complex systems, which are very sensitive to even minor changes in the composition and/or manufacturing technology. The so called multi-phase steels therefore offer very attractive combinations of strength and ductility which are due to the coexistence of the different microstructural components, their different mechanical behavior and their mutual interactions.

Multi-phase steels can, for example, contain a relatively soft matrix phase being responsible of good mechanical properties as a result of the presence of a hard second phase as in the case of dual phase steels, which brings high strength. It is possible to vary the mechanical properties and to tailor them for the respective application foreseen by adjusting type, morphology and orientation and above all volume fraction, size and distribution of the different phases.

Welding and heat treatment becomes of primary importance when it comes to the top performance of both types of Advanced Steels components. The comprehensive detailed heat treatment procedure needs to be carefully determined for every particular grade for every particular application. The thermal treatment during production and the microstructures of wrought Advanced Steels provided good performance characteristics, but had limitations in the as-welded condition. It should be mentioned that the largest part of the studies on these grades including those on the microstructure and precipitation kinetics was performed on wrought conventional grades so far. However, modern grades still became a challenge to investigators.

These modern grades appeared at the same time period of increased activity in the offshore industry. This industry required always materials that could handle aggressive environments. Even, some other grades as conventional ones could also stand up to these aggressive environments, some of their components at the time drove up their prices. All of these factors combined to encourage the offshore oil industry to take a close look at Advanced Steels.

A remarkable recent progress in the production techniques and understanding of the metallurgy has led the development of Advanced Steels towards higher alloying with chromium,

molybdenum and even nickel. The phase equilibrium in these alloys has become even more complex and the precipitation behavior of these grades can attain new features in the presence of new alloying elements. However, a profound knowledge of important aspects of these grades under study is requested in order to avoid problems in service and eventually damages or failures.

The major goal of the present thesis is to study the phase transformation in solid state of various Cr-Mn and Cr-Ni Duplex Stainless Steels. Therefore, different investigations were carried out. Appropriate phase descriptions are determined. Besides analyze the effects of metallurgical features on the properties of DSS and Advanced High Strength Dual Phase (DP) steels. One of the tasks was to study the plastic deformation effects after heat treatment in diverse duplex grades.

CHAPTER 3

3

Literature review

CHAPTER 3

Literature review

3.1 ADVANCED HIGH STRENGTH STEELS

3.1.1 Fundamentals of Advanced High Strength Steels

Advanced High Strength Steels (AHSS hereafter) have unique metallurgical properties and processing capabilities that enable the automotive industry to meet requirements, while keeping low cost. The global steel industry has met the demand through the development of new AHSS grades. This section presents an overview of AHSS fundamental characteristics.

3.1.1.1 Development of AHSS

The steel industry has responded to competition from alternative materials for light-weighting and performance enhancements, by developing new steel grades with superior product attributes to leverage steel as the optimal automotive material. As the motivation to reduce the mass of vehicles continues to intensify, automakers seek to maximize the efficiency of their materials selection.

In 1963, microalloying with strong carbonitride forming elements (V, Nb, and Ti) started to be developed widely. High Strength Low Alloy (HSLA) steels, as a type of typical low-carbon low-alloy structural steel, was developed when the fine precipitation of Nb carbides was found to increase mechanical properties of the material; exhibits an outstanding combination of high strength, resistance to brittle fracture and good weldability (J. Fernández, 2007; B. K. Show, 2010). By 1975, the average vehicle contained 3.6% medium and high-strength steel for a total vehicle content of 61%, mostly mild (Hall, 2011).

In the 1980's, the use of interstitial free (IF) and galvanized steels grew for complex parts, as styling, corrosion and cost were key considerations. IF steel was initially developed as a highly formable material and used extensively for deep drawn applications requiring high ductility and resistance to thinning.

Since this period microalloying practice with low alloy of Nb, V, Ti elements start receiving more attention. In 1994, a consortium of 35 sheet steel producers began the UltraLight Steel Auto Body (ULSAB) program to design a lightweight steel auto body structure that would meet a wide range of safety and performance targets (Figure 3.1). The body-in-white (BIW) revealed in 1998 validated the design concept of the program. After that, a new generation of AHSS including Hot Formed (HF) and Dual Phase (DP) steels was incorporated into BIW structures, even DP were developed in the late 1970 (ASM, 1993).

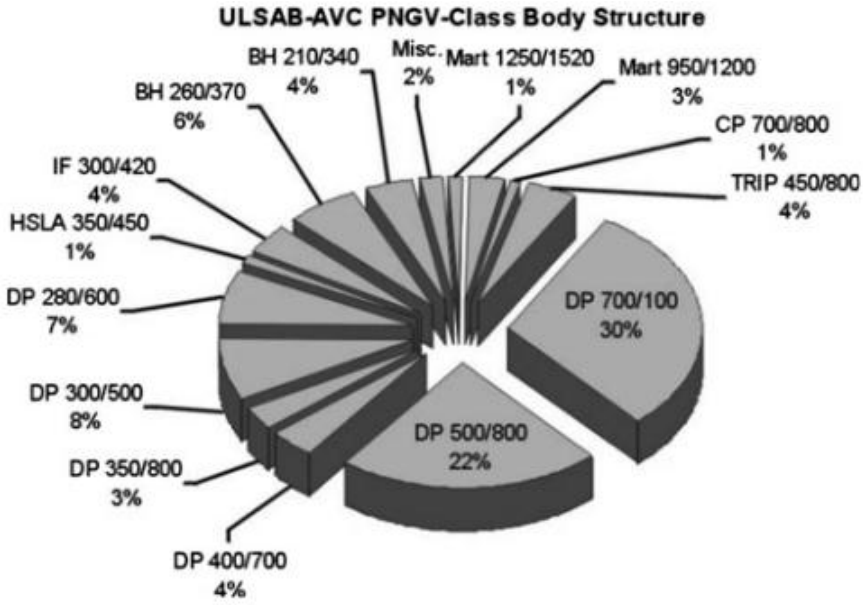

Figure 3.*1 Material selection in ULSAB project (Y. Weng, 2011)*

Essential for the growing use of AHSS has been the simultaneous development of new processes and equipment to produce and form the material. DP and Transformation Induced Plasticity (TRIP) steels are the focus of automotive applications based in the many advantages as: safety improvement through high crash resistance, better appearance over elevated dent resistance, better performance increasing fatigue strength, cost reduction and cost savings through materials cost compared to aluminum and magnesium (ASM, 1993).

3.1.1.2 Essential Qualities

These new steels have enhanced strength and formability achieved through the development of more complex microstructures controlling cooling processes, hardened by phase transformation. The microstructure may include Martensite, Bainite and retained Austenite. Compared with conventional low to high-strength include IF, BH (bake hardening) and HSLA, which have yield strength of less than 550 MPa and ductility that decreases with increased strength.

AHSS are more complex, particularly in their microstructures, which are usually multiphase for an improved combination of strength and ductility. The balance is carefully constructed to reach performance requirements while maintaining excellent formability (J. R. Shaw, 2011). Moreover, provide other advantageous mechanical properties, such as high strain-hardening capacity. Since the production of AHSS requires fast cooling, inadequate cooling capacity has to be compensated by adding more alloying elements. The addition of alloying elements deteriorates both the properties and increases the environmental problem (Z. Xiaodong, 2011).

3.1.1.3 Classification and Applications

The first generation of these AHSS is ferrite based. This classification is divided into six categories as follows:

- Dual phase (DP), which have a microstructure of martensite dispersed in a ferritic matrix and provides a good combination of ductility and high tensile strength, *(More detailed description will be given in subchapter 3.1.2.3).*

- Ferritic-bainitic (FB). Including stretch-flangeable (SF), is also a DP, with soft ferrite and hard bainite. It's finer than the typical DP steel, however, can be more finely tuned to be SF. It's suited to carry vibration loads, often used for profiles, mechanical parts, cross beams, reinforcements and wheels.

- Complex phase (CP), presents a mixed microstructure with a ferrite/bainite matrix containing bits of martensite, retained austenite and pearlite. Microalloying elements such as titanium or niobium may also be precipitated. Presents properties as high yield strength and high elongation at tensile strengths similar to DP. Besides, it can have good edge stretchability, as well as good wear characteristics and fatigue strength. In automotive sector CP has several applications, particularly in body structure, suspension and chassis components.

- Martensitic (MS), in this case all austenite is converted to martensite. The martensitic matrix contains a small amount of very fine ferrite and bainite phases. Increasing carbon content, high strength and hardness could be reached. It has relatively low elongation. However, post quench tempering can improve ductility. These grades are recommended for bumper reinforcement and door intrusion beams, rocker panel inners and reinforcements, side sill and belt line reinforcements, springs and clips (E.J. Petit, 2010).

- Transformation Induced Plasticity (TRIP), microstructure constitute with a soft ferrite matrix embedded with hard phases. The matrix contained a high amount of retained austenite, 5% at least, plus some martensite and bainite. Receive its name for its unique behavior during plastic strain, also to the dispersal of hard phases, the austenite transforms to martensite, which allows the high hardening rate to endure at very high strain levels. Automotive applications include body structure and ancillary parts.

- Hot-formed, boron based containing 0.002% and 0.005% boron, also named "boron steel". In direct hot forming, is blanked at room temperature and then heated to high enough temperature for austenization. The steel is then formed while hot and quenched in the forming tool, developing martensitic microstructure. Post-forming work may be required for exceptionally high strength pieces. Reinforcements for A and B pillars, roof bows, side wall members and beams for crash management structures are some of their applications.

The second generation of AHSS are more austenite based included the Twinning Induced Plasticity (TWIP), which is austenite based. It sits apart from conventional and first generation AHSS on the elongation tensile strength diagram (Figure 3.2).

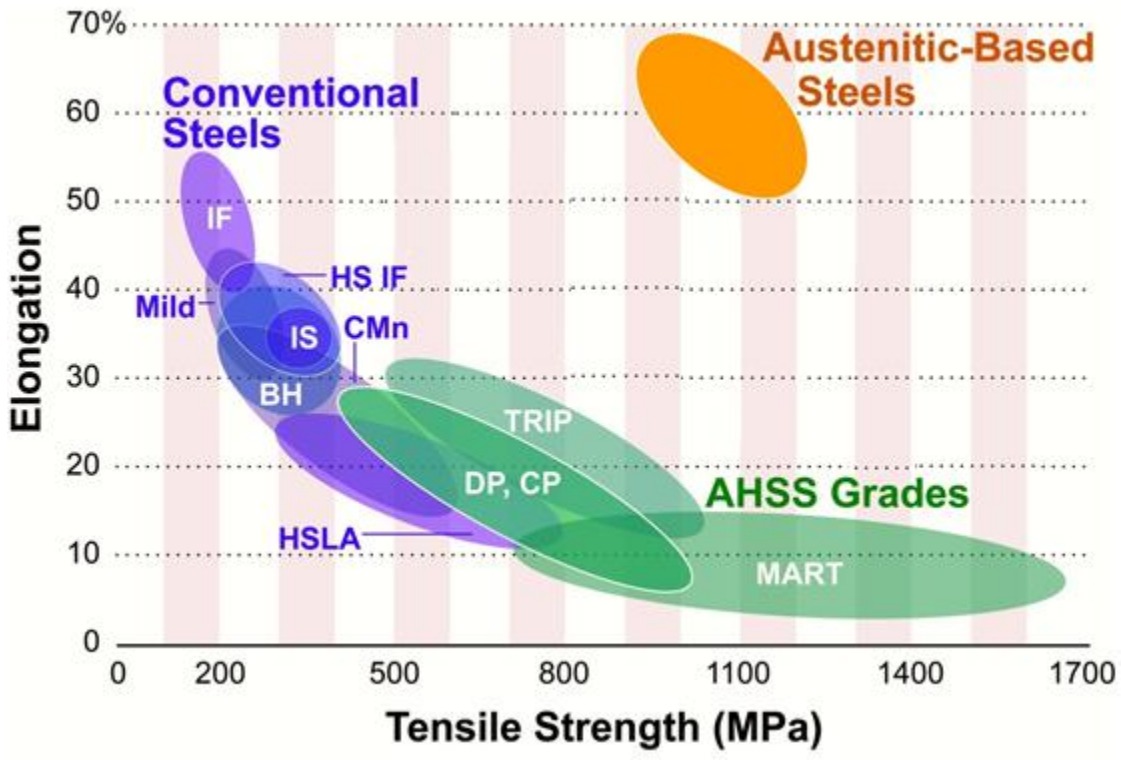

Figure 3.2 *Comparison of elongation tensile strength diagram between traditional C steels, High Strength Steels and AHSS* (Kovieczny, 2003)

3.1.2 Physical Metallurgy and Properties

Despite carbon is the most important element for strengthening steel, presents deleterious effects on many technological properties such as weldability, therefore the addition is limited. Specifically on the steels discussed in the present dissertation a subsequent brief description of the physical metallurgy is provided.

3.1.2.1 Processing

Strengthening and hardening mechanism are often used in various combinations to reach specific requirements, such as fatigue strength or dent resistance. The most important is grain refinement which leads to an improvement or both strength and toughness (N.Maruyama, 1998; Ashwin Pandit, 2005). Ferritic grain refinement will result in an increase in yield strength, is achieved by the maximization of the total interfacial area per unit volume of austenite grain before the γ→α, which control rolling through the rolling passes and the retardation of austenite recrystallization.

To obtain the optimal grain refinement and strengthening the finishing temperature, the coiling temperature and the cooling rate have to be controlled. Increasing the cooling rate in the run out table (ROT) and lowering the coiling temperature (CT) conduct to refinement of the ferrite, since the precipitation hardening is mainly influenced by the cooling path from the finish rolling temperature is critical (Ardo, 2003).

The Hall-Petch equation quantifies the effect of grain refinement to the increase of strength.

$$\sigma_y = \sigma_i + k_y d^{-\frac{1}{2}} \tag{3.1}$$

Where σ_i is the strength of the material considered as a single crystal in the annealed condition and $k_y d^{-\frac{1}{2}}$ is the hardening contribute due to mean size of grains. The microalloying elements precipitate contributes to the overall strength through precipitation hardening (M. Murayama, 2001; E. V. Pereloma, 2006). Particles as NbC, VC, TiC mainly precipitated on crystalline defects in either austenite or ferrite, provided dispersion strengthening (Ardo, 2003). Transformation strengthening is the principal strengthening mechanism employed in manufacturing AHSS. Alloying elements and faster cooling rates depress the temperature of transformation of austenite to ferrite and, ultimately, the effect will be sufficient to cause transformation to bainite or martensite. Figure 3.3 shows the consequence of this progression. Hence, the strength is increased progressively with the introduction of lower temperature transformation products, losing toughness and ductility.

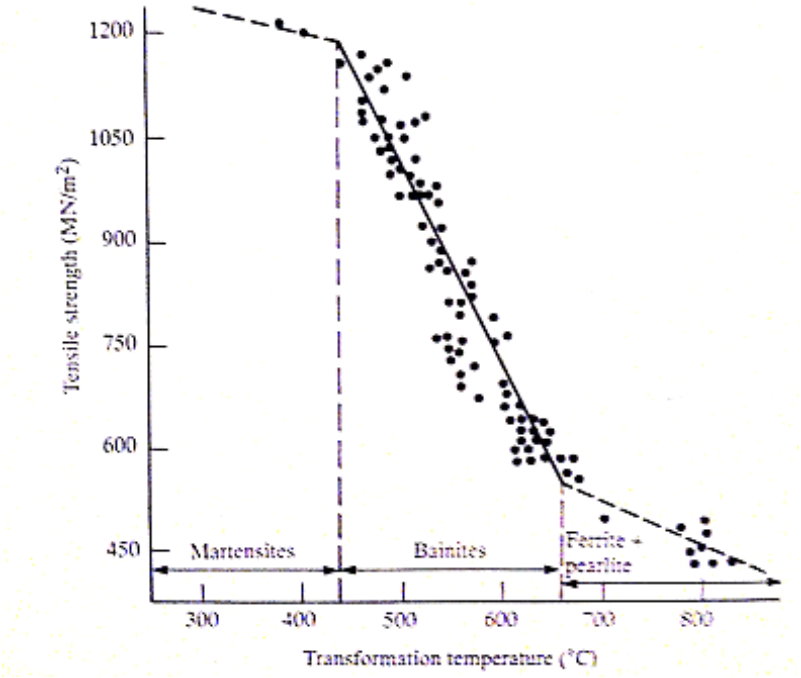

Figure 3.3 *Relationship between 50% transformation temperature and tensile strength* (Pickering, 1960)

One of the important step in the production of these steels is heating cycles, temperature and cooling rates must be carefully controlled within tight windows in order to develop the desired microstructures.

3.1.2.2 Mechanical Properties

The increase formability allows for greater part complexity, which leads to fewer individual parts (cost savings) and more manufacturing flexibility. Fewer parts mean less welding (cost and cycle-time savings) and weld flanges (mass and weight savings).

Depending on design, the higher strength can translate into better fatigue and crash performance, while maintaining or even reducing thickness. Table 3.1, highlight the potentiality of DP and TRIP the mechanical properties evolution (IISI, 2006)

Table 3.1 *Mechanical properties of AHSS compared to common HSLA* (*ULSAB-AVC, 2009)*

STEEL GRADE	YS (MPa)	UTS (MPa)	Total EL (%)	n Value (5-15%)	r Bar	K Value (MPa)
BH 210/340	210	340	34-39	0.18	1.8	582
BH 260/370	260	370	29-34	0.13	1.6	550
DP 280/600	280	600	30-34	0.21	1	1,082
IF 300/420	300	420	29-36	0.2	1.6	759
DP 300/500	300	500	30-34	0.16	1	762
HSLA 350/450	350	450	23-27	0.14	1.1	807
DP 350/600	350	600	24-30	0.14	1	976
DP 400/700	400	700	19-25	0.14	1	1,028
TRIP 450/800	450	800	26-32	0.24	0.9	1,690
DP 500/800	500	800	14-20	0.14	1	1,303
CP 700/800	700	800	10-15	0.13	1	1,380
DP 700/1000	700	1,000	12-17	0.09	0.9	1,521
Mart 950/1200	950	1,200	5-7	0.07	0.9	1,678
Mart 1250/1520	1,250	1,520	4-6	0.065	0.9	2,021

YS and UTS are minimum values

Tol. EL (Total Elongation) is a typical value for a broad range of thicknesses and gage lengths

To compare different steels or grades of the same class the stress-strain curves instrument is given. Figure 3.4 the behavior of different DP steels grades, compared to a mild steel, is emphasized.

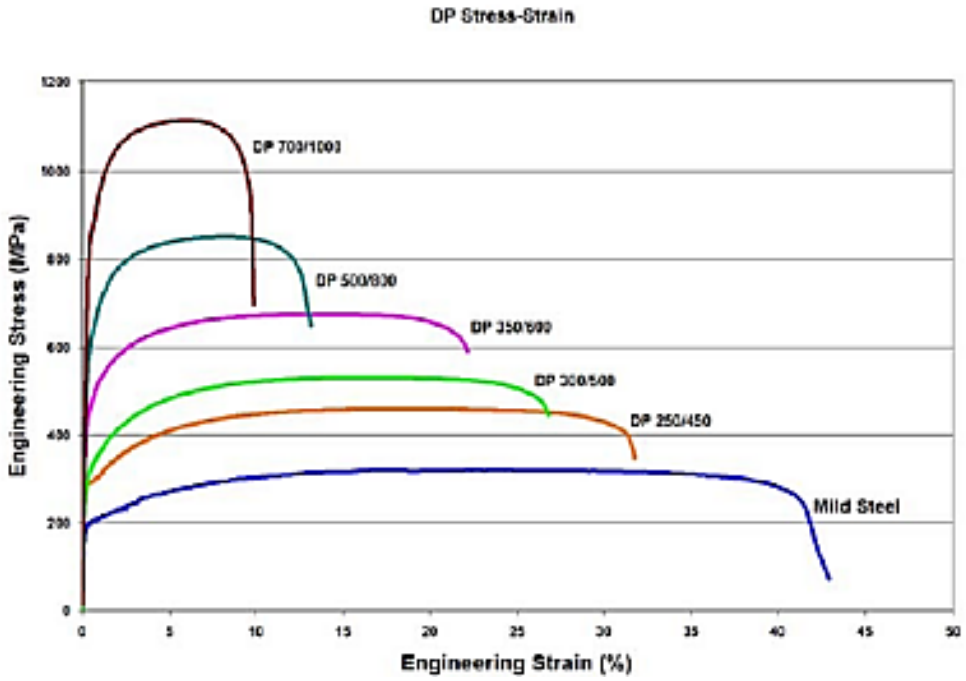

Figure 3.4 *Engineering stress-strain of different Dual Phase steels grades* (S. P. Bhat, 2001)

DP steels having increase values of work hardening exponent, due to the particular balanced microstructure, can present greater stretchability and crash energy absorption than HSLA steels,

which can be derived from the total elongation obtained in a standard tensile test, previously shown on Figure 3.2.

DP steels presents higher fatigue limit compare to conventional HSLA, as shown in Figure 3.5. The reasons are mainly metallurgical, as it was found that the dispersed fine martensite island presented on these grades retard the propagation of fatigue cracks (Chapetti, 2005).

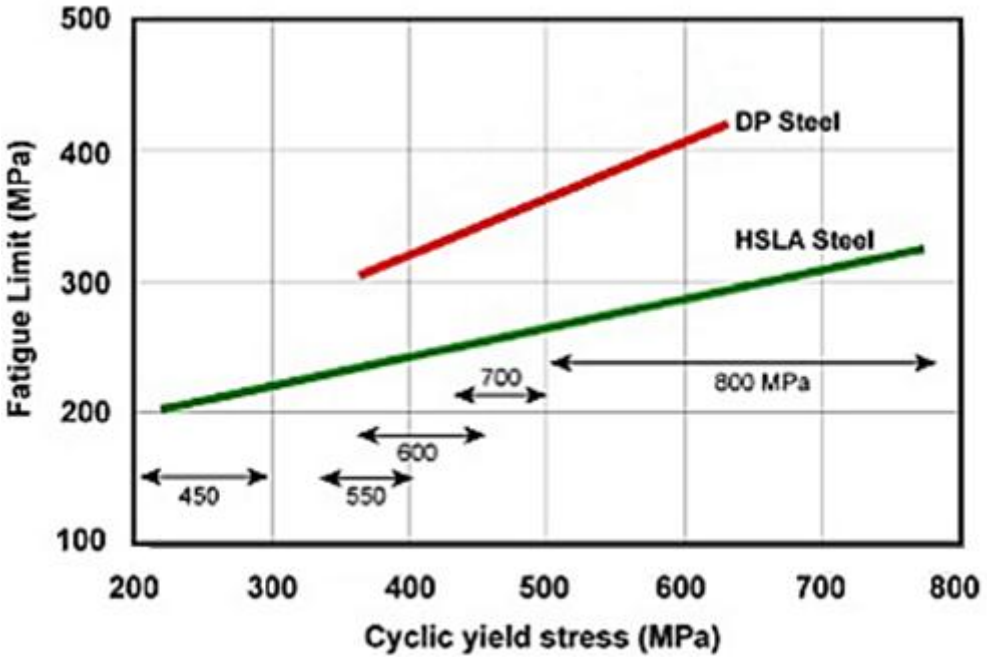

Figure 3.5 *Fatigue limits of HSLA and DP steels* (Chapetti, 2005)

3.1.2.3 Dual phase steels

Dual phase steels are gaining in popularity with the vehicle makers. Consist of a ferritic matrix containing a hard martensitic second phase in the form of islands. Increasing the volume fraction of hard second phases generally increases the strength. The dual phase is produced by annealing in the ($\alpha + \gamma$) region followed by cooling at a rate which ensures that the γ-phase transforms to martensite, although some retained austenite is also usually present leading to a mixed martensite-austenite (M-A) constituent. To allow air-cooling after annealing, microalloying elements are added to low-carbon-manganese-silicon steel, particularly vanadium or molybdenum and chromium (Kovieczny, 2003)

Vanadium in solid solution in the austenite increases the hardenability but the enhanced hardenability is due mainly to the presence of fine carbonitride precipitates which are unlikely to dissolve in either the austenite or the ferrite at the temperatures employed and this inhibit the movement of the γ/α interface during the post-anneal cooling.

Depending on the composition and process route, hot-rolled steels requiring enhanced capability to resist stretching on a blanked edge (as typically measured by whole expansion capacity) can have a microstructure containing significant quantities of bainite.

Figure 3.6 shows a schematic microstructure of DP steel. The soft ferrite phase is generally continuous, giving these steels excellent ductility. When these steels deform, strain is concentrated in the lower-strength ferrite phase surrounding the islands of martensite, creating the unique high work-hardening rate exhibit by these steels.

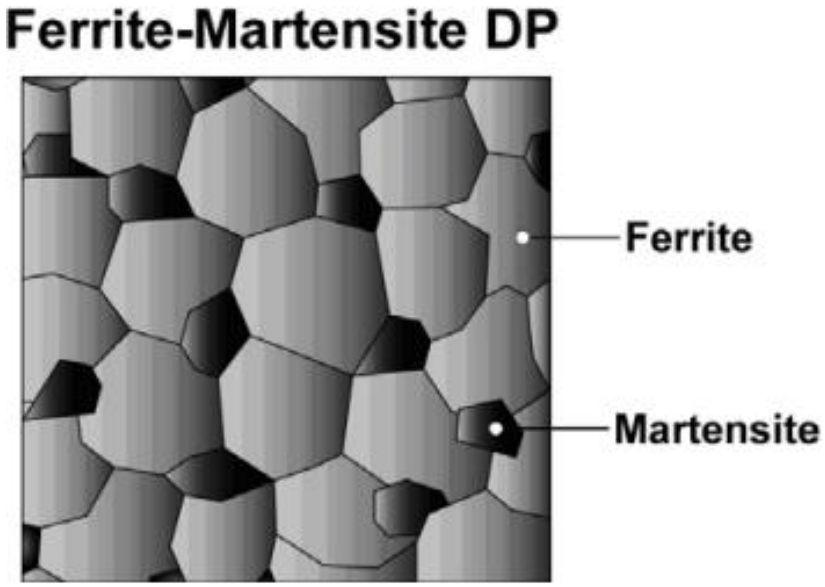

Figure 3.6 *Schematic microstructure of Dual Phase Steel.*

The martensite structure found in DP steels is characteristic of plate martensite having internal microtwins. The retained austenite can turn to martensite during straining thereby contributing to the increased strength and work-hardening. Interruption of the cooling, following intercritical annealing, can lead to stabilization of the austenite with an increased strength of subsequent deformation. The ferrite grains, approximately 5μm, adjacent to the martensite islands are generally observed to have a high dislocation density resulting from the volume and shape change associated with the austenite to martensite transformation.

The work hardening rate plus excellent elongation creates DP steels with much higher ultimate tensile strengths than conventional steels of similar yield strength. The engineering stress-strain curve for HSLA steel is compared on Figure 3.7 to a DP steel curve of similar yield strength. The DP steel exhibits higher initial work hardening rate, higher ultimate tensile strength and lower YS/TS ratio than the similar yield strength HSLA.

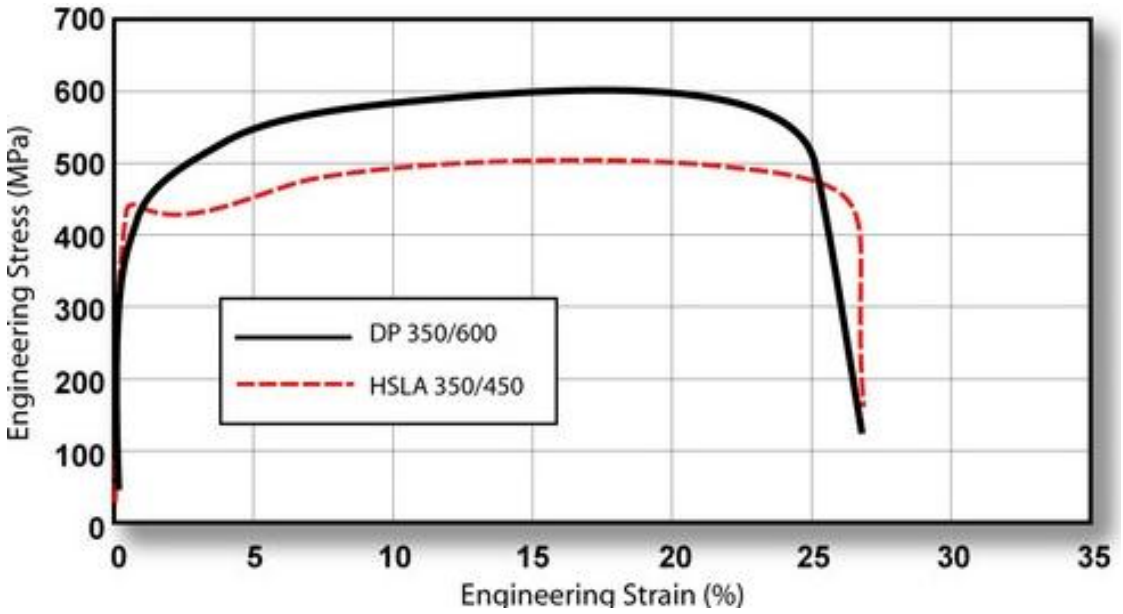

Figure 3.7 *Engineering stress-strain curves of HSLA and DP steels with the same yield strength*

DP and other AHSS also have a bake hardening effect that is an important benefit compared to conventional higher strength steels. The bake hardening effect is the increase in yield strength resulting from elevated temperature aging (created by the curing temperature of paint bake ovens) after prestraining (generated by the work hardening due to deformation during stamping or other manufacturing process) (S. P. Bhat, 2001). However, when welding the highest strength grade (DP700/1000) to it, the spot weldability may require adjustments to the welding practice, which is detailed in the following subchapter.

3.1.3 Joining Process

AHSS are readily welded by any of the welding processes, including shielded metal arc, submerged arc, flux-cored arc and gas metal arc process. Became a fundamental process due the growing used especially in the automotive industry. These steels owning a particular microstructural features, can be modified by following heat technological operation, the welding parameters have to be strictly controlled without losing the favorable mechanical properties which characterize them. Higher heat inputs strongly affect the microstructure, resulting a martensite and/or bainite phases in the weld metal and Heat Affected Zone (HAZ) with a consequent loss in toughness.

DP steels can be welded satisfactory with suitable processes and parameters, laser and spot welding are the most used joint techniques due to their lower heat inputs if compared with other welding techniques.

3.1.3.1 Cold Metal Transfer

"Cold" is a relative term in perspective to welding. Cold Metal Transfer welding is commonly referred to as CMT. The workpieces to be joined as well as the weld zones remain considerably "colder" in the cold metal transfer process (CMT) than they would with conventional gas metal arc welding.

The cold metal transfer process is based on short circuiting transfer, or more accurately, on a deliberate, systematic discontinuing of the arc. Results are a sort of alternating "hot-cold-hot-cold" sequence. The "hot-cold" method reduces significantly the arc pressure. During a normal short circuiting transfer arc, the electrode is distorted while being dipped into the weld pool, and melts rapidly at high transfer arc current. A wide process window and the resulting high stability define the cold metal transfer process. Automation and robot-assisted applications is what the process is designed for.

The major advancement is that the motions of the wire have been integrated into the welding process and into the overall management of the procedure (S. Schreiber, 2010). Every time short circuiting occurs, the digital process control interrupts the power supply and controls the retraction of the wire. The forward and back motion takes place at a rate of up to 70 times per second. The wire retraction motion helps droplet detachment during the short circuit.

The fact that electrical energy is converted into heat is both a defining feature and sometimes critical side effect of arc welding. Ensuring minimal current metal transfer will greatly reduce the amount of heat generated in the cold metal transfer process. The restricted discontinuations of the short circuit leads to a low short-circuit current. The arc only inputs heat into the materials to be joined for a very short time during the arcing period because of the interruption in the power supply.

The reduced thermal input offers advantages such as low distortion and higher precision. Benefits include higher-quality welded joints, freedom from spatter, ability to weld light-gauge sheet as thin as 0.3 mm, as well as the ability to join both steel to aluminum and galvanized sheets.

3.2 DUPLEX STAINLESS STEELS

3.2.1 Fundamentals of Duplex Stainless Steels

Duplex Stainless Steels (DSS) are stainless steels containing two primary phases: face-centered cubic (fcc) austenite and body-centered cubic (bcc) ferrite. In the 1920s, these alloys were first observed while an outgrowth of studies on austenitic stainless steels was carried out. The equality between the good corrosion resistance and mechanical properties has made them an important part of stainless steel family of alloys. In the following section a DSS summary is presented.

3.2.1.1 Development of DSS

The development of a duplex microstructure is a natural outgrowth of the metallurgy of the Fe-Cr-Ni system, which is the basis of all stainless steels. In 1927, Bain and Griffith developed a two-phase stainless alloy (E. C. Bain, 1927). Afterwards, by 1929 Avesta Jernverk named 453E as a first commercial DSS whose chemical composition was approximately 25%Cr-5%Ni (Gunn, 1997). Sweden and Finland start producing the duplex stainless steel in cast since 1930, which was mostly used in the sulfite paper industry (Alvarez, 2008).

Since 1936 a patent was granted in France for a cast duplex Uranus 50 (UR 50), it was noticed that a balance of ferrite and austenite had better resistance to chloride stress-corrosion cracking than a fully austenitic microstructure.

Nevertheless, plate products remained sensitive to edge cracks (Gunn, 1997; Soulignac, 2010). The use began in oil refinement, food processing, pulp and paper, which started to use exactly weighed alloying additions. The latter patent included copper additions in order to improve the corrosion resistance in several solutions. In 1940, another patent with molybdenum (Mo) and chromium (Cr) additions (Holtzer, 1953), was subjected to hardening effects by heat treatment in the 400-500° C range without losing corrosion resistance properties and embrittlement effects. After World War II, the Swedish grade 3RE60 (AISI Type 329) was extensively used for heat exchanger tubing for nitric-acid service. Industries start to require DSS in various applications including vessels, heat exchangers and pumps.

The DSS welded condition began to limit theses classes of steels, even when their provided good performance characteristics, the HAZ of welds had low toughness because of excessive ferrite and the lower corrosion resistance (Soulignac, 2010).

The DSS grades were developed to reduce intergranular corrosion problems in the high carbon austenitic stainless steels. DSS wrought evolution in 1970-1980 periods was particularly rapid, there were two main factors which advanced the development and use of duplex alloys. Firstly, nickel shortage increases the price of austenitic steels, in combination with increased activity in the offshore oil industry.

Secondly, steel production techniques improved rapidly with the introduction of the Vacuum (VOD) and Argon Oxygen Decarburization (AOD), which made possible to produce much cleaner steels with a very low carbon level with controlled nitrogen content.

In the 70s Langley Alloy developed a famous superduplex grade, known under the name of Ferralium 255 (UNS S32550) with 25% Cr and high Mo additions. This grade had nitrogen

additions but far behind today grades, it also remained difficult to weld. With the new process routes VOD/AOD plus continuous casting was possible to melt and transform at lower cost DSS, but weldability remained poor and manufacture of vessels stayed low and challenging. In the 90s new generations of nitrogen additions were developed. N additions contribute several properties, including the high temperature stability of the two-phase microstructure precisely in welded regions.

Table 3.2 list the chemical compositions of the second generation wrought DSS and of the cast DSS. First generation and the common austenitic stainless steels are included for comparison.

Table 3.2 *Chemical composition (wt. pct) of wrought and cast Duplex Stainless Steels*, austenitic grades exhibit for comparison (IMA, 2001)*

Name	UNS No.	EN	C	Cr	Ni	Mo	N	Cu	W
Wrought Duplex Stainless Steels									
First-Generation Duplex Grades									
329	S32900	1.4460	0.08	23.0-28.0	2.5-5.0	1.0-2.0	**	–	–
3RE60 ***	S31500	1.4417	0.030	18.0-19.0	4.3-5.2	2.50-3.00	0.05-0.1	–	–
Uranus 50	S32404		0.04	20.5-22.5	5.5-8.5	2.0-3.0	–	1.00-2.00	–
Second-Generation Duplex Grades									
2304	S32304	1.4362	0.030	21.5-24.5	3.0-5.5	0.05-0.60	0.05-0.20	–	–
2205	S31803	1.4462	0.030	21.0-23.0	4.5-6.5	2.5-3.5	0.08-0.20	–	–
2205	S32205	1.4462	0.030	22.0-23.0	4.5-6.5	3.0-3.5	0.14-0.20	–	–
DP-3	S31260		0.03	24.0-26.0	5.5-7.5	5.5-7.5	0.10-0.30	0.20-0.80	0.10-0.50
UR 52N+	S32520	1.4507	0.030	24.0-26.0	5.5-8.0	3.0-5.0	0.20-0.35	0.50-3.00	–
255	S32550	1.4507	0.04	24.0-27.0	4.5-6.5	2.9-3.9	0.10-0.25	1.50-2.50	–
DP-3W	S39274		0.03	24.0-26.0	6.8-8.0	2.5-3.5	0.24-0.32	0.20-0.80	1.50-2.50
2507	S32750	1.4410	0.030	24.0-26.0	6.0-8.0	3.0-5.0	0.24-0.32	0.50	–
Zeron 100	S32760	1.4501	0.030	24.0-26.0	6.0-8.0	3.0-4.0	0.20-0.30	0.50-1.00	0.50-1.00
Wrought Austenitic Stainless Steels									
304L	S30403	1.4307	0.030	18.0-20.0	8.0-12.0	–	0.10	–	–
316L	S31603	1.4404	0.030	16.0-18.0	10.0-14.0	2.0-3.0	0.10	–	–
317L	S31703	1.4438	0.030	18.0-20.0	11.0-15.0	3.0-4.0	0.10	–	–
317LMN	S31726	1.4439	0.030	17.0-20.0	13.5-17.5	4.0-5.0	0.10-0.20	–	–
904L	N08904	1.4539	0.020	19.0-23.0	23.0-28.0	4.0-5.0	0.10	1.0-2.0	–
254 SMO	S31254	1.4547	0.020	19.5-20.5	17.5-18.5	6.0-6.5	0.18-0.22	0.50-1.00	–
6%Mo	Various	Various	0.030	19.5-22.0	17.5-25.5	6.0-7.0	0.18-0.25	1.00	–
Cast Duplex Stainless Steels									
CD4MCuN Grade 1B	J93372		0.04	24.5-26.5	4.4-6.0	1.7-2.3	0.10-0.25	2.7-3.3	–
CD3MN Cast 2205 Grade 4A	J92205		0.03	21.0-23.5	4.5-6.5	2.5-3.5	0.10-0.30	–	–
CE3MN Atlas 958 Cast 2507 Grade 5A	J93404	1.4463	0.03	24.0-26.0	6.0-8.0	4.0-5.0	0.10-0.30	–	–
CD3MWCuN Cast Zeron 100 Grade 6A	J93380		0.03	24.0-26.0	6.5-8.5	3.0-4.0	0.20-0.30	0.5-1.0	0.5-1.0
Cast Austenitic Stainless Steels									
CF3 (cast 304L)	J92500	1.4306	0.03	17.0-21.0	8.0-12.0	–	–	–	–
CF3M (cast 316L)	J92800	1.4404	0.03	17.0-21.0	9.0-13.0	2.0-3.0	–	–	–

* Maximum, unless range or minimum is indicated. Significant figures shown accordance with ASTM A 751.

** Not defined in the specifications.

*** This grade was originally made without a deliberate nitrogen addition; without such an addition, it would be considered a first-generation duplex.

The previous DSS generation with rather low N additions had big coarsened ferritic grains in the HAZ with nitrides precipitations, which had detrimental effects on both toughness and corrosion resistance of welded grades (A. Fanica, 2007; Tuomi, 2000). The highly N alloyed grades were recognized as the alternative to expensive Mo high Ni austenitic grades, from then strong developments occurred with new superduplex chemistry dedicated to specific corrosion resistance applications (Groenewoud, 1982).

The most common duplex grade today is EN1.4462 or 2205 (UNS S31803/S32205), with 22% Cr, 5% Ni, 3% Mo and 0.16% N as chemical composition, is used in many applications and variety of product forms. They become commonly known by a number which evidence their typical Cr and Ni contents. The 2205 is a Ni enhanced DSS alloy, which Ni serves to improve the corrosion resistance properties. Moreover, exhibits a yield strength that is more than double of AISI Type 304, 316 and 317 austenitic stainless steels. Forward, new duplex grades have been introduced in the market place, the main targets of such developments are specifies by:

- Economy and overall cost benefits
- Easy of fabrication
- Improvements in design properties
- Increased availability
- Increased know-how overcoming the fear of change

The Lean Duplex development is due to replace the expensive Ni, with higher content of N and Mo. (D. S. Bergstrom, 2003) proposed an economical alternative to the common 2205 DSS with lower alloy content, particularly Ni and Mo, the mechanical properties and resistance to pitting crevice corrosion was indeed similar to 2205 DSS. Simultaneously at the wrought of Lean DSSs, the known Hyper Duplex Stainless Steels (HDSS) have been recently developed for long life and high temperatures applications, combining an excellent corrosion resistance and extra high strength.

3.2.1.2 Essential Qualities

In DSS the austenitic phase to be stabilized requires quite high Ni and Cr contents. DSS have been designed to have 50% δ-ferrite/50% γ-austenite microstructure, there chemistry is characterized by significant contents of Cr plus Mo while Ni content remains about 50% of the austenitic grades with similar corrosion resistance properties. The concerns of the costs particularly Ni and Mo, have had a drastic impact on austenitic grades, duplex have always be an alternative answer very cost competitive, particularly for thicker gauges. Substitutions of 316, 317 904L (N) grades by 2205 duplex grades is a cost strategy, cheaper grade while corrosion properties and high mechanical properties are given. For lean duplex including 2304 duplex grade versus 304 have been observed the similar outcomes. Likewise Superduplex being an alternative to superaustenitic and, in some other cases, to expensive Ni alloys (Alfonsson, 2010).

The chief reasons for using DSS are their good resistance to oxidation, corrosion and stress corrosion, all of these while keeping superior mechanical properties. These characteristics offer powerful driving forces for a further increase duplex uses in newly applications.

3.2.1.3 Classification and Applications

Such as austenitic stainless steels, the DSS are a family of grades, which classification in corrosion performance depends on their alloy content. The evolution of DSS has continued, and four modern groups of DSS can be divided as follows:

- ***Lean Duplex Stainless Steels*** has been replacing 316 and even 304 austenitic grades, own a higher content of N and Mo, and replace part of the Ni by Mn. These grades can certainly improve the progress of the duplex steels since it is possible to retain quality and reduce material cost.

- ***2205***, the standard DSS which covers approximately the 80% of the duplex use. The Cr content is approximately 22%, is used primarily due to its quite low cost and good availability.

- ***25 Cr DSS***. The 44LN, Carpenter 7Mo, Ferralium 255, Uranus 47N and Sumitomo DP3 are some examples of this subdivision. Copper additions were made to improve corrosion resistance in reducing acids and alloying with tungsten, was used to further improve the pitting resistance (Liljas, 2008).

- ***Superduplex***, present in some applications, higher corrosion resistance than 6% Mo. These grades are currently available and are widely used in the production of seamless tubes. They pledge cost-effective alternatives to superaustenitic or nickel-based for heat exchangers cooled by seawater.

Chemical composition is used also for the classification of DSS by calculating pitting resistance equivalent PRE (Table 3.3), but is not applicable in all environments. Sometimes also called PREN since consider the N content (J. O. Nilsson, 1992)

$$PREN = [wt.\%Cr] + 3.3[wt.\%Mo] + 16[wt.\%N] \quad (3.2)$$

The addition of W in some DSS can increase corrosion resistance, for these grades a PREW is expressed as follow:

$$PREW = \%Cr + 3.3\%Mo + 1.65\%W + 16\%N \quad (3.3)$$

PREN and PREW value is often used to distinguish the family to which alloy belongs. The classification taking in account the PRE is as follow:

- For Lean Duplex lower than 30.
- Standard Duplex having 30 as PRE.
- Superduplex with 40.
- Hyperduplex >45.

One of the important characteristic of DSS is the partitioning of the alloying elements between the constituent phases, which gives many peculiarities in mechanical and corrosion properties. The ferritic phase is enriched in δ-stabilizing elements (Cr, Mo, Si), and the austenitic phase in

γ-stabilizing elements (Ni, N, Cu, Mn). The distribution of the alloying elements between the phases is described by the partition coefficient, the ratio of the content of an element in ferrite in wt. % to that in austenite (Smuk, 2004).

Table 3.3 *Chemical compositions in wt. % of some most common wrought duplex stainless steel grades arranged with ascending PREN value* (Soulignac, 2010)

Grade	Standard	Cr	Mo	Ni	N	Other elements	PREN
2101	UNS S 32101	21	0.3	1.5	0.22		25
2202	UNS S 32202	22	-	2	0.20		26.5
2304	UNS S 32304	23	0.2	4.0	0.10		25
2205	UNS S 31803	22	3.0	5.3	0.17		35
2507	UNS S 32750	25	4	7.0	0.27		>40
Zenon 100	UNS S 32760	25	3.6	7.0	0.25	0.7 Cu, 0.7W	41
2707 HD	UNS S 32707	27	4.8	6.5	0.4		49
3207 HD	UNS S 33207	32	3.5	7	0.5		50

Duplex stainless steels present fine-grained structure, Ni alloying and biphasic mixture, which gives a high mechanical strength. One important application is to be employed in many corrosive environments within the temperature range of approximately -50°C to less than 300°C. In refining and petrochemical industry, the chloride containing process media or cooling water is very common. In oil and gas extraction applications, production tubes that transport oil up from the source to the oil-rig are used.

Type 22Cr and 25Cr are typical used against Sulfide containing process, which ferritic steels and high strength steels suffers cracking. These type of materials in annealed condition, have a yield point limit about 550 MPa, which could be increased with a cold rolled finish but his also limits the resistance of the material to stress corrosion caused by H_2S (Armas, 2008).

Some of main areas where they are applied: Oil production specifically heat exchangers and crude distillation (when SCC is a risk), petrochemicals (avoiding corrosion problems, 2205 and 2507 as the commonly used), desalination plants (2507 as effective option to austenitic 300 series) and automotive applications with the favorable combination of high strength, formability and high energy absorption in crash situation.

3.2.2 Physical Metallurgy and Properties

The chemical composition of DSS has been adjusted to reach the 50% ferrite and 50% austenite base metal microstructure. The Fe-Cr-Ni ternary phase diagram is a guide of the metallurgical behavior of these steels category. Figure 3.8 illustrate that DSS solidify as ferrite, part of it then transform to austenite as the temperature drops about 1000°C (IMOA, 2009)

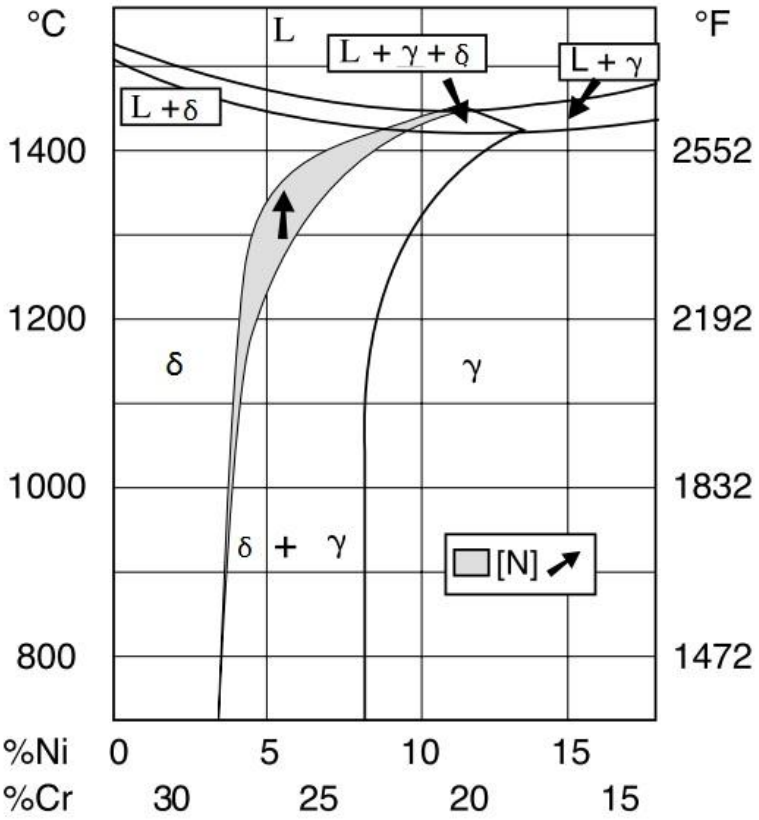

Figure 3.8 *Fe-Cr-Ni ternary phase diagram at 68% Fe* (IMOA, 2009)

Thermodynamically, because the austenite is formed from ferrite, it's impossible for the alloy to go past the equilibrium level of austenite. However, as cooling continues to lower temperatures, carbides, nitrides, sigma and other intermetallic phases are all possible microstructural constituents. Minor amendments in composition can cause a large effect on the relative volume fraction δ-ferrite and γ. The aim of maintaining the desired phase balance is achieved firstly by adjusting Cr, Mo, Ni and N contents while controlling also the thermal history. Although, because the cooling rate determines the amount of δ-ferrite that can turn into γ, cooling rates following high temperature exposures influence the phase balance (Charles, 1995).

N is the one who raises the temperature at which the austenite begins to form the δ-ferrite. Hence, even at relatively cooling rates, the equilibrium level of γ can almost be reached. The δ-ferrite excess was controlled with N, in the second DSS generation. The use of N means that Cr nitrides may be formed of δ/δ and or δ/γ boundaries. Other detrimental phases, such as sigma,

alpha prime and carbides can form in a matter of minutes at certain temperatures (Experimentation of harmful precipitation phases are presented in Chapter 5 and 6).

Figure 3.9 presents an isothermal precipitation diagram for 2507 DSS. Cr nitrides, σ- and χ-phase precipitation begins at the relatively "slow" time of 1-2 minutes at temperatures, which is slower than ferritic grades or highly alloyed austenitic grades. This advantage is due, in part, to the high solubility of C and N in the low Ni austenite phase and possibly to a retarded effect of N on the carbide precipitation.

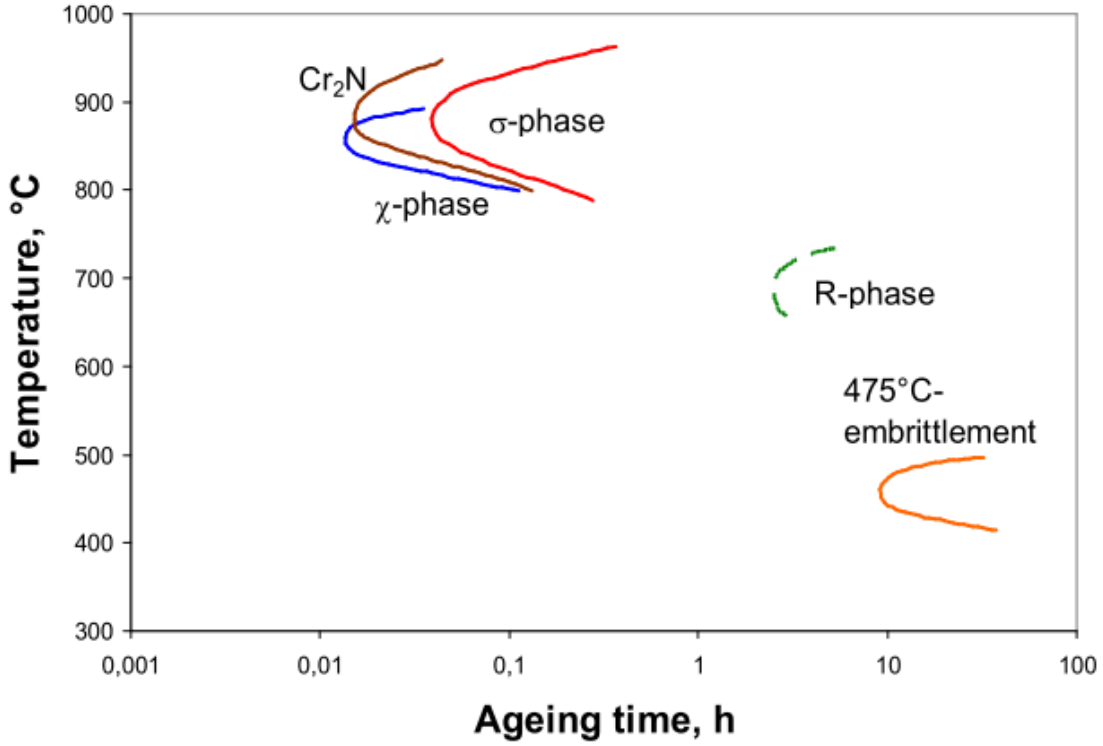

Figure 3.9 Experimentally determined TTT-diagram of SAF 2507 showing the C-curves of Cr 2 N, χ-phase, σ-phase, R-phase and spinodal decomposition. The C-curve of R-phase is dashed as it is supposed to be a precursor of the more stable σ-phase (J. -O. Nilsson, 2010)

Consequently, duplex grades are quite resistant to sensitization on cooling, formation kinetics of carbides and nitrides are only affected by Cr, Mo and Ni in these grades. Sigma and chi precipitation occurs when higher temperatures are reached while carbide and nitride precipitation at the same time. Duplex grades with more Cr, Mo and Ni content will present more rapid sigma and chi kinetics than those with lower alloy content.

3.2.2.1 Processing

Duplex stainless steels are manufactured as various wrought products, such as hot-rolled plates, cold-rolled sheets, tubes, pipes, bars, wires, different forgings and castings.

Production of complex shapes from DSS with significant amount of welding involved in the design can meet severe problems or become very costly considering difficulties with workability and weldability of DSS. The manifolds on oil platforms or valve bodies or similar equipment where castings are not possible because of the integrity issues can be examples of such components. In such cases the methods of powder metallurgy (P/M) can become efficient (Smuk, 2004).

Powder metallurgy is a manufacturing process of compacting metallic or ceramic powder by applying high temperature and/or high pressure. The compaction is usually carried out by one of the following methods:

- Sintering;
- Powder forging
- Cold Isostatic Pressing (CIP)
- Hot Isostatic Pressing (HIP)

Atomizing is widely used for the duplex stainless steel production, which is a process to obtain raw material for pressing. Powders are manufactured by spraying a molten alloy stream into small droplets inside a special chamber (atomizer) using gas jet, usually nitrogen or argon. The droplets solidify with the cooling rate of 102 to 105 °C/s producing ultrafine grain structure.

Powder is packed into a special container manufactured from low-alloy steel, usually by welding (Chen, 2001). The design and fabrication of container itself is one of the most important aspects of the HIP process, because can affect the quality of the end product. These are carefully inspected and the oxidized surface layers near the welds must be removed to ensure contamination-free end product.

Filling of the container is usually accompanied with vibration to provide the packing density as close to the maximal theoretical value (for spherical particles -65 -70 %) as possible. The container is evacuated to 10-2-10-4 torr, often at temperatures of 300-500 °C to facilitate the removal of internal gases. Finally, the container is sealed by welding, then placed in a special vessel with inert gas at high pressure (100-150 MPa) and high temperature (1100-1200°C).

The powder particles yield, grain boundaries creep and the diffusion occurs, giving rise to coalescence of powder particles to produce densified material with no porosity. HIPping can be interpreted as three-dimensional forging. After the HIPping process is finished, the container metal is removed by machining or by acid pickling.

3.2.2.2 Phase Transformations

In DSS ferrite phase is essentially unstable because of the high content of alloying elements.

Therefore, a large variety of secondary phases may precipitate in DSS in the temperature range of 300-1000 °C during isothermal aging or other heat treatment. Precipitation of secondary phases in DSS is usually considered in two separate temperature regions as shown in Figure 3.10, which may occur below 600 °C and from 600 to 1000 °C.

The following phases observed: σ phase, Cr_2N, CrN, secondary austenite γ_2, χ phase, R phase, π phase, M_7C_3, $M_{23}C_6$, and τ phase. In grades which contain copper it can also precipitate as copper-rich ε-phase. Additionally, spinodal decomposition of ferrite can occur in the temperature range of 300-500 °C.

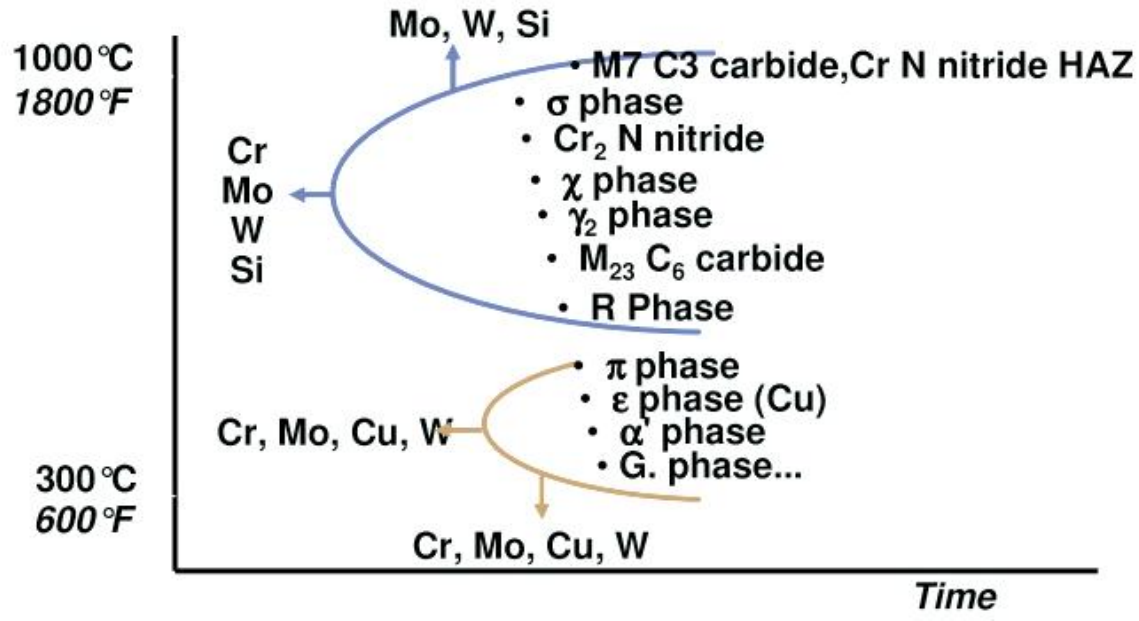

Figure 3.10 *Phase precipitation which may occur in Duplex grades (Charles, 1991)*

Long exposure times are usually required for this. Some parameters of the phases are listed in Table 3.4. σ phase is undoubtedly the most important of the listed secondary phases because of its significant volume fraction and its strong influence on toughness and corrosion behavior, besides 4 vol. % of σ phase can result in decrease of impact toughness down to the value of less than 27 J from 230-300 J.

Table 3.4 Lattice parameters and critical temperature range of secondary phases in DSS (J. O. Nilsson, 1992)

Precipitate	Nominal composition	Lattice type	Space group	Temperature range (°C)	Lattice parameter (nm)
σ	Fe 35-55 Cr 25-40 Mo 11-25	BCT	P42mnm	600-1000	*a*=0.880, *c*=0.454
Chromium nitride	Cr2N	Hexagonal	P31m	700-900	*a*=0.480, *c*=0.447
Chromium nitride	CrN	Cubic	Fm3m	N/A	*a*=0.4130-0.447
χ	Fe36Cr12Mo10 Fe 35-50 Cr 20-35 Mo 20-22	BCC	I43m	700-900	*a*=0.892
R	Fe 30-40 Cr 17-20 Mo 25-45	Hexagonal Rhombohedral	R3	550-650	*a*=1.0903, *c*=1.9342 *a*=0.9011, α=74°27'30"
π	Fe7Mo13N4	Cubic	P4132	550-600	*a*=0.636-0.647
τ	Not determined	-	Fmmm	550-650	*a*=0.405, *b*=0.484, *c*=0.286
Carbide	M7C3	-	Pnma	950-1050	*a*=0.452, *b*=0.699, *c*=1.211
Carbide	M23C6	FCC	Fm3m	600-950	*a*=1.0560-1.065

Sigma phase σ, is a hard brittle intermetallic compound enriched with Cr, Mo and Si (Y. Maehara, 1983), is formed in a large variety of DSS, as well as in some austenitic stainless steels (H. D. Solomon, 1979). Precipitation often starts at triple junctions or at ferrite/austenite boundaries (J. O. Nilsson, 1992), and continues at incoherent twin boundaries and finally intragranularly (Stickler, 1972). Sigma precipitates in high volume fractions, which affects strongly the mechanical and corrosion properties (B. Josefsson, 1991; Calliari, 2010). The temperature range of precipitation is from 600-1000°C. However, the fastest precipitation rate is between 850-900°C (C. V. Roscoe, 1984; A. J. Strutt, 1986). Sigma precipitation could be controlled by modifying solution annealing temperature (B. Josefsson, 1991; Chen, 2001).

Chi phase χ, is commonly found in DSS after aging at temperatures 700-900 °C. Appears often with σ phase, although the "nose" of its C-curve appears at somewhat lower temperatures and shorter exposure times (J. O. Nilsson, 1992). The volume fraction of χ phase is not usually very high, it consumes significant amounts of chromium and molybdenum from the parent matrix, and simultaneously forming secondary austenite becomes depleted of these elements.

The effects of χ phase on toughness and corrosion properties are detrimental; however, it is often difficult to separate them from those of σ phase. This can lead to a decrease of the pitting

corrosion temperature (J. O. Nilsson, 1992). Investigations indicate that the former precipitation of χ phase can support σ phase precipitation (T. H. Chen, 2002; K. Karlsson, 1992).

Chromium nitrides, precipitation takes place at temperatures 700-900 °C during fast cooling from high solution annealing temperatures, presumably because of the supersaturation of the ferritic phase with nitrogen, or during isothermal heat treatment, becoming an important issue with the increased use of high nitrogen content in modern DSS.

In the former case, Cr_2N particles precipitate mostly intragranularly with the crystallographic relationship $< 0001 >_{Cr_2N} \parallel < 011 >_{\delta}$. In the latter case, nitride particles precipitate intergranularly at δ/δ grain boundaries or γ/δ phase boundaries. Also likewise in the case of χ phase, simultaneously forming secondary austenite became depleted in Cr (Vogt, 2001).

Secondary austenite γ_2, the duplex structure is the result of quenching from high temperatures, at which the equilibrium share of ferrite is higher, so, decomposition of ferrite can take place at lower temperatures, following mechanism are mentioned (J. O. Nilsson, 1992):

- Eutectoid reaction $\delta \rightarrow \sigma + \gamma_2$ is facilitated by rapid diffusion along δ/γ boundaries and produces a typical eutectoid structure of σ phase and austenite in former δ-ferrite grains.

- Widmannstätten precipitates, with various morphologies form at temperatures above 650 °C, involving fast diffusion rates (Smuk, 2004).

- Martensitic process, Austenite precipitates isothermally and obeys the Nishiyama-Wasserman orientation relationship. Diffusionless character of the transformation with respect to the substitutional elements.

Carbides, occurs preferentially at δ/γ phase boundaries (P. D. Southwick, 1980), however, were also observed at δ/δ and γ/γ boundaries (T. Thorvaldsson, 1985). Either carbides, M_7C_3 and $M_{23}C_6$, precipitates at temperatures 950- 1050 °C and below 950 °C, respectively, in DSS, relatively rich in carbon.

R phase, is an intermetallic compound enriched in molybdenum. Precipitation occurs in the range of 550-700 °C. It has complicated trigonal crystal structure with the unit cell consisting of 159 atoms.

π phase, has a cubic crystal structure and it precipitates intragranularly in isothermally at 600 °C aged material, discovered by Nilsson and Liu 1991 (J. O. Nilsson, 1991).

Copper particles, were found to pin the growing δ/γ phase boundaries. Investigation leads to a refinement of the microstructure of DSS after aging at 850 °C associated with the copper precipitates (R. W. K. Honeycombe, 1982).

3.2.2.3 Mechanical Properties

One of the advantages of biphasic microstructure in DSS is the exceptional mechanical properties. These properties are highly anisotropic, which means that they may vary depending on the orientation. This is caused by the elongated grains and crystallographic texture due to hot or cold rolling.

Tensile strength, ferrite is usually stronger than austenite for the same interstitial content. The solubility of C or N in austenite is much higher than that in ferrite. Therefore, in duplex structure nitrogen is partitioned in a way that austenite can become stronger than ferrite (J. Johansson, 1999; M. Oden, 2000).

The amount of nitrogen dissolved in austenite in a super DSS was as high as 0.45 wt. % at average content of 0.27 wt. %. (Charles, 1991). Besides, tensile strength is grain-size dependent. The grain size in DSS is usually smaller than in both ferrite and austenite of the corresponding chemical composition (J. O. Nilsson, 1992). Then in practice a duplex alloy achieves higher strength values than its constituents. If the effects of grain size and partitioning of interstitials is compensated, the strength of a DSS is controlled by the stronger ferrite component (S. Floreen, 1968).

Fatigue, is associated to the yield strength (Jacobsson, 1991). This property can be evidently improved by stress-relieving heat treatments resulting in formation of small amounts of σ phase. In Figure 3.11 the typical yield strengths of several duplex stainless steels are compared with and 316L austenitic stainless steels between room temperature and 300°C.

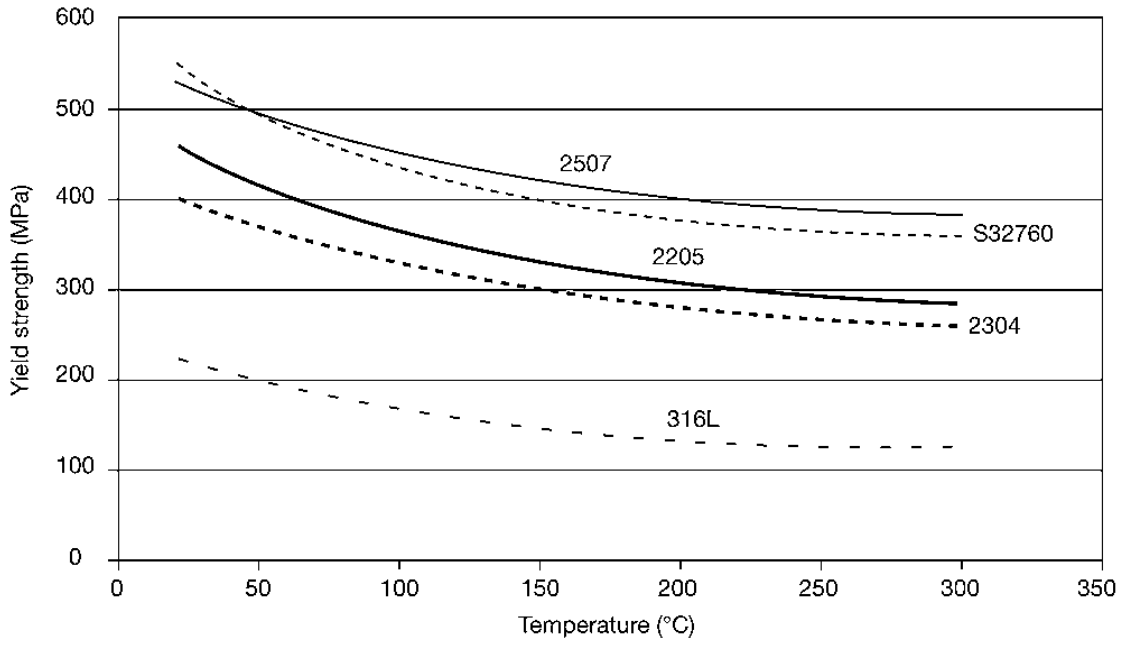

Figure 3.11 *Duplex Stainless Steels grades comparison to a 316L Austenitic Stainless Steel, room temperature and 300°C* (IMOA, 2009)

In order to find the balance among the duplex microstructure, the improved fatigue resistance and reduction in impact toughness and corrosion resistance because of precipitated secondary

phases is challenging, the dilemma is often solved in favor of as low amount of intermetallic secondary phases as possible.

It was also recognized that fatigue cracks grow preferentially in the ferritic phase and the austenite phase retards the crack growth, the non-modified spherical inclusions are more corrosion resistant and smaller phase size and homogeneous microstructure resist better crack initiation and growth.

Toughness, DSS achieve good toughness properties due to the presence of the austenite phase (S. Floreen, 1968). Austenite retards the cleavage fracture of ferrite. However, high alloying results in some decrease of the impact toughness. A comparison of the mechanical properties of some DSS grades is shown in Table 3.5.

Table 3.5 *Typical mechanical properties values of some annealed DSS. Austenitic and ferritic stainless steels shown for comparison* (J. O. Nilsson, 1992)

Grade	Standard	Yield strength 0.2%, [Mpa]	Ultimate tensile strength, [Mpa]	Elongation, [%]	Impact toughness at RT, [J]	Fluctuating tension fatigue strength, [Mpa]
AISI 304	UNS S30400	210	515-690	45	> 300	120± 120
AISI 430	UNS S43000	205	450	20	-	-
23Cr-4Ni (SAF 2304)	UNS S32304	400	600-820	25	300	245±245
22Cr-5Ni-3Mo (SAF 2205)	UNS S31803	450	680-880	25	250	285±285
25Cr-7Ni-4Mo (SAF 2507)	UNS S32750	550	800-1000	25	230	300±300

Toughness is very sensitive to the precipitation of secondary phases. In the temperature range of 600-900 °C σ, χ, R and π phases can precipitate, while at the temperatures below 500 °C spinodal decomposition of ferrite takes place. Subsequently, this means that sufficiently high cooling rates must be provided to avoid the precipitation (J. O. Nilsson, 1992; Sieurin, 2006; Calliari, 2010).

Corrosion is defined by a series of factors as the average of chemical composition of the grade, grain size, precipitation of intermetallic secondary phases, surface quality to mention some of them. This property is described as the ability to passivate and to remain in the passive state in a given environment. Cr, Mo and N are the most important alloying elements in duplex stainless steels with respect to corrosion properties.

Austenite phase is in general the weakest phase. Stress corrosion cracking (SCC) resistance increases with higher Cr and Mo contents, DSS are less sensitive to these damage phenomenon compared with common Ni alloyed austenitic steels, due to the increase ferrite amount (R. B. Hutchings, 1991).

3.2.3 Lean Duplex Stainless Steel

Duplex (ferritic/austenitic) stainless steel grade with superior machinability and easier to machine, Table 3.6 shows the chemical composition of the different grades. The ductility is less than austenitic grades, in case of cold working an intermediate annealing is recommended. Intermetallic phases precipitate after shorts times such as carbides and nitrides, which are less harmful to properties.

The impact toughness is slightly reduced due to the low Ni content (H. D. Solomon, 1979); on the other hand, fracture mechanism has a brittle behavior. Lean duplex has been used for blast walls on oil platforms based on the high strength combined with sufficient corrosion resistance. They are also used to replace construction steels, like bridges, storage tanks and also for transport vehicles.

Table 3.6 *Chemical composition (wt.%) of Lean Duplex Stainless Steels 2101, 2304 and 2404* (AB)

	UNS	EN	C	N	Cr	Ni	Mo	Others
LDX 2101®	S32101	1.4162	0.03	0.22	21.5	1.5	0.3	5Mn
2304	S32304	1.4362	0.02	0.1	23	4.8	0.3	
LDX 2404™	S82441	1.4662	0.02	0.27	24	3.6	1.6	3Mn

Outokumpu **LDX 2101®** (Liljas, 2008), with high Mn and N contents presents high strength and good corrosion performance also in welded condition, with UNS S32101 and 1.4162 in the American and European standard systems. DSS 2101 presents good resistance to localized corrosion including intergranular, pitting and crevice corrosion. The good oxidation resistance is also applied for high temperatures, however, suffers embrittlement if held at temperatures above 300°C, which can be amended by a full solution annealing treatment.

The high strength of 2101 makes bending and forming more difficult, hence, the operation will require larger capacity than austenitic stainless steels. Weldable by all standard electric methods, using 2209 as a filler metal. The heat input must be kept low and no pre or post heat should be given. Even so, unlike other duplex grades welding of 2101 without filler metal is possible.

Sandvik introduced **SAF 2304,** which was created to minimize the raw material cost with low Ni contents, compensated with Mn and N. Is characterized because it has almost no Mo, therefore is a cost-effective option to 316 in some applications. Likewise LDX 2101, 2304 is not suitable for using at temperatures above 300°C, however, provides good general corrosion resistance in most environments. The high strength of this type makes bending and forming more difficult and their ductility is less than austenitic grades, but can be welded by all standard process.

Filler metal is required in order to avoid excessive ferrite formation; the N added to the shielding gas will ensure the adequate austenite balance.

LDX 2404™ (Outokumpu) is a molybdenum-containning duplex grade with high content of Cr and N. Due to the lower alloy content, mainly Mo, the precipitation of damage intermetallic phases is more retarded than conventional grades, like 2205. The grade combines a higher mechanical strength than for other common duplex, is also well suited for optimal desings, reduced maintenance, durability and long-term cost efficiency.

2404 provides a good corrosion resistance and is also better than 4404 grade, pitting and crevice corrosion resistance is satisfactory. Mechanical properties of these grades are presented in Table 3.7

Table 3.7 Mechanical properties of Duplex stainless steels LDX 2101, 2304 and 2404 respectively (AB)

Grade	Tensile Strength (Mpa)	Yield Strength 0.2% Proof (Mpa)	Elongation (% in 50mm)	Hardness	
				Rockwell C (HR C)	Brinell (HB)
2101	650	450	30		250 max
2304	600	400	25	32 max	290 max
2404	680	480	25		290 max

3.2.3.1 Martensitic transformation

Deformation-induced martensitic (α'-martensite) transformation may occur in metastable austenitic stainless steels, where austenite phase evolves to the thermodynamically more stable α'-martensite phase due to the plastic deformation. The martensitic transformation takes place with a cooperative movement of atoms crating a very precise orientation relationship between the parent austenite and the product martensite. Some authors concurred on the transformation of austenite to lath martensite trough adifussional process which could be promoted by dislocations and twins accumulations introduced in the material during plastic deformation. (Bain, 1924) was the first to introduce a theory to explain the martensitic transformation from *fcc* austenite, to *bcc* or *bct* martensite with a minimum of atomic movement.

(Sachs, 1930) and (Nishiyama, 1934) using X-ray diffraction found that these important planes and directions were not really parallel, in some cases detecting deviations of more than a few degrees. Thus, the corresponding cells in the martensite and the parent are also rotated with respect to each other. Important planes and directions were no longer precisely parallel and it became clear that the martensite-parent orientation relation was irrational.

However the experimental results were found to follow a theory which includes both the Bain distortion and the presence of an invariant plane. In the so called phenomenological theory the martensitic transformation is accomplished by the Bain distortion and a shear deformation, slip or twinning, at the interface between austenite and martensite. Figure 3.12 represents the stages

of the martensitic transformation: the shape change following Bain's theory (a), the shear at the interface between parent austenite and new martensitic phase (b) and the twinning at the interface between austenite and martensite (c).

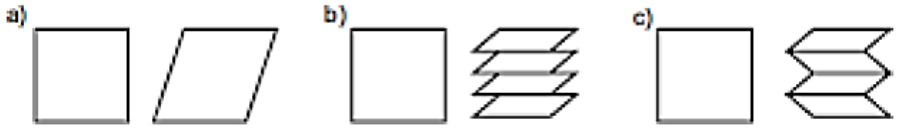

Figure 3.12 *Martensitic transformation: shape change following* (Bain, 1924) *theory (a), shear at the interface between parent austenite and new martensitic phase (b) and twinning at the interface between austenite and martensite (c)*

In order to form metastable austenite, two different types of deformation-induced occur. In the beginning of cold deformation and at low levels of strain hcp, paramagnetic ε-martensite seems to be favored, while at higher levels of strain bcc, ferromagnetic α'-martensite predominates. The increasing amount of α'-martensite with increasing of deformation and the contemporary decreasing till complete disappearance of ε-martensite led to suppose the following sequence of martensite transformation from metastable austenite (Prohászka, 2005):

$$\gamma \rightarrow \varepsilon \rightarrow \alpha' \tag{3.4}$$

Nevertheless, in some case only direct $\gamma \rightarrow \alpha'$ transformation seems to take through a dislocation reaction (I. Alternberger, 1999). Both transformations may occur in stainless steel according to recent studies (C. X. Huang, 2007; A. Das, 2008), stated that during the Ec. 3.4 evolution, the ε-martensite seems to act as the precursor phase of α' in both metastable austenitic stainless steels and high N austenitic grades. Preferential sites for α'-martensite nucleation can be the intersections of ε-martensite (Prohászka, 2005), the intersections between ε-martensite and slip bands (K. Spencer, 2009), intersections between mechanical twins and shear bands (Jin, 1997).

The presence of α'-martensite may affect the uniform elongation through its influence on the work-hardening rate (Talonen, 2007), proposed two alternative strengthening mechanism of α'-martensite. For α'-martensite content till 30%, α'-martensite particles dispersion harden the softer austenite phase, and the plastic deformation is accommodated mainly by the austenite phase.

3.2.4 Standard and Superduplex Stainless Steels

Standard Duplex stainless steel (2205) was developed as a product which could improve upon some of the technical weaknesses of the standard austenitic and ferritic stainless steels that are available in the market. It's the most widely used, due to both excellent corrosion resistance and high strength.

The standard duplex S31803 composition has been refined over the years by many steel suppliers, and the resulting restricted composition range was endorsed as UNS S32205 in 1996. Duplex S32205 gives better guaranteed corrosion resistance, but for much of the Duplex S31803 currently produced also complies with Duplex S32205. 2205 is not generally suitable for using at temperatures above 300°C as it suffers from precipitation of brittle micro-constituents, not below -50ºC because of its ductile-to-brittle-transition.

This duplex grade is a nitrogen-enhanced, the N serves to significantly improve the corrosion resistance properties of the alloy, which also exhibits a yield strength that is more than double that of conventional austenitic stainless steels; especially in the welded condition. Earlier duplex alloys have had moderate resistance to general corrosion and chloride stress-corrosion cracking, but suffered a substantial loss of properties when used in the as-welded condition.

The 2205 duplex stainless steel provides corrosion resistance in many environments that is superior to the AISI Type 304, 316 and 317 austenitic stainless steels. This duplex stainless steel is often used in the form of welded pipe or tubular components, as well as a formed and welded sheet product in environments where resistance to general corrosion and chloride stress corrosion cracking is important. The increased strength creates opportunities for reduction in tube wall thickness and resists handling damage.

Nevertheless, the extraordinary corrosion resistance (and other properties) of 2205 may be greater than is required in some applications. In certain SCC applications, while 2205 would provide an acceptable technical solution, it may not be an economical replacement alloy for Type 304, 316 or 317 stainless steel.

The higher cost of 2205 is due primarily to the amounts of the alloying elements Ni (nominal 5.5%) and Mo (nominal 3%). Thus, it is desirable to provide a weldable, formable duplex stainless steel that has greater corrosion resistance than the Type 304, 316 or 317 austenitic stainless steels shown in Table 3.8, and has a lower production cost than the commonly used 2205 duplex stainless steel.

Table 3.8 *Corrosion and Mechanical Properties of some Stainless Steels, 2205 Duplex grade, austenitic Type, 304, 316 and 317 and Duplex Developed under the Patent of* (D. S. Bergstrom, 2003)

Alloy	**Chemical comp. (wt. %)**		**PCR**	**SCC**	**Mechanical Properties**		
	Ni	**Mo**	**CPT**	**CSCC**	**Tensile Strength (Mpa)**	**Yield Strength 0.2% Proof (Mpa)**	**Elongation (% in 50mm)**
S31803	5.7	3.1	35°C	20°C	620	450	25
Type 304*	8-10.5	-	-	2.5°C	515	205	40
Type 316*	10-14	2-3	15°C	-3°C	515	205	40
Type 317*	11-15	3-4	19°C	2°C	517	206	35
US6551420B1[(a)]	3-4	1.5-2.0	31°C	**	786	572	37

Continuance to this idea (D. S. Bergstrom, 2003) attended an economical alternative to the known 2205 DSS with lower alloy content, particularly nickel and molybdenum. Bergstrom's duplex stainless steel exhibits mechanical properties comparable to 2205 along with resistance to pitting/crevice corrosion that is significantly greater than the Type 316 and 317 stainless steels. Table 3.8 resumes the important corrosion and mechanical properties of the new duplex steel created under the US Patent No. 6551420 B1 in comparison with pre-existing stainless steels. The success of the 2205 grade led to the development of an entire family of duplex alloys, which range in corrosion resistance depending on their alloy content.

This grade is well-welded by all standard process, ER 2209 is used as filler metal which provides a ferritic-austenitic weldment offering good properties of both phases, is over-alloyed with respect to Ni, to ensure the right ferrite balance in the weld metal.

A **Superduplex Stainless Steel** is a type of Duplex stainless steel with enhanced corrosion resistance which is categorized by its PRE_N being greater than 40, containing 25% Cr, 6.8% Ni, 3.7% Mo and 0.27% N, with or without Cu and/or W additions (SAF 2507, UR52N, DP3W, Zeron100). This is the most highly alloyed grade for wrought products, requiring both high mechanical strength and resistance to corrosion in extremely aggressive environments likewise chloride-containing acids (C. Bopper, 1994).

The high contents of Cr, Mo and N give the alloy a very high strength and simultaneously a good workability (see Table 3.9) for extrusion into seamless tubes. The yield point in tension exceeds 758 MPa in the extruded and annealed condition. Besides exhibiting excellent mechanical properties, this new alloy has a high resistance to pitting corrosion and crevice corrosion in chloride environments as well as a high resistance to stress corrosion cracking caused by hydrogen sulphide. In addition, the alloy is suited for applications that require welding, such as butt-welded seamless tubes and seam-welded tubes for various coiled tubing applications.

Consequently, it is especially appropriate for hydraulic tubes, such as umbilical tubes, which are used in order to control platforms in oil field. Besides, it is used extensively for offshore oil and

gas applications and can be found in flow lines, risers, process vessels, separators, coolers, manifolds, and process piping. Onshore, it can be found in heat exchangers, boilers, and pressure vessels in petrochemical and chemical processing plant.

In the expanding offshore oil & gas industry there was a need for high performance materials and 6Mo austenitic steels were selected due their high resistance to seawater. However, superduplex grades such as Zeron 100® and SAF 2507 were developed to compete with the superaustenitic grades with good success. Today, large quantities of superduplex tubing are used in umbilicals for the control of sub-sea systems.

Also in the offshore industry, lean duplex steel has been used for blast walls on oil platforms based on the high strength combined with sufficient corrosion resistance. Other areas where DSS have partly replaced austenitic alloys are flue gas cleaning systems and seawater desalination plants. In the latter case a combination of duplex grades is used to meet different aggressive environments.

Table 3.9 *Chemical and Mechanical Properties of Duplex grades, S31803, S32205, 2507, Zeron 100®* (Bergstrom, 2007)

Alloy	**Chemical comp.** (wt.%)		**Mechanical Properties**				
			Tensile Strength (Mpa)	Yield Strength 0.2% Proof (Mpa)	Elongation (% in 50mm)	**Hardness**	
	Ni	Mo				Rockwell C (HR C)	Brinell (HB)
S31803	5.7	3.1	620	450	25	31 max	293 max
S32205	5.7	3-5	655	450	25	31 max	293 max
2507	6	3	795	550	15	32 max	310 max
Zeron 100®	7	4	750	550	25	28 max	

3.2.5 Forming

3.2.5.1 Cold work

Duplex grades have shown good formability in wide fabrications. In some applications a simply forming is required, such as the rolling of cylindrical sections, press forming, vessel and tank head forming by pressing or rolling. The primary concern is the high strength of these grades and the power of the forming equipment. A typical first estimate is that a DSS will respond to forming similar to a 300 austenitic grade at twice the thickness. Figure 3.13 exhibit a comparison of the minimum in bending for several stainless steels.

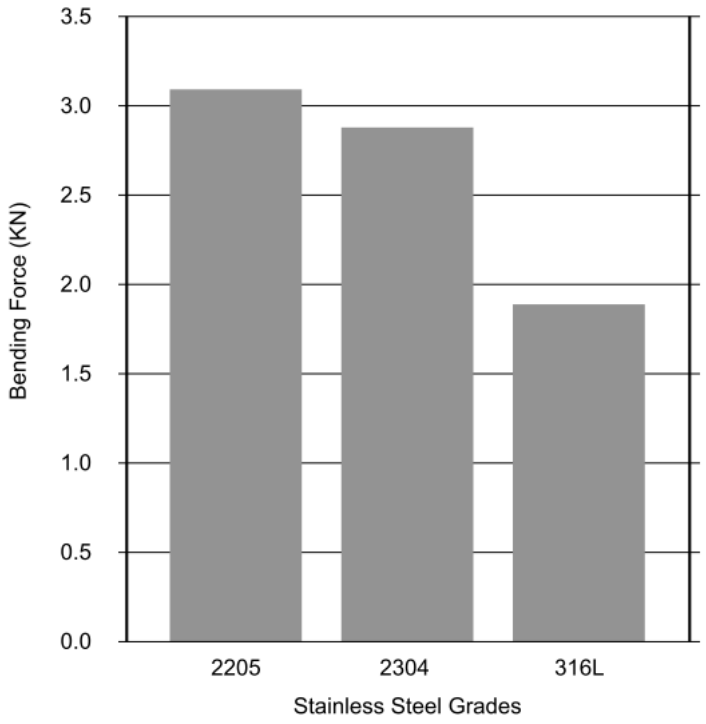

Figure 3.13 *Minimum force required to start Deformation in bending of 2304, 2205 and 316L. Test sample 50x2 mm* (Avesta, 2001)

The high strength of DSS can still proffer problems, even when the equipment has sufficient power. The lower ductility of duplex grades compared with austenitic ones must be taken into account. DSS have a minimum required elongation in most specifications of 15% to 25% in comparison with austenitic grades. For these grades a more generous bend radius than austenitic grades is required, in some cases intermediate anneals in severe or complex forming because of their lower ductility. The effect of cold work on the mechanical properties of 2205 is shown in Figure 3.14.

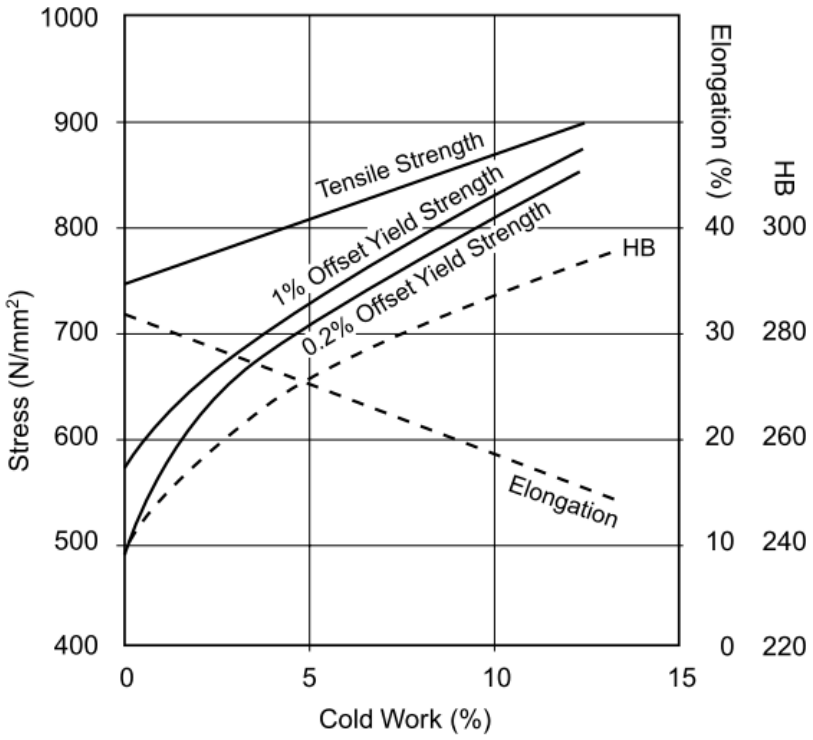

Figure 3.14 *Effect of cold work on the mechanical properties of SAF 2205 DSS* (Avesta, 2001)

DSS in many cases represent a replacement for a part that has been optimized for an austenitic and ferritic grade or carbon steel. The first attempt is often made without a change of thickness, however, a higher strength of DSS would justify a reduction of thickness, and the cost of redesign may postpone taking advantage of the cost and weight savings.

Duplex grades show some anisotropy of mechanical properties because of the rolling of the duplex structure, even so its practical effect is smaller than with ferritic steels due to the greater ductility of the duplex.

3.2.6 Welding

In Duplex grades providing a very good hot cracking resistance, is rarely a consideration when welding these steels, compared with austenitic grades which is a huge problem. However, HAZ can reduce corrosion resistance, toughness or pots-weld cracking in DSS. To avoid these problems, the welding procedure should focus on minimizing total time at temperature in the "red hot" range rather than managing the heat input for any one pass.

Preheating is not recommended because can be detrimental, relatively heat input can be tolerated and finally postweld heat treatment can be performed, but should be a full solution anneal followed by water quenching. Table 3.10 provides the temperatures for the solution annealing of Duplex grades (Hertzman, 1998).

Table 3.10 *Minimum solution Annealing Temperatures of DSS* (ASTM, 1996)

Grade	**Minimum Annealing Temperature**	
	°C	**°F**
Lean Duplex (2304)	980	1800
2205	1040	1900
25 Cr Duplex	1040	1900
Superduplex (depend on grade)	1050-1100	1925-2010

3.2.6.1 Submerged Arc Welding

This welding process allows the deposition of relatively large welds with less total time at temperature for the HAZ than would be possible for a larger number of passes with less deposition per pass. The SAW can provide to the DSS a minimal risk of hot cracking because of the ferrite solidification and duplex transformation of the weld metal. However, it is necessary to make some adjustment of joint design or welding parameters relative to austenitic grades in order to obtain full penetration welds (G. B. Holloway, 1991).

SAW is a cost efficient and technically satisfactory approach to welding duplex stainless steels it's also commonly used to manufacture heavy wall DSS pipe. Table 3.11 presents the typical parameters for this welding process in DSS.

Table 3.11 *Typical Submerged Arc Welding parameters for DSS with various size of filler metal* (Avesta, 2001)

Electrode diameter		**Current**	**Voltage**
mm	**inch**	**A**	**V**
2.5	0.094	250-450	28-32
3.25	0.125	300-500	29-34
4	0.156	400-600	30-35
5	0.203	500-700	30-35

Chapter 4

Effect of brazing speed on the microstructure and mechanical properties of Dual Phase steels

CHAPTER 4

Effect of brazing speed on the microstructure and mechanical properties of Dual Phase steels

This chapter[1] encloses the study of the interfacial microstructures and intermetallic compounds produced by Cold Metal Transfer welding plates of galvanized DP600 Dual Phase steel with CuSi3 as filler metal. A general description of the Dual Phase steels applications in automotive industry is presented. Next, the experimental procedures applying a CMT braze welding for different joining speeds, the description of the microstructural characterization and mechanical tests performed are explained. Steels have been widely using for construction, automobile, machinery, energy, transportation, daily life, etc. still steels play an important role to our society in the future. More advanced steel products with the characteristics of high performance, low cost, easy fabrication, low tolerance and environment benign have been developed to meet the demands from both market and environment protection. It seems there is no stop of this advancing trend.

The development of steel products is dependent on the steel knowledge we have. Although there have been a good accumulation of steel knowledge since the massive production of liquid steel, the new phenomena and roles in steels have still been investigated in recent years. Now people involved in steel research, steel processing and steel applications are concerned more and more with the progresses of steel science and technology than ever before, and have made great contributions to steel knowledge. This is one of the reasons why steel products are widely used in many applications.

[1] Portions of this chapter have been published in (A. F. Miranda Pérez, 2012) *et al.* and (I. Rampin, 2010)

4.1 Motivation

Dual Phase steels offer an outstanding combination of strength and drawability as a result of their microstructure, in which a hard martensitic or bainitic phase is dispersed in a soft ferritic matrix (Senuma, 2001). These steels having high strain hardenability give good strain redistribution capacity and thus drawability as well as finished part mechanical properties, including yield strength, which is further increased by the paint baking (also called Bake Hardening, BH) process. High finished part mechanical strength lends these steels excellent fatigue strength and good energy absorption capacity, making them suitable for using in structural parts and reinforcements. The strain hardening capacity of these steels combined with a strong bake hardening effect gives them excellent potential for reducing the weight of structural parts and even skin parts.

The interest in DP steels has been increasing in automotive industry, due to the possibility of reducing weight of vehicles and increasing the passenger safety at a very competitive cost. Automotive applications particularly well suited for structural body and safety parts such as longitudinal beams, cross members and reinforcements, unavoidably entail welding and joining in the manufacturing process and the fatigue resistance of welded joints due to the integrity and safety requirements (see Figure 4.1).

The variation of welding parameters (voltage, current and speed of welding) affects weld performance, mechanical, and metallurgical properties.

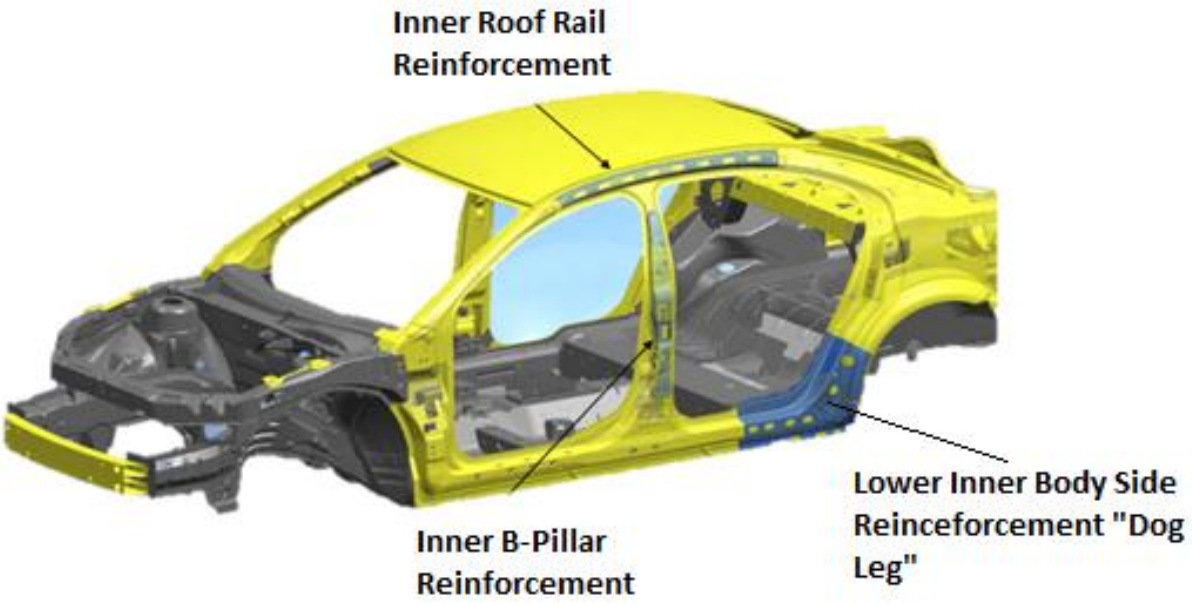

Figure 4.1 *Automotive structural body, Inner roof rail and B-Pillar reinforcement made from Dual Phase steel* (Cannon, 2011)

The CMT (Cold Metal Transfer) braze welding is a relatively new technology that partially decouples the arc electrical transients from the filler wire feed rate. It allows reducing the heat required for welding and permits higher joining speeds. One of the characteristic is the

reduction of spatter and also the lowest heat input that it is required for the joint (H. T. Zhang, 2008; Schwartz, 1987).

4.2 Case of study

Galvanized DP steel plates have been tested in some automotive designs; these are extensively used because of their excellent mechanical properties and superior corrosion resistance. Segregation of alloying elements during joint is still a problem; besides the formation of oxides on the steel surface often have a deleterious effect on coating adhesion during the galvanizing process. Although, a particular concern regarding reducing CO_2 emissions and the drive of having better fuel economy have already enthused the car manufacturer to use the weight materials having better mechanical properties. DP 600 provides a large potential for weight reduction and improved crash performance.

The aim of this study case is to analyze the interfacial microstructures and intermetallic compounds produced by cold metal transfer welding of two plates of galvanized DP600 dual phase steel with CuSi3 as filler metal. The study was performed by applying a CMT braze welding with three different joining speeds. The welded microstructures and microhardness were determined and related to the welding process conditions.

4.3 Experimental procedures

4.3.1 Galvanized Dual Phase 600

The materials were galvanized DP600 steel plates (Figure 4.2) of 119x130x1, 2 mm, whose composition is shown in Table 4.1.

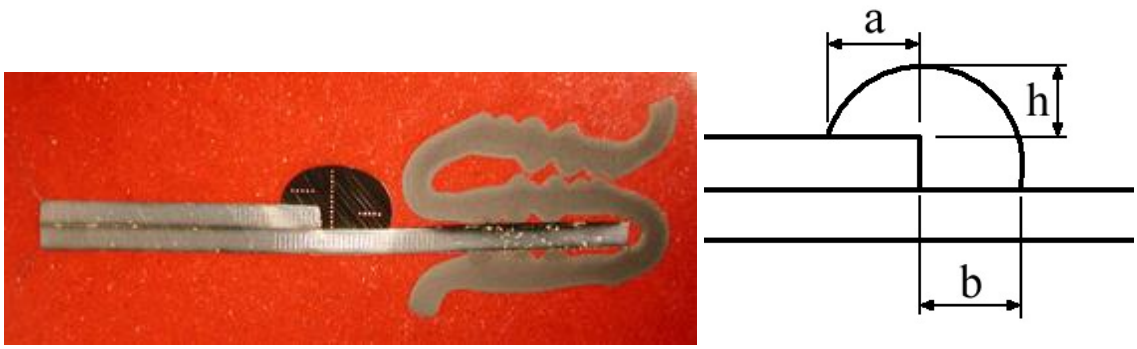

Figure 4.2 Dual Phase 600 steel plate, measurement scheme a, b and c for the specimens

The filler metal used in the braze-welding process was ER CuSi-A, the chemical composition is shown in Table 4.2. The wire alloy of 2 mm was used as filler metal during welding process. The filler metal was yellow-brown with two dark bands, approximately of amplitude 3 mm, extended along the sides, probably generated by the arc power required by the CMT process.

Table 4.1 *Composition of the base metal (wt %)*

C	**Mn**	**Si**	**N**	**Al**	**Ti**	**Nb**
0,115	0,155	0,186	0,0032	0,035	0,002	0,003
V	**B**	**Cu**	**Cr**	**Ni**	**Mo**	**Sn**
0,002	0,0003	0,012	0,347	0,026	0,110	0,003

Table 4.2 *Composition of ER CuSi-A (wt. %)*

Mn	**Si**	**Other**	**Cu**
0,75-0,95	2,80-2,95	Max. 0,5	Balance

For the mechanical tests, microhardness profiles were performed in accordance with the UNI EN ISO 6507-1 standard test method (ISO, 1999) using a load of 100 g. The tensile strength of welded joints was evaluated by Galdabini Sun 2500® testing machine. For tensile test actually does not exist a guideline for these kinds of samples, furthermore the (ISO, 2000) was used approaching to those for tensile shear test.

4.3.2 Welding parameters

The joint was carried out using the CTM method with the following parameters: V=10, 4 V and I=125 A. For this study different welding rates were considered. Table 4.3 presents the joining rates and the heat input.

Table 4.3 Welding rate parameters during braze welding and heat input.

	DPWB9	**DPWB3**	**DPWB16**
v (mm/s)	700	800	900
$\mathbf{H_n}$ (J/mm)	100,3	87,75	78

4.4 Results and Discussion

4.4.1 Material Characterization

The overview of the cross-section OM image of the base material along the longitudinal section is presented on Figure 4.3a, while the transversal side is on Figure 4.3b. It is constituted by ferritic matrix, with grains elongated in the rolling direction, and martensitic phase dispersed in parallel bands distributed in the same direction.

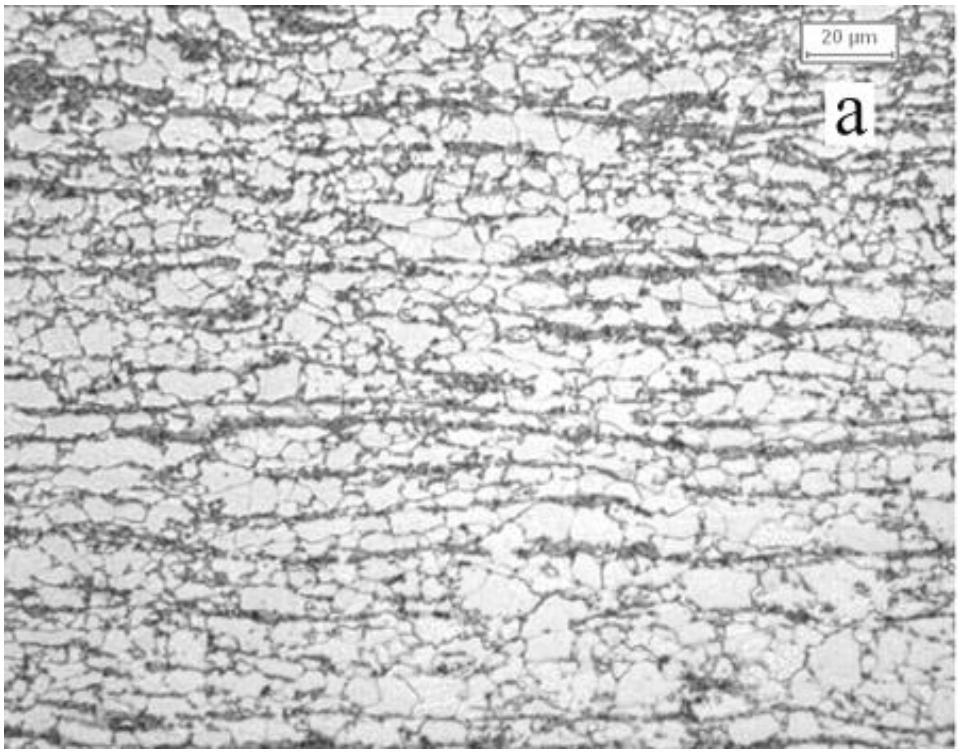

Figure 4.3a *Microstructure of base metal, DP600 steel, along the longitudinal section of the plate*

The HAZ adjacent to the unaffected area is constituted by coarse ferritic grains shown in Figure 4.4a, which was confirmed by SEM observation and microhardness values. Moving toward the joint martensite and bainite phases were observed, which are typical for the AHSS welded (E. Keehan, 2006).

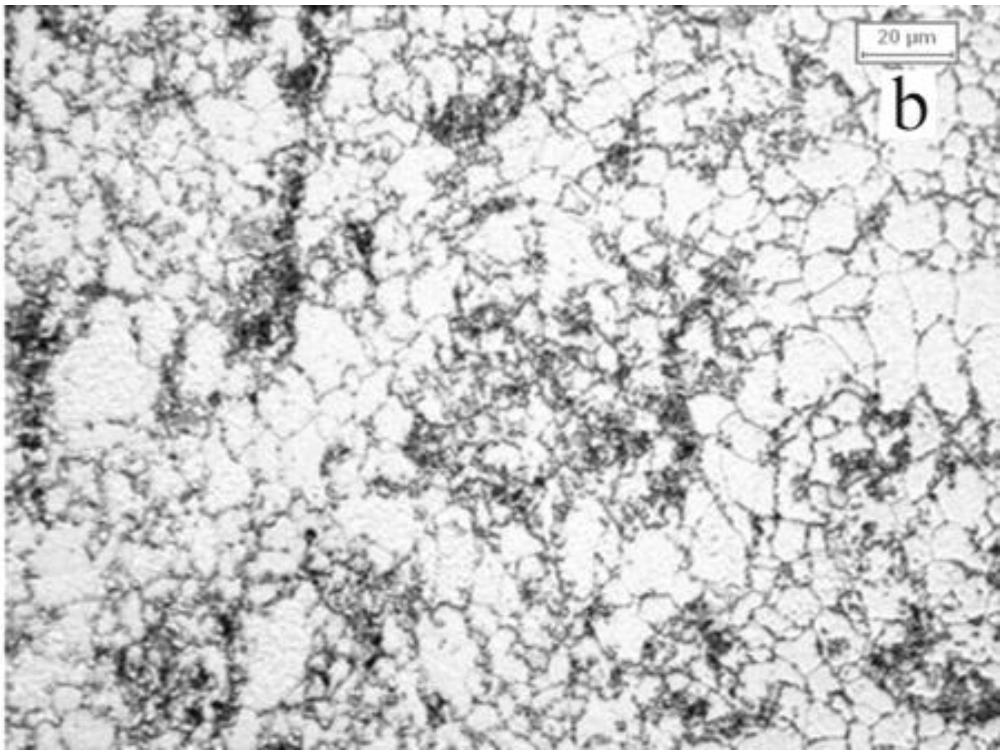

Figure 4.3b *Microstructure of base metal, DP600 steel, along the transversal side of the plate*

Continuing in the HAZ of the upper plate a completely martensitic structure is observed with strips of martensite that are more developed near the welding line (Figure 4.4a-b).

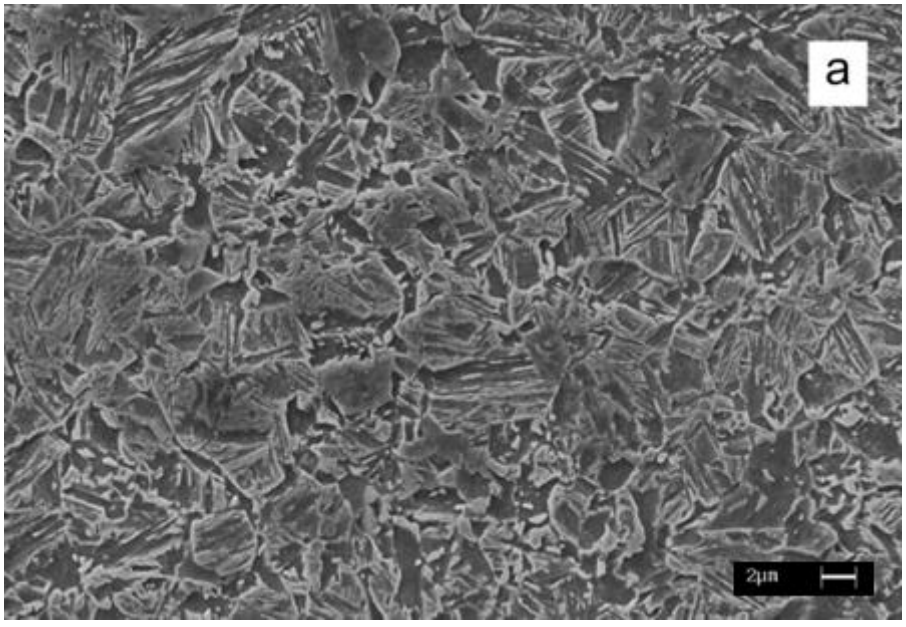

Figure 4.4a *Scanning electron micrographs of HAZ in the upper plate.*

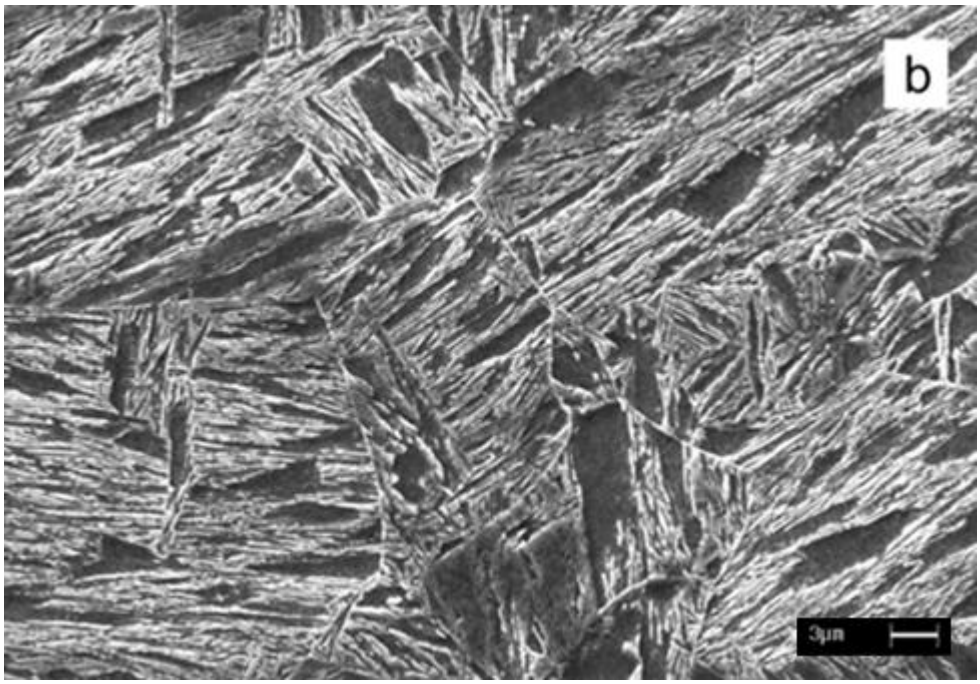

Figure 4.4b *Scanning electron micrographs of HAZ in the lower plate.*

This microstructural sequence was investigated in all the three samples considered in this study. The differences due to welding rate are the size and quantity of martensitic phase. Considering the same areas in different samples, the sample brazed at higher *v* has more martensite grains.

Table 4.4 *Values of the length of HAZ in the samples*

	DPWB9 (mm)	**DPWB3 (mm)**	**DPWB16 (mm)**
$l_{HAZ, Up}$	3,75	2,50	3,25
$l_{HAZ, Low}$	7,00	5,75	6,00

The length of HAZ is correlated to the welding rate parameter, in fact, increasing the welding rate, the Heat Affected Zone becomes smaller because the heat input is lower. Moreover, increasing the welding speed, the cooling rate is higher so that the sample DP16 shows a larger martensitic area.

The SEM analysis reveals a layer of intermetallic compounds, which growth at the interface steel-cordon. This is not uniform along the whole section: there are compact layers (Figure 4.5a) alternate with thicker inhomogeneous zones (Figure 4.5b). The compact zone has a uniform thickness of about 3 µm and it is divided into two layers (I and II). The composition of the layers I and II are shown in Table 4.5 for the three samples.

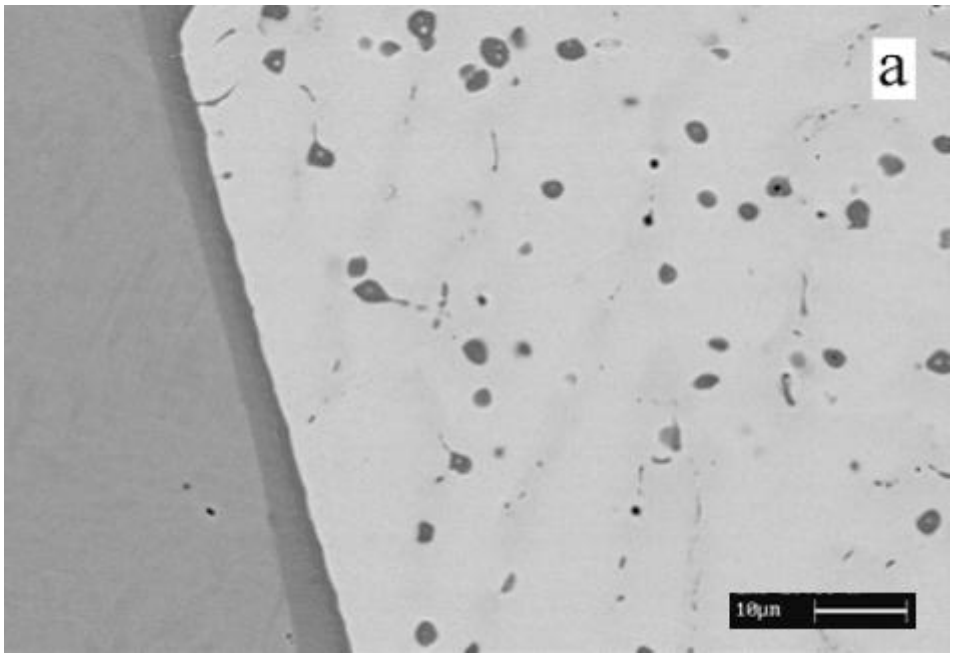

Figure 4.5a *Intermetallic compounds at steel-cordon interface: compact layer*

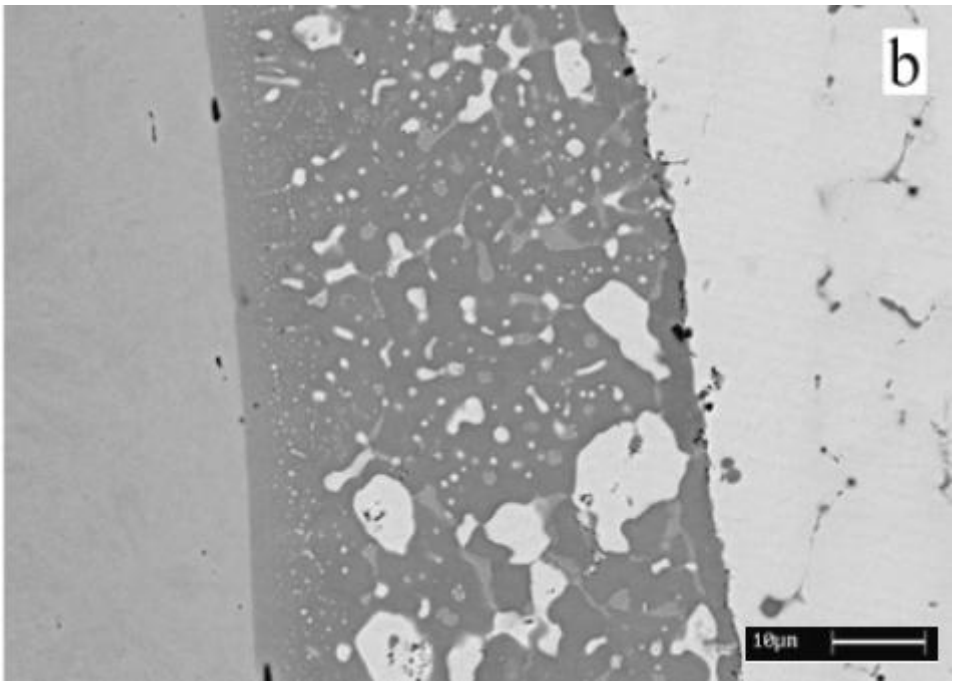

Figure 4.5b *Intermetallic compounds at steel-cordon interface evidence an irregular layer*

As indicated in Table 4.5, ternary Fe-Cu- Si compounds are formed. The proportions among the three elements are different in I and II layers. The following proportions can be identified: I layer: $Fe_{7.26}$-$Cu_{0.34}$-Si; II layer: $Fe_{3.48}$-$Cu_{0.52}$-Si.

Table 4.5 *Composition of the compound layers*

		Si (wt.%)	**Mn (wt.%)**	**Fe (wt.%)**	**Cu (wt.%)**
DPWB9	I	6,1	1,2	88,0	4,7
	II	10,8	1,5	74,9	12,8
DPWB3	I	8,2	1,2	84,6	6,0
	II	11,5	1,7	76,1	10,7
DPWB16	I	7,0	1,3	86,3	5,4
	II	11,8	1,2	78,7	8,3

The layer of non-homogeneous intermetallic compounds is rich in Fe and Si and their concentration increases towards the seam weld. This layer contains zones with high concentrations of Cu, Fe and Si and gray areas with higher concentrations of Cu.

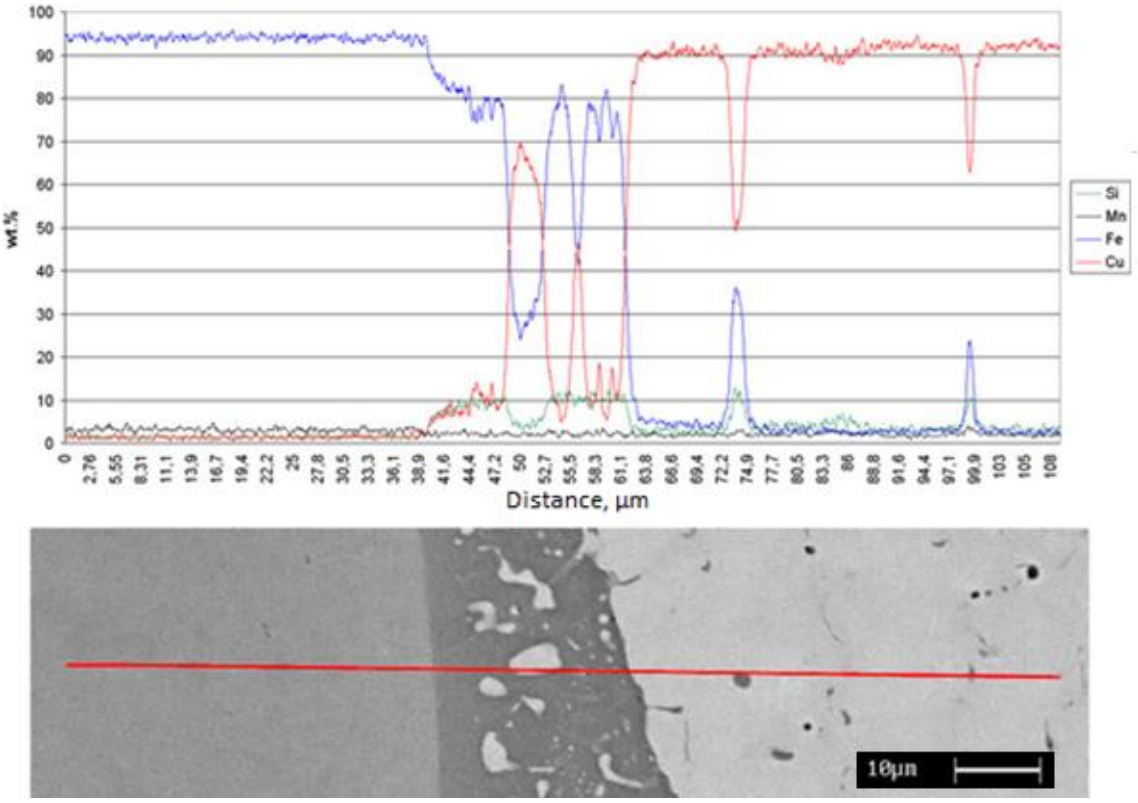

Figure 4.6 *Composition profile through the intermetallic compact layer*

The same areas are enclosed by small precipitates rich in Cu. As it can be seen in Figure 4.6, some intermetallic compounds are observed in the copper filler zone due to the strong stirring

force of the arc, which fragments the stick-like compounds at the interface solid/liquid so that many particles can be swept into the filler zone and grow by an Ostwald ripening mechanism (Y. Zhi-shui, 2006).

4.4.2 Microhardness Test $HV_{0.3}$

In order to observe the resistance to permanent or plastic deformation a microhardness test was performed. Figure 4.7 evidence the indentation point applied to the specimens in order to effect the measurement.

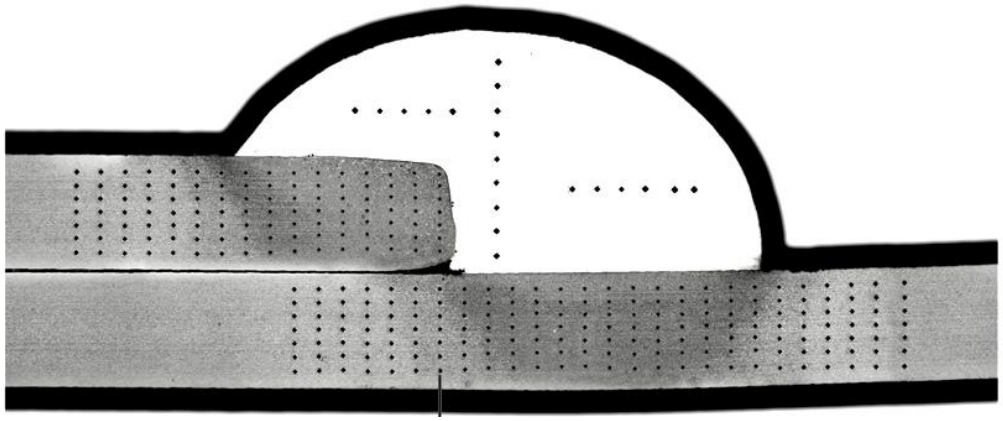

Figure 4.7 *Scheme of indentation points for microhardness $HV_{0.3}$ test*

The results of microhardness tests performed on three samples are summarized in Figure 4.8. The graphs confirm that with the increase of the weld rate, the size of the areas with hardness martensitic (375-450 $HV_{0.3}$) increases too, and in particular in DPWB3 and DPWB16 is noticed in the zones (very limited in the first, much more extensive in the second) higher hardness up to 425 $HV_{0.3}$. It is also noted that a v higher correspond HAZ more contained, but with increases more abrupt of microhardness.

Focusing instead on the bottom plate, it can be seen in DPWB3 and DPWB16 an area in the lower zone of the plate higher microhardness. The origin of these analysis, confirmed the observation of smaller amounts of martensite at the heart of the plates, there could be the coalescence of the central part of the plates after the braze welding process.

It can also be noted that at higher *v* the Heat Affected Zone has a smaller size and a more abrupt increase of microhardness. Lastly, it can be seen that the profiles made at 150 μm from the upper surface of the plates, have markedly higher hardness values, in particular on the lower plate. This confirms the OM observation that points out a greater concentration of martensite in these areas.

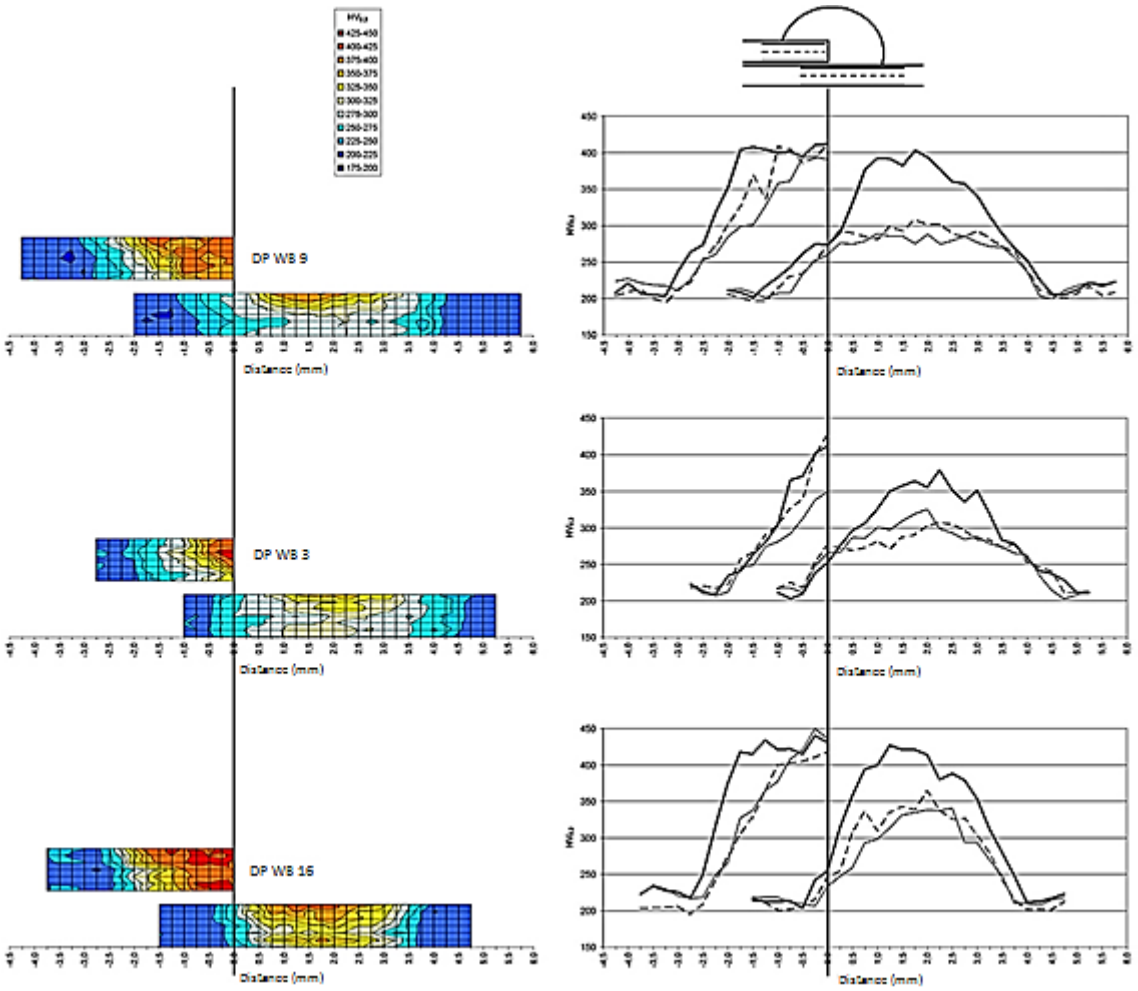

Figure 4.8 *Vickers's microhardness profiles*

4.4.3 Factographic study

The study of the characteristics of simply braze welding CMT analyzed concludes with a series of tensile tests, which finality is to quantify the mechanical strength of the joints and to identify possible influences of the speed braze on the mechanical characteristics observed. From the specimens analyzed (three for weld speed) their width varies from 23.25 mm to 24.75 mm. This factor must be considered in the calculation of the fracture strength σ_R. The maximum load achieved by each test was normalized on the section of a slab of the specimen in question (ax1.2 mm2).

Tensile-shear test was performed, which indicates the assembly state of stress in the specimen. Due to its particular shape, in the sample automatically drawn there are efforts to cut (between the upper surfaces of the plates and seam weld) and traction (between vertical surface of the upper plate and seam weld).

Tensile tests results, which are grouped for the three specimens under study, are summarized in Table 4.5

Table 4.5 *Tensile tests results of the nine specimens. a: amplitude of the specimen, F_R: breaking load, σ_R: fracture strength calculated, σ_{Rm}: fracture strength medium for each braze welding, dev.st (σ_{Rm}): standard deviation of the averages calculated, η_M: average efficiency of junction (= σ_{Rm}/σ_R, base metal)*

	DPWB9			**DPWB3**			**DPWB16**		
Specimens	**A**	**B**	**C**	**D**	**E**	**F**	**G**	**H**	**I**
a (mm)	24,00	23,95	23,60	23,45	24,75	23,90	23,25	23,90	23,85
F_R (N)	11376	10352	9586	7212	9365	9841	7425	7286	7699
σ_R (MPa)	395,0	360,2	338,5	256,3	315,3	343,1	266,1	254,0	269,0
σ_{Rm} (MPa)	**364**			**305**			**263**		
dev.st(σ_{Rm})	**28**			**44**			**8**		
η_m (%)	55%			46%			40%		

The efficiencies of junction η_M averages indicate that this type of brazing does not reach the mechanical strength of the base metal (σ_R = 664 MPa), and are obviously lower in processed samples to v higher. The fact that the mechanical resistance decreases with the increase of the speed of the process can be explained considering the depth of the bond steel-bead reached in the joint.

By reducing the supply of heat, the penetration for capillarity of Cu melted between the plates (key stage in the process of brazing) reduces too, and also the spread of Cu atoms in the steel. In addition, it has been observed that by decreasing the supply of heat, the amount of intermetallic compounds that are formed at the interface of the braze welding is reduced.

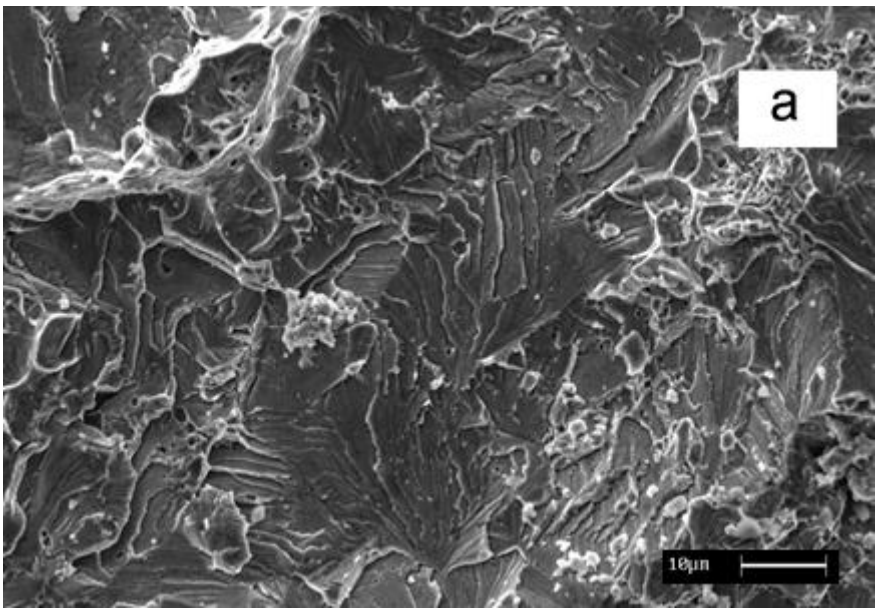

Figure 4.9 *Brittle fracture in the intermetallic layer*

The presence of intermetallic compounds at the plate-filler interface has an embrittlement effect, causing the fracture of the joint. Subsequently, the fracture propagates in a ductile way until failure. Figure 4.9 highlights the typical brittle mechanism of fracture, characterized by cleavage

planes, in the intermetallic layer area while Figure 4.10 refers to the fracture of the cordon. In this case the mechanism is ductile, characterized by small dimples.

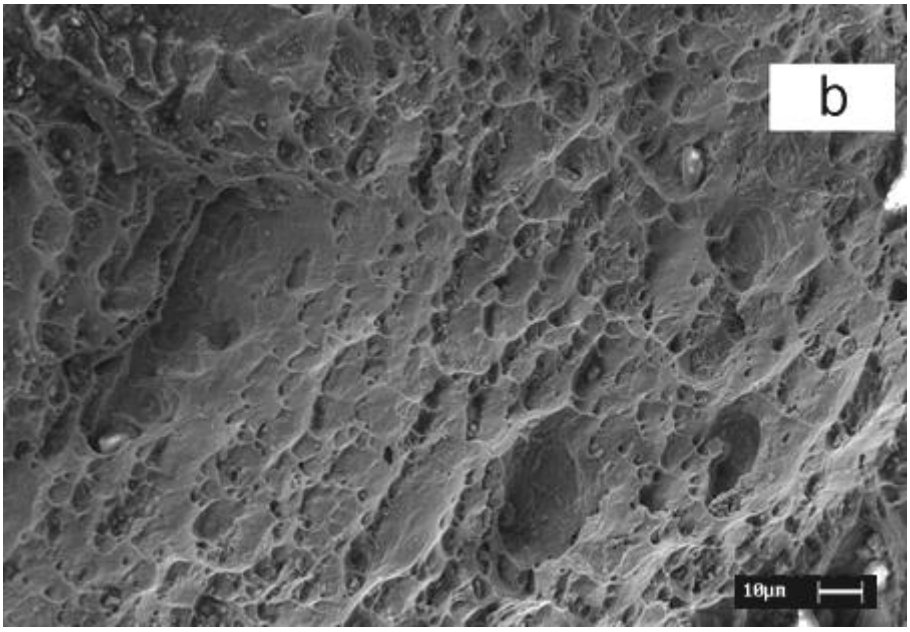

Figure 4.10 *Ductile fracture presented in the cordon*

Considering the brazing design, it comes up that the “L” edge of the upper plate covered by the filler metal increases the stress in the vertical edge of the upper plate.

4.5 Final remarks

The size of the Heat Affected Zone is relatively small (max. 7 mm). The microstructure of HAZ is constituted by an area with coarse grains, followed by a fine grain area (bainitic and ferritic phases). Approaching the seam weld, the quantity and size of martensitic grain increase, in the area next to the joint the microstructure is markedly martensitic. The microhardness values confirm the structure observed by the optical microscope, showing higher hardness in the areas with more martensite.

At the interface steel plates-Cu filler metal an intermetallic compound layer was formed. Along the interface there are zones where the intermetallic layer is uniform and compact with 3 μm thickness and others where the layer is inhomogeneous with a maximum thickness of 40 μm. Little rounded or elongated intermetallic precipitates were formed in the Cu-filler near the interface with steel plates. In all the cases the compounds are ternary Fe-Cu-Si intermetallic phases, whose composition, calculated on the two layers of compact zones, are $Fe_{7.26}$-$Cu_{0.34}$-Si and $Fe_{3.48}$-$Cu_{0.52}$-Si.

The variation of speed in brazing affects the width of HAZ that decreases at the increasing of the welding rate, but the size and amount of martensite phase in this area increases. The SEM and microhardness analysis show the effects of the coalescence in the heart of plates, probably due to the difference between the cooling rate on the surface and the inner zone of the plates. The joining rate also affects the thickness of the inhomogeneous intermetallic zones, where these areas are smaller when the process is quicker.

Moreover, at the increasing of the welding rate, the copper concentration in the intermetallic layer decreases due to the minor shorter diffusion time. In the samples where the input H is minor, the penetration of molten copper between the plates is reduced, as well as the capillary diffusion of Cu and the formation of intermetallic compounds; these factors adversely affects the mechanical strength of the joint. Moreover, the fractographic study of the samples failed after shear tensile revealed an embrittlement effect of the intermetallic layer. The CMT technique is considered adequate for joining dual phase galvanized steel. In particular the best results were obtained with the higher heat input due to the increasing of the mechanical strength of the joint.

Chapter 5

5

Influence of heating cycles on the precipitation of secondary phases in Duplex Stainless Steels

CHAPTER 5

Influence of heating cycles on the precipitation of secondary phases in Duplex Stainless Steels

The study on the transformation in the microstructure due to diverse heating cycles, such as isothermal heat treatments and/or welding is consider in this chapter[1]. Duplexes have great potential for expanding future structural design possibilities, enabling a reduction in section sizes leading to lighter structures. The duplex grades offer combination of higher strength than austenitic grades as well as a great majority of carbon steels with similar or superior corrosion resistance. Because of the advantages of their superior corrosion resistance, strength or both, Duplex stainless steels are commonly used for diversely applications.

Owing higher ferrite content than austenitic steels, they are more ferromagnetic and present higher thermal conductivity and lower thermal expansion, the ferrite matrix suffers a decomposition process when aged in the temperature range 650-950 °C.

Hence precipitation of austenite, sigma (σ), chi (χ), carbides and nitrides is developed, which are known as deleterious intermetallic phases that reduce the corrosion resistance and mechanical properties for this type of materials. Up to now, DSSs have been encountering some problems in the actual processing, such as difficult thermal processing, easy cracking and low productivity, mainly due to their sensitivity to precipitate harmful sigma phase.

Sigma precipitation can drastically decrease the toughness and corrosion properties of these grades (J. O. Nilsson, 2000; J. O. Nilsson, 1993; Y. S. Ahn, 2002). These phases must be avoided or well controlled, in order to prevent the resultant harmful effects due to their presence, such as embrittlement of the corrosion resistance reduction.

Almost all DSS contain significant percentages of nitrogen which, together with nickel and manganese, allows stabilizing the austenitic phase.

---

[1] Portions of this chapter have been published in (E. Ramous, 2012) and (A. F. Miranda Pérez)

For this reason, the exposure of the material within the critical temperature range can cause precipitation of nitrides, predominantly of chromium, which is the main alloying element (A. J. Ramirez, 2003).

An overall theoretical description of the precipitation of secondary phases in DSS is presented and the harmful consequences in their mechanical properties, following with a case of study which discusses the intermetallic phase formation as a consequence of isothermal heat treatments and welding in the critical temperature range for various types of Cr-Ni and Cr-Mn DSS.

5.1 Motivation

Over the last 20 years, significant developments have occurred in materials processing, providing a range of stainless steel material characteristics to suit the demands of various engineering applications. This is due to the aesthetic appearance, high corrosion resistance, ease of maintenance, smooth and uniform surface, high fire resistance, high ductility and impact resistance, reuse and recycling capability, as well as ease of construction of stainless steel structural members.

Nickel stabilizes the austenitic microstructure and therefore contributes to the associated favorable characteristics such as formability, weldability, toughness and high temperature properties (Baddoo, 2008; Gardner, 2005).

Their good mechanical properties are chiefly due to the structure constituted of ferrite (δ) and austenite (γ). However, the morphology of both phases is also an important factor which is known to control the mechanical properties (R. Badji, 2008; H. Sieurin, 2006; I. Calliari, 2007). Applications of the duplex grades are typically straightforward, since they can be formed and welded with standard equipment and techniques.

For the fabrication process in industrial applications of DSS such as chemistry, food, pharmacy and marine are often welded under large heat input alike in submerged arc welding (SAW) (V. Olden, 2008; P. Johansson, 2002; S. Tsuge, 2011), afterward isothermal heat treatment if and where it is possible, which causes to modify the texture and thus the final properties of the weld joint (H. Sieurin, 2006; I. Calliari, 2007; M. C. Young, 2007). During fusion welding, the DSS base material is subjected to a series of thermal cycles. Therefore, microstructural transformations occur, affecting the δ/γ balance in the steel. Precipitation of undesired secondary phases begins to appear, even after few minutes (3-5 min) and especially in the range 850-950°C (I. Calliari, 2007).

The intermetallic precipitates led to dangerous effects of embrittlement and reduction of the corrosion resistance. The formation of these harmful phases has been the subject of many studies (Nilsson, 1992; Charles, 2008), aimed to the identification of such phases and to the analysis of the precipitation conditions, which generally are different and specific for each type of steel.

The most important and interesting embrittling phases are the intermetallic Sigma (σ) and Chi (χ) phase, which their precipitation kinetics and transformation in various DSS grades have been extensively studied (I. Calliari, 2010; I. Calliari, 2011). Additionally, those known as carbides and nitrides, which are formed above 600 °C, the precipitation of carbides in DSS is less important than in the other types of stainless steels, owing to the low carbon content of DSS which makes the detrimental effects less important than those produced by other phases.

However, almost all the DSS contain significant percentages of nitrogen (typically in the range 0.1-0.3%), which represents an important alloying element because, together with nickel and manganese, allows to stabilize the austenitic phase, in order to confer to these steels the optimum microstructure, which is composed by almost equivalent volume fractions of ferrite and austenite (Nilsson, 1992; A. Weisbrodt, 2006). For these reasons, the content of nitrogen in DSS can be ten times higher than Carbon, hence makes possible and easier for nitrides formation, mainly of chromium, which is the main alloying element. Nitrides precipitation

causes a local depletion of chromium, making the steel more susceptible to localized corrosion and, furthermore, the presence of such structural discontinuities inside the microstructure increases the number of preferential sites for the cracks initiation, compromising the resistance characteristics of the steel.

5.2 Case of study

In this particular case of study two heating cycles are discussed. Firstly is described the effect of time during isothermal treatment at 850°C and 900°C on the microstructure of SAF 2205 Duplex Stainless Steels welded plates. The alloy commonly denoted as SAF 2205, is a usual duplex stainless steel which is used for corrosive service due to its higher corrosion resistance compared to conventional austenite stainless steels like types 304 and 316 (T. R. Parayil, 2011; M. B. Cortie, 1997).

Previous studies evidenced that DSS 2205 submerged arc weldments using proper welding parameters gives satisfactory δ-γ phase balance in the heat-affected-zone (H. Sieurin, 2006; V. Olden, 2008). Their crystallographic texture results from the recrystallization and phase transformation phenomena occurring in each of the two phases at various stages of the isothermal treatment. However, at high temperatures, DSS are prone to intermetallic phase transformation such as σ and χ, resulting in pernicious effects on impact toughness and corrosion resistance (I. Calliari, 2007; J. O. Nilsson, 1996; S. S. M. Tavares, 2005).

Sigma phase can occur at a temperature range between 650-950°C (Davis, 1994; N. Sathirachinda, 2010; J. Michalska, 2006), and the precipitation rate depends on alloy level of mainly chromium and molybdenum. Is mainly formed by decomposition of the ferrite, known as a non-magnetic, hard and brittle phase and in the initial state it is usually seen as precipitates at triple junctions and δ-γ boundaries (S. Wessman, 2010; J. Michalska, 2006; R. Badji, 2008).

The corrosion properties can be decayed given that Mo and Cr accumulate in the sigma phase; even so sigma is the most critical for the mechanical properties (Magnabosco, 2009; Y. -J. Kim, 2004). The aim of this first part is to evidence the morphology of sigma phase, and obtained a quantitative analysis of precipitation nucleated after aging SAF 2205 welded duplex stainless steels.

In the second part of this study has been performed as a part of a wide research on phase transformation in DSS. Specifically, the nitrides formation after isothermal heat treatments in the critical temperature range for various types duplex grades. The formation of nitrides in DSS is possible and has already been studied (N. Sathirachinda, 2010), also in Cr-Ni DSS, although in these steels the main undesired effects are due to the presence of other phases, such as σ and χ-phase. However, the presence of nitrides seems to be more important and conditioning in the most recent DSS grades, both in Cr-Ni DSS, with a higher content of alloying elements (and particularly nitrogen) such as Superduplex (SDSS), and Lean Duplex due to a minor content of Ni and Mo and in which nitrogen plays a fundamental role for the formation of the optimal microstructure.

The nitrogen contents which are generally present in DSS are above the solubility limit in the ferritic phase for temperatures around 1000°C. Nevertheless, the solubility in austenite is not compromised. This difference in solubility in the two phases has an important implication in the precipitation of nitrides in these alloys. The predominating chromium nitride is the Cr_2N type, with a hexagonal structure, even if CrN nitrides with a cubic structure has been observed in the heat affected zone of the weldments in a SAF 2205 (S. Hetzman, 1986).

The Cr_2N formation can occur in two different forms, depending to the thermal process which the steel is subject. Precipitates can grow intragranularly, as a result of a too rapid cooling from

temperatures of the order of 1000-1300°C, or intergranularly during isothermal heat treatments at lower temperatures. Intragranular is formed probably, because, at those temperatures the solubility of ferrite against nitrogen increases, reaching values comparable for austenite and therefore bringing the ferrite in the state of supersaturated solid solution. If the subsequent cooling is too rapid, the nitrogen is unable to diffuse completely and to be distributed into the austenite, but precipitates in the form of nitrides of elongated shape.

On the contrary, the intergranular nitrides are formed as a result of isothermal heat treatments carried out within the critical temperature range for DSS (700-950°C). Also the intergranular nitrides are related to the super-saturation conditions of ferrite, but precipitate in globular form and decorate both ferritic grain boundaries and the grain boundaries between austenite and ferrite (Nilsson, 1992).

Moreover, nitrides precipitation during the isothermal heating is often accompanied by the formation of secondary austenite (γ_2) (A. J. Ramirez, 2003), which contains lower levels of N, Cr and Mo if compared with the primary austenite. Secondary austenite increases the toughness of the material but is deleterious for the corrosion resistance, particularly against pitting corrosion, and its appearance is much more frequent in multiple-pass weldments, due to the subsequent heating on the same welding zone.

5.3 Experimental procedures

5.3.1 Base metal of duplex grades

Different grades of DSS were analyzed: SAF 2101, 2304, 2205, 2507, 2510 and Zeron100, received in form of bars or plates, and whose chemical compositions are reported in Table 5.1. All the investigated steels, in the as-received conditions, were subjected to a solution annealing treatment at the optimum temperature, followed by a water quench.

Table 5.1 *Chemical composition of the examined DSS (wt. %)*

	C	Si	Mn	Cr	Ni	Mo	Cu	W	P	S	N
2101	0.026	0.69	3.95	22,57	1.10	0.07	-	-	0.030	0.001	0.13
2304	0.030	0,56	1.40	23.20	4.30	0.18	-	-	0.027	0.001	0.10
2205	0.030	0.56	1.46	22.75	5.04	3.19	-	-	0.025	0.002	0.16
2205*	0.019	0.5	1.5	21.9	5.7	3	-	-	0.021	0.001	0.16
2507	0.015	0.24	0.83	24.80	6.89	3.83	0.23	-	0.023	0.001	0.27
Zeron100	0.020	0.72	0.56	25.24	7.46	3.67	0.59	0.61	0.025	0.001	0.28
2510	0.020	0.44	0.37	25.30	9.90	4.00	-	-	0.018	0.001	0.28

*SAF 2205 welded plates using submerged arc welding (SAW) with ER 2209 as filler metal

5.3.2 SAF 2205 Welding procedure*

SAF 2205* duplex stainless steel, received as a welded plate of 30x30 mm of thickness, commercially produced by Outokumpu Stainless Steels, which plates were welded together to form butt joints along the longitudinal direction using submerged arc welding (SAW) that allows the deposition of relatively large welds with less total time at temperature for the HAZ than would be possible for a larger number of passes with less deposition per pass using ER 2209 as filler metal.

The chemical compositions of the filler materials is given in Table 5.2

Table 5.2 *Chemical composition (wt. %) of weld material (SAF 2205), 30 mm thickness*

	C	Si	Mn	Cr	Ni	Mo	P	N
Weld wire	0.020	0.7	1.2	22.5	9	3	0.025	0.15

The welding parameters are listed in Table 5.3

Table 5.3 *Submerged arc welding parameters*

Electrode	ER 2209 (AWS)
Interpass temp	150 °C
Voltage	30.5 V
Amperage range	450-500 A
Weld speed range	4-5 mm/s

SAW is a cost efficient and technically satisfactory approach to welding duplex stainless steels is also commonly used to manufacture heavy wall DSS pipe.

5.3.3 Heat treatments on SAF 2205, Zeron 100 and SAF 2205*

The isothermal heat treatments were performed in the temperature range 600-1000°C. Relatively short treatment times (from 3 to 120 minutes) were chosen in order to measure small amounts of secondary phases and to study the kinetics of precipitation, while longer treatment times (up to about 750 h) were employed only for the study of Cr-Mn Lean DSS. The continuous cooling tests, performed on 2205 and Zeron100 grades, were carried out in a Setaram "Labsys TG", in argon atmosphere, and have involved a heating at 10°C/min from room temperature, a permanence in temperature for 5 min and a controlled cooling at different rates (from 0.02 to 0.4°C/min). Some works concerning σ and χ formation have been already published by (I. Calliari, 2011).

On SAF 2205* case, isothermal ageing treatments of specimens, previously solubilized at 1100°C and water quenched, were carried out in the temperature range 850-900 °C for 3 and 6 hours followed by water quenching. This part of the research was performed at the Royal Institute of Technology.

5.3.4 Characterization techniques

Metallographic sections were prepared for optical metallography using standard techniques of mechanical polishing. The total volume fraction of the intermetallic phases including χ phase, were measured by image analysis in unetched metallographic samples for SAF 2205* by means of S-3700N Hitachi Scanning Electron Microscope (SEM), in backscattered-electrons mode (BSE) at the Royal Institute of Technology.

In order to determine the chemical composition of the phases present in the microstructure, an energy dispersive X-ray spectrometer (EDX) system attached to the scanning electron

microscope was used. The data elements were quantified by a ZAF correction method using Quantax computer program included in the SEM.

For the other grades, the different phases were identified on the unetched samples, by means of a Leica Stereoscan 440 Scanning Electron Microscope (SEM), in backscattered-electrons mode (BSE), coupled with a Philips EDAX Energy Dispersive Spectroscope (EDS) for the determination of the phases chemical compositions.

Through the SEM-BSE observations, ferrite appears slightly darker than austenite, while the intermetallic phases are lighter, owing to the higher content of molybdenum, with the χ-phase brighter than the σ-phase. On the contrary, nitrides and carbides appear as small black particles. Finally, the amount of secondary phases was estimated using image-analysis software on SEM-BSE micrographs.

In this study, a thermodynamic modelling of the investigated DSS's phase diagrams, obtained by the CALPHAD method (L. Kaufman, 1970), is reported. The method is based on the minimization of the Gibbs free energy of the phases provided by the multicomponent system Fe-C-Si-Mn-Cr-Ni-Mo-N and the calculations were performed by means of the Thermo-Calc software (B. Sundman, 1985), using the thermodynamic database TCFe3 and TCFe6.

5.4 Results and Discussions

5.4.1 Equilibrium data

An examination of the pseudo-binary phase diagrams of the considered steels and from the Thermo-Calc calculations Figure 5.1, it is possible to distinguish that nitrides are equilibrium phases, which are expected at the thermodynamic equilibrium for temperatures below 950-1000°C.

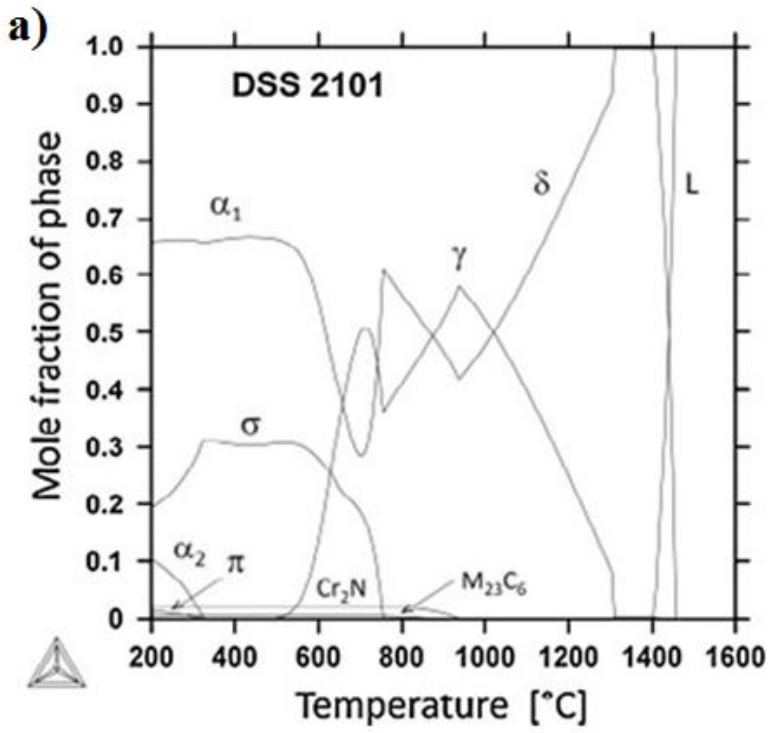

Figure 5.1 a *Thermo-Calc calculated equilibrium fractions of each phase vs. temperature for Lean Duplex 2101*

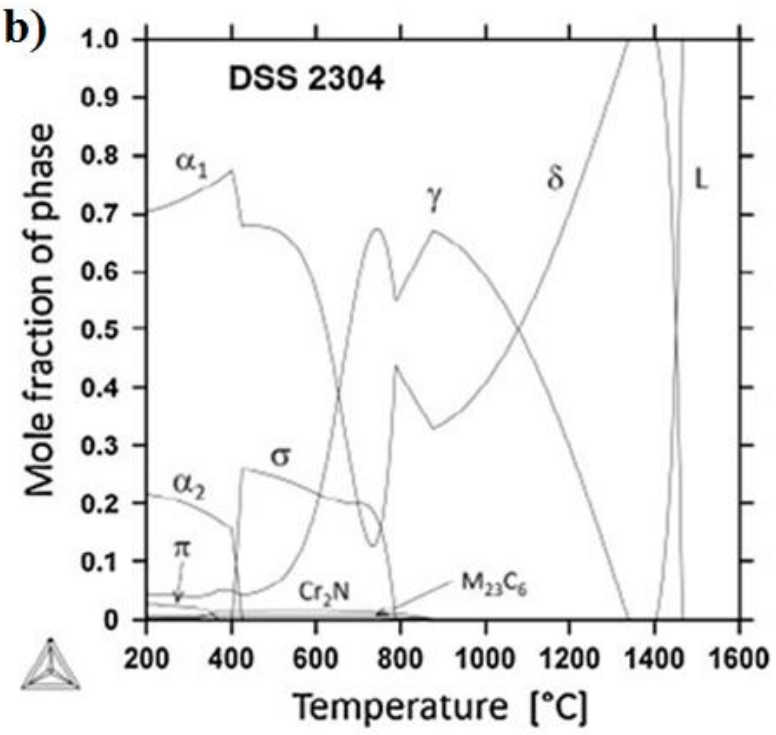

Figure 5.1 b *Thermo-Calc calculated equilibrium fractions of each phase vs. temperature for Lean Duplex 2304*

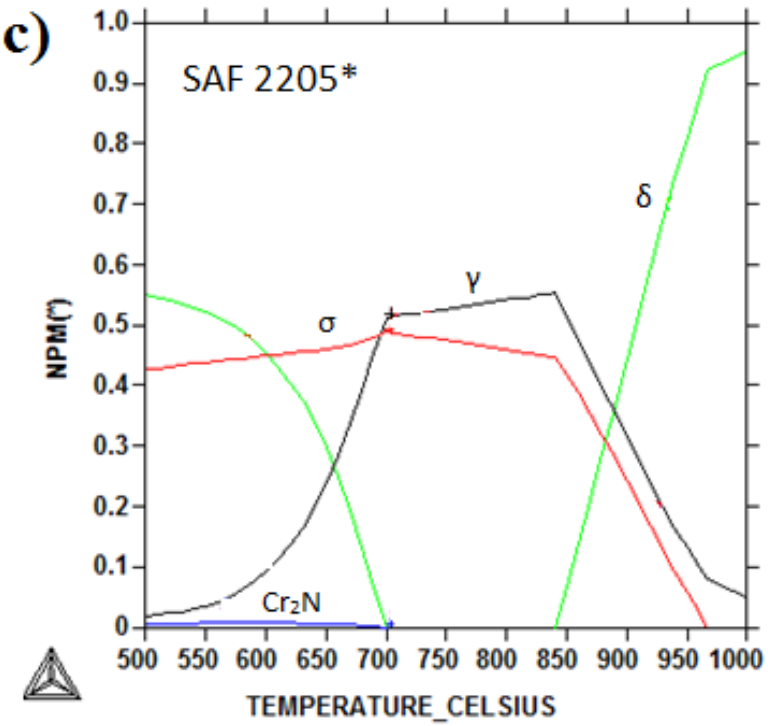

Figure 5.1 c *Thermo-Calc calculated equilibrium fractions of each phase vs. temperature for Standard Duplex SAF 2205**

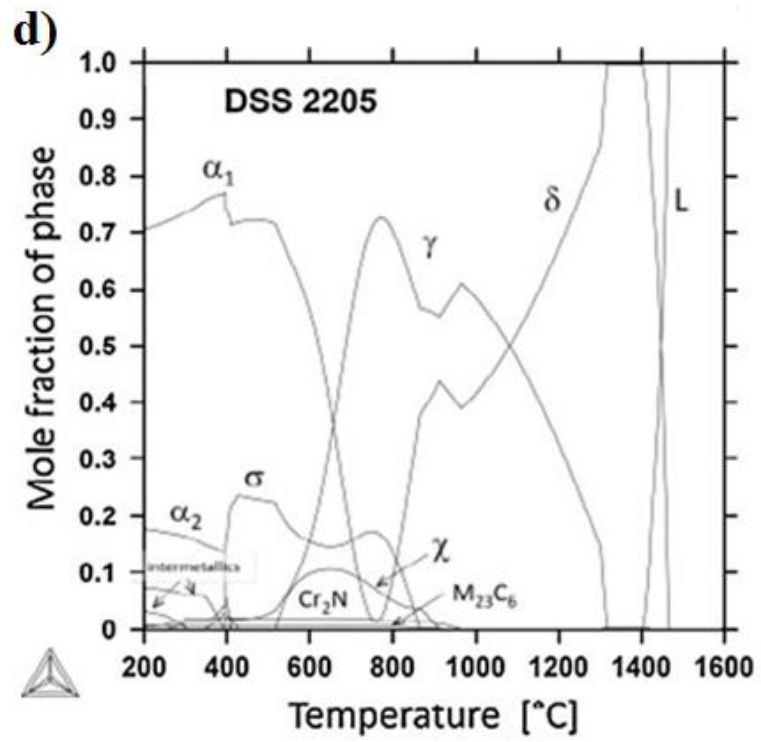

Figure 5.1 d *Thermo-Calc calculated equilibrium fractions of each phase vs. temperature for Standard Duplex SAF 2205*

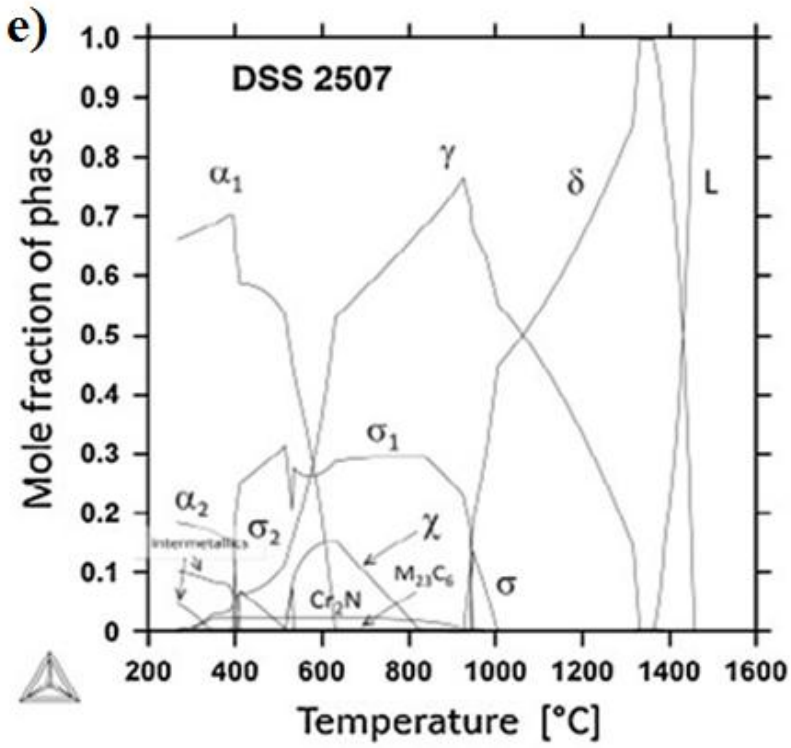

Figure 5.1 a *Thermo-Calc calculated equilibrium fractions of each phase vs. temperature for Superduplex 2507*

The secondary phases observed in DSS are even more from those presented in the diagrams, but Thermo-calc and other similar programs are unable to predict all of them as they are not sufficiently well described thermodynamically. It is even quite likely that some of the listed phases are non-equilibrium phases. σ-phase gradually becomes the dominating phase due to a lower free energy, as can be observed in Thermo-calc diagrams for all duplex grades (Figure 5.1 a-e). However, σ-phase and Cr_2N play an increasingly important role as the risk of formation becomes higher in modern highly alloyed DSS. Adding molybdenum, chromium and nitrogen is a mixed blessing as these elements increase the resistance to pitting corrosion but, at the same time, create a material that is increasingly difficult to produce.

The amount of nitrides depends on the nitrogen concentration in the alloy and from the overall composition of the steel, and ranges from a minimum of about 1.5-2% of the volume fraction in 2205 to about 4-5% in the high-alloyed Cr-Ni grades. As expected, nitrogen is mainly dissolved in austenite, while in ferrite it is present in low concentrations. Consequently, in the non-equilibrium microstructure obtained by rapid cooling from high temperature, the ferrite is generally supersaturated in nitrogen.

5.4.2 Lean Duplex grades

In these duplex grades, the balanced microstructure is obtained by adding higher levels of γ-former elements, such as Mn and N, and the low content of Mo allows for a significant reduction of the secondary phases precipitation, such as χ- and σ-phase. In fact, in 2101 and 2304 grades, the isothermal treatments do not cause the precipitation of χ- and σ-phase, as usually occurs in Cr-Ni DSS, also for very long treatment times which exceed the 750 hours (I. Calliari, 2011).

Beside the reduced Mo content, the lack of σ and χ-phases precipitation could be justified by the effect of the increased nitrogen content, which lowers the activity of chromium and molybdenum, thus lowering the driving force for σ- and χ-phase precipitation. This precipitation delay probably can derive from the lowering of the partitioning ratio for chromium and molybdenum in the ferrite (J. Li, 2011).

2101 Lean duplex, isothermally heat treated in the temperature range 600-950°C, was only characterized by nitrides precipitation, located at the ferritic grain boundaries and between ferrite and austenite. The precipitates, analyzed by means of EDS (close to the resolution limit), appeared to be enriched in chromium and can be identified as chromium nitrides, even if cannot be excluded that some of them may be chromium carbides, since through SEM-BSE investigations an accurate distinction is not possible. At 600-650°C and for ageing times less than 40 min the precipitation has not occurred, but for longer times the nitrides begin to appear at the ferritic grain boundaries. On the contrary, at 750°C the precipitation has occurred after only 20 min and nitrides continue to be present even after 20 hours of treatment. Increasing the temperature (Figure 5.2), the particles become coarser and also precipitate at the grain boundaries between ferrite and austenite.

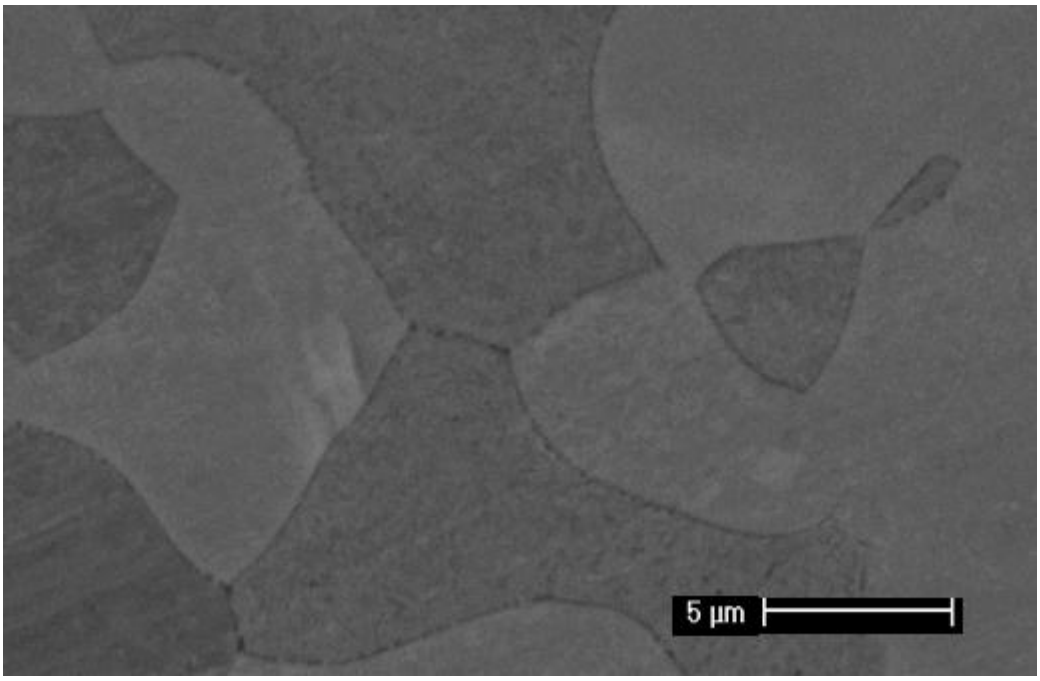

Figure 5.2 *2101 Lean DSS specimen treated at 750°C for 45 min (SEM-BSE)*

In Figure 5.3, a schematic of the precipitation kinetics of these particles and a SEM-BSE micrograph is reported.

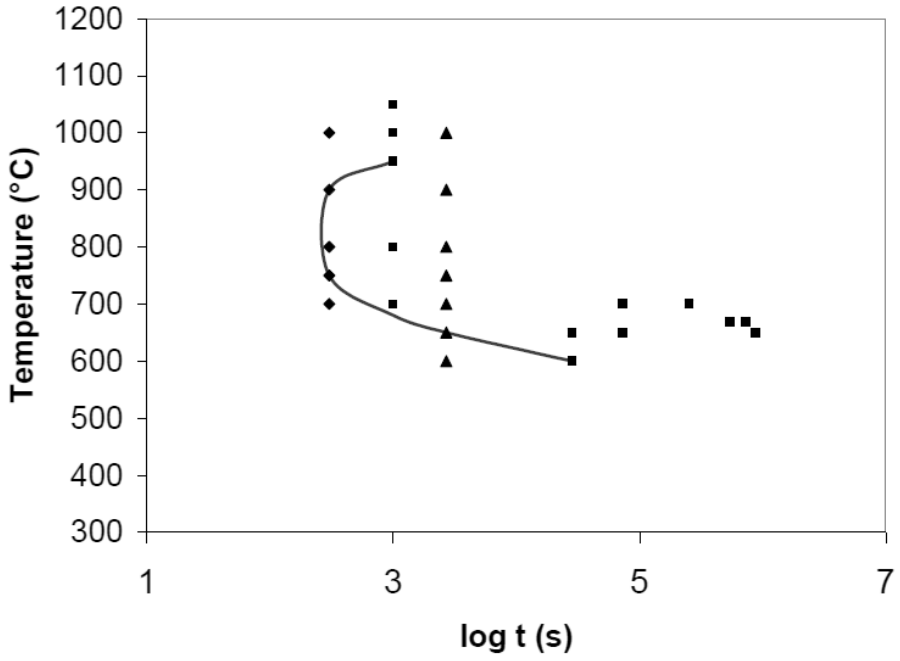

Figure 5.3 *2101 Lean DSS nitrides precipitation kinetic*

Hence, in 2101 DSS, the nitrides at the grain boundaries represent the only phase which is formed for temperatures above 750°C and which is responsible for serious embrittling effects, causing a decrease in impact toughness of more than 100 J (I. Calliari, 2009)

Lean duplex 2304, after isothermal heat treatments at 550-650°C, does not evidence any precipitation of nitrides. However, a moderate precipitation of these particles was determined after 40-45 min of permanence at 750°C and 850°C. In this case, the precipitation of nitrides has required higher temperatures and longer times, if compared to the 2101 grade.

The precipitates are mainly located in the vicinity of the grain boundaries between ferrite and austenite, but were also identified within the austenitic grains (Figure 5.4). This can be explained by the fact that, as a result of the treatments, the precipitation of nitrides has occurred together with the formation of secondary austenite (P. Johansson, 2001)

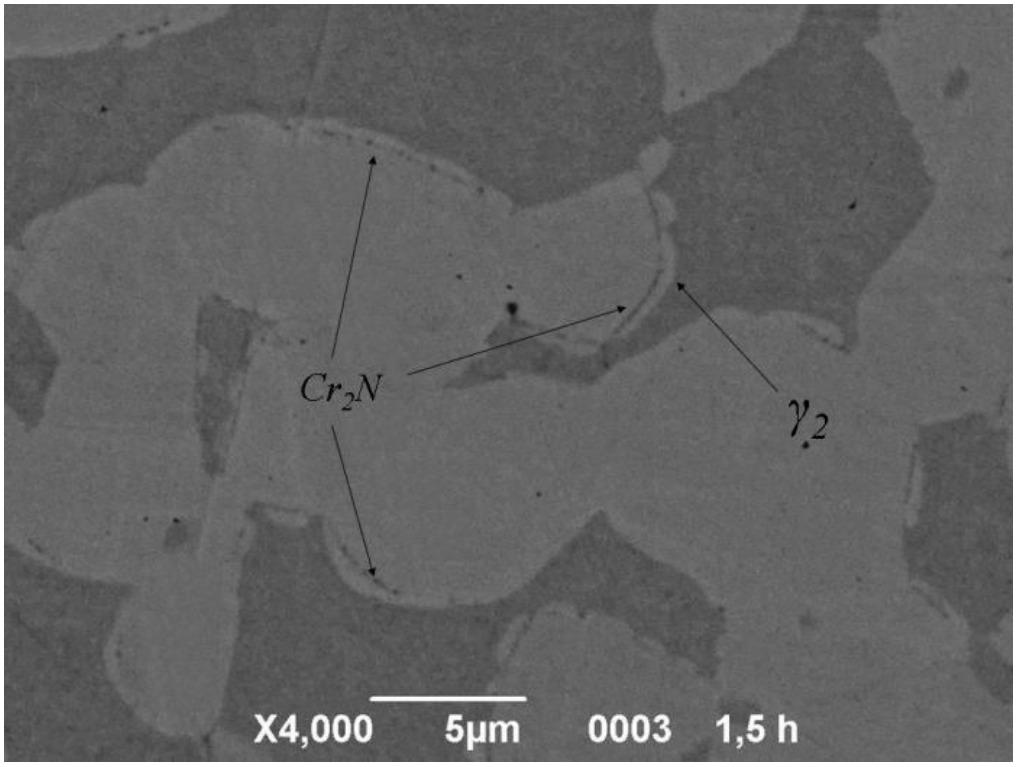

Figure 5.4 *SEM-BSE micrographs of nitrides precipitation in 2304 DSS treated at 750°C for 90 min*

As a consequence of the 750°C treatment, the amount of austenite estimated has increased from 50% to 53.1% of volume fraction after 45 min of permanence and has reached 54.6% after 90 min.

The EDS analyses of the detected phases have revealed that the weight concentration of Cr in ferrite and austenite is approximately 28% and 22%, respectively, while in γ_2 is 19%. The Ni concentration was instead estimated as 3.2% and 6.5%, respectively for ferrite and austenite, and about 5% in γ_2. This reduction of the chromium content in the secondary austenite can be ascribed to the nitrides formation. In fact, these Cr-depleted regions were initially ferritic and have been subsequently enriched in Ni, which has diffused from the surrounding austenitic regions. Hence, the process which involves the γ_2 formation seems to be characterized by a depletion of Cr and a concurrent enrichment in Ni of those regions which undergo the

transformation. The appearance of γ_2 involves a rearrangement of the austenitic grains, which move toward the ferritic matrix, thus nitrides remain trapped within the austenitic island and, if the treatment time is sufficiently long, are dissolved therein. On the other hand, the low Ni content in the 2101 grade may be the reason for which the secondary austenite formation seems to not occur (in this duplex grade nitrides remain always localized to the grain boundaries).

A previous work on the impact toughness at room temperature of the 2304 grade isothermally treated (I. Calliari, 2009) shows that the material is always ductile, although nitrides are present, and the observed decrease in toughness is about in the order of 60 J. However, the same study on a 2101 grade isothermally treated (I. Calliari, 2009), evidences that the presence of nitrides strongly affect the toughness of the material, causing a progressive weakening of the microstructure by increasing the amount of precipitates. These different behaviors can be ascribed to the formation of γ_2, which substantially reduces the embrittling effects due to the intergranular nitrides.

5.4.3 Other duplex grades: 2205, 2507, Zeron100 and 2510

For this class of DSS, which are high-alloyed than the previous Cr-Mn grades, the isothermal heat treatments in the temperature range 780-950°C have mainly caused the precipitation of intermetallic compounds, such as σ- and χ-phase. Only the 900°C and 950°C treatments have determined a slight precipitation of nitrides at the grain boundaries, while temperatures below 900°C should not be considered critical for the nitrides formation. In Duplex the Cr-Ni, then, the very small quantity of nitrides observed brings this type of secondary phases in second place as compared to the more harmful harmful σ- and χ-phase, whose detrimental effects on mechanical properties and corrosion resistance have been already widely discussed (J. O. Nilsson, 2000)

In the 2205 DSS, the observed amount of nitrides is lower than in the other grades, also in the equilibrium microstructure, and has been estimated as about 1.5% of the volume fraction. After isothermal treatments between 700°C and 900°C (I. Calliari, 2011) and after continuous cooling from the solubilization temperature (I. Calliari, in press), the nitrides precipitation was very limited and not easily detectable by means of conventional metallographic techniques. In this steel, the SEM-BSE observations are not very effective, due to the small size of the particles, but by means of TEM they appear as small and rare particles at the ferrite/austenite grain boundaries. Nitrides always accompany the precipitation of σ- and χ-phases which, being in larger quantities can be considered as the ones which affect the material properties.

The 2507, Zeron100 and 2510 are DSS with a high content of alloying elements than SAF 2205. Zeron100 differs from 2507 for the addition of tungsten and more amounts of copper, the 2510 is the most alloyed one and they all have nitrogen content higher than 0.25%.

The isothermal treatments between 700°C and 950°C allows in these steels a rapid precipitation of both σ- and χ-phase, even after few minutes (3-5 min) and especially in the range 850-950°C. In the same temperature range and for similar permanence times, the treatments have also caused the concurrent precipitation of chromium nitrides (Figures 5.5), initially in the form of particles at the grain boundaries, finally as fine precipitates inside the supersaturated ferritic matrix.

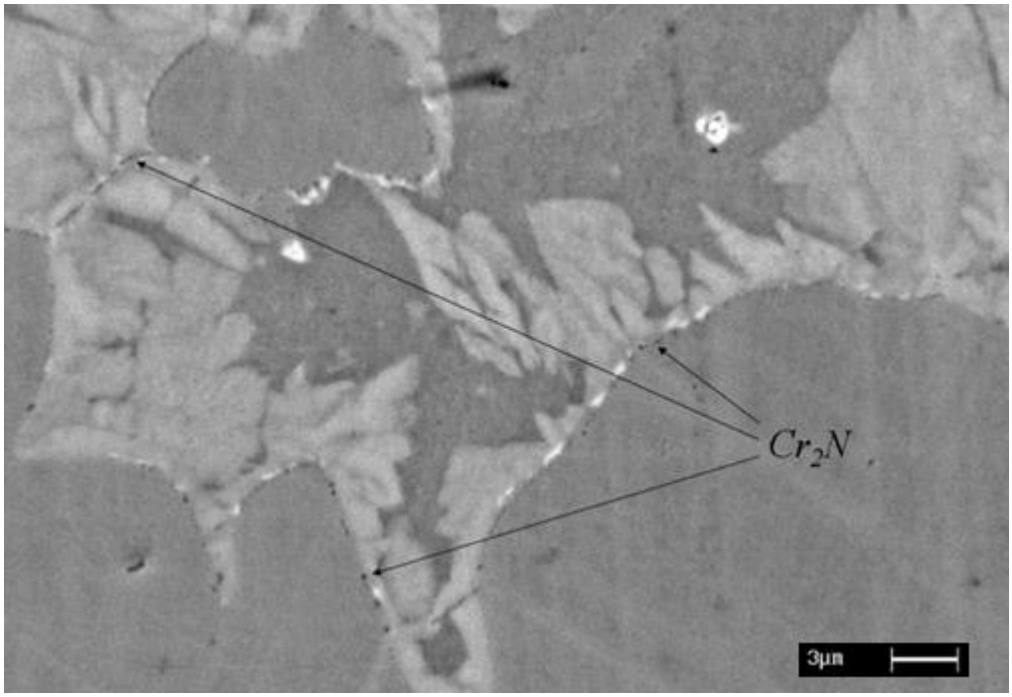

Figure 5.5 *SEM-BSE micrographs of Superduplex 2510 treated at 900°C for 5 min*

In these cases, the particles are coarser than in 2205 and therefore detectable by means of SEM-BSE, through which appear as dark particles, well distinguishable from σ and χ which instead have lighter colors. Figure 5.6 evidence that only in the 2510 grade the formation of nitrides is associated with the formation of secondary austenite, with the consequent rearrangement of the grain boundary.

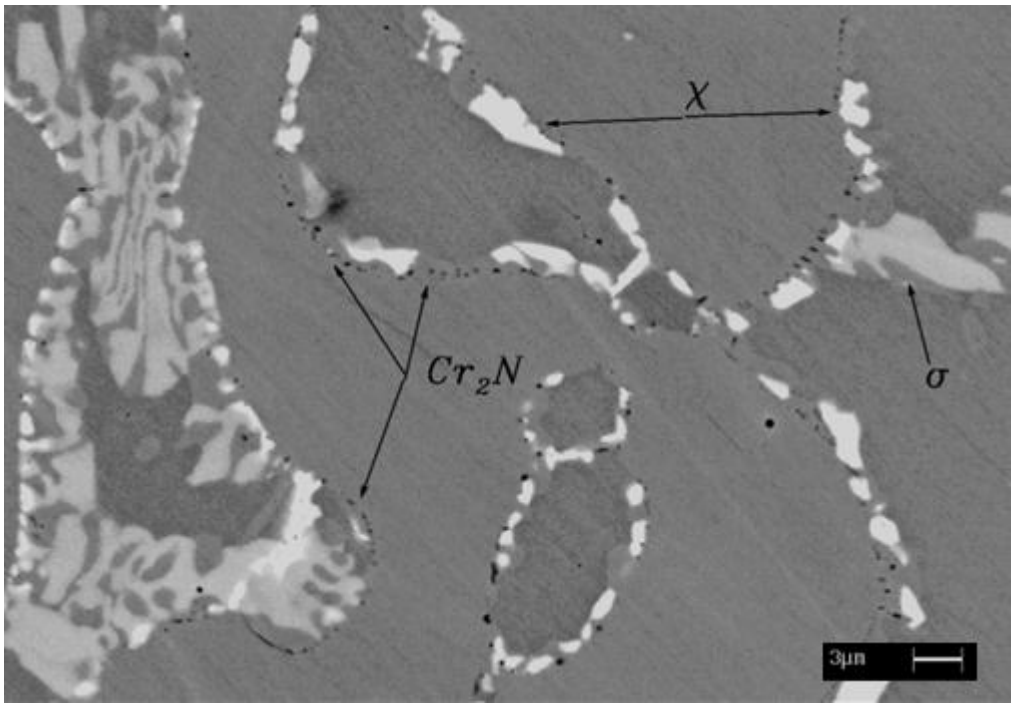

Figure 5.6 *SEM-BSE micrographs of Superduplex Zeron100 treated at 950°C for 5 min*

In all these duplex grades, the amount of nitrides increases with the treatment time but always remains within 1% of volume fraction, while the other phases exceed the 10% after only ten minutes treatment. Nitrides also precipitate during the continuous cooling tests, when the times for diffusion are obviously lower than in the isothermal treatments. In these conditions the precipitation kinetics are different, thus σ-phase appears by first and is followed by χ and nitrides, by decreasing the cooling rate (I. Calliari, in press)

Nitrides contribute to the embrittlement of DSS when exposed to isothermal heat treatment in the critical temperature range. This fact is particularly evident in those samples in which a limited amount (1-2%) of harmful phases was detected but in which the greatest decrease in toughness have been observed (J. O. Nilsson, 1993; I. Calliari, 2010). Consequently, those samples which are slightly affected by the precipitation must be considered as the most critical samples, while, for higher volume fractions of intermetallic compounds, the effect of the nitrides may be neglected, because the toughness resistance is already worsened.

5.4.4 SAF 2205 welded case*

In this part the precipitation of sigma phase is considered. The microstructure of the base material consists of a ferrite matrix with elongated austenite grains approximately 51% of fraction shown in Figure 5.7.

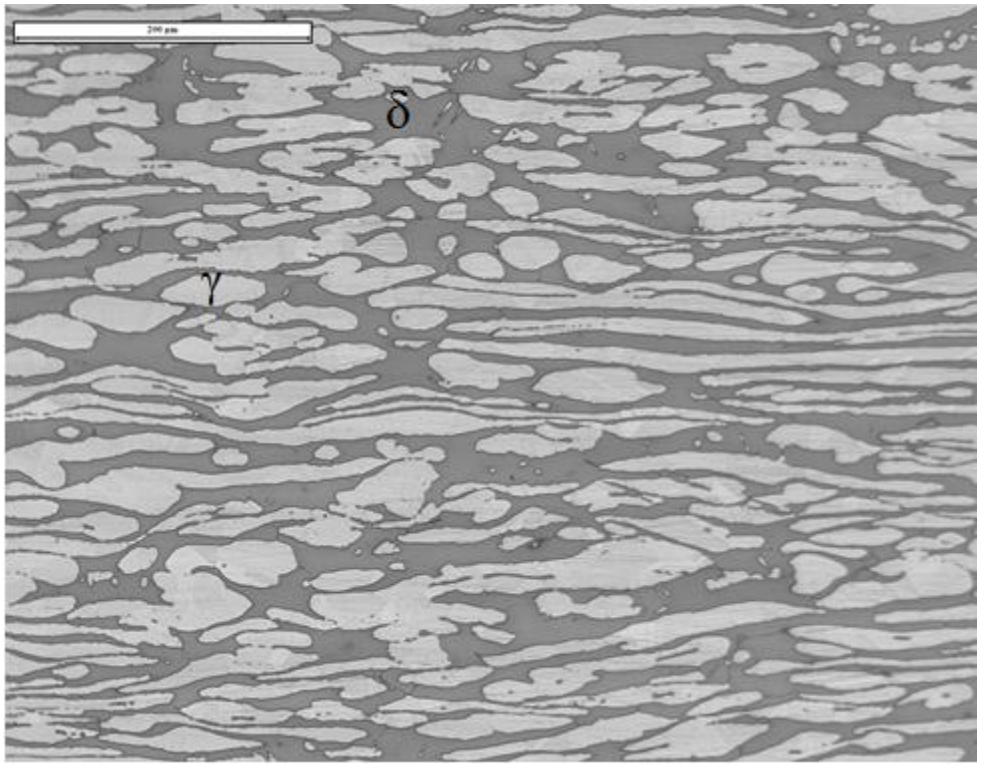

Figure 5.7 *Optical micrograph of the base material. Ferrite is dark and austenite is white*

The coarser microstructure in the weld material austenite phase is restructured, growing as Widmanstätten plates (Figure 5.7a), within approximately 52% of ferrite matrix. The heat affected zone (HAZ) adjacent to the fusion line (Figure 5.8b) presents a lower amount of austenite compared to the melted zone, while the ferrite matrix content increases dramatic liken in the weld zone approximately 65%. During the welding procedure the structure in this region is fully transformed to ferrite, and the austenite grains then reform on cooling to room temperature. The chromium during the weld thermal cycles has insufficient time to diffuse through the ferrite phase; consequently the ferrite/austenite transformation occurs partially during cooling.

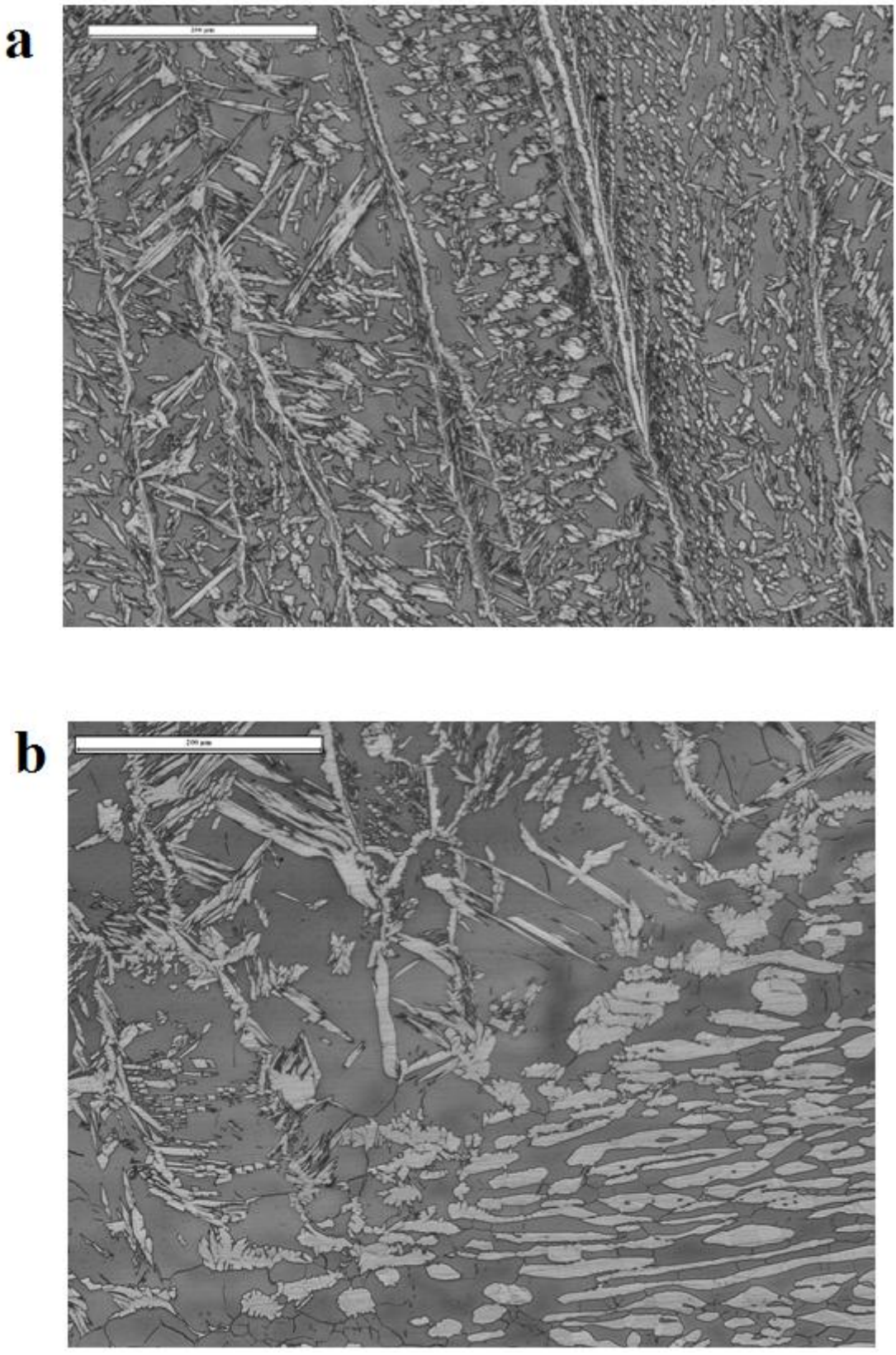

Figure 5.8 *Optical micrographs of a 30 mm material a) Weld metal cross section, b) HAZ, weld material on the left sided superior and base material on the right*

Furthermore the adjacent zone to the base metal (Figure 5.8b) has a major grain growth than the melt zone; coarser austenitic grains are presented within a ferrite matrix. In the weld metal and HAZ the grain size increase as a function of heat input.

On Figure 5.9 the microstructure of the 850°C heat treated sample at 3 hours is reported, evidencing a decreasing of ferrite phase with elongates sigma precipitates through the δ/γ interface, which are known as preferential nucleation sites for the heterogeneous precipitation. Presence of chi (χ) phases along the micrograph can be appreciated however it is not considered in this work, because of their lower content.

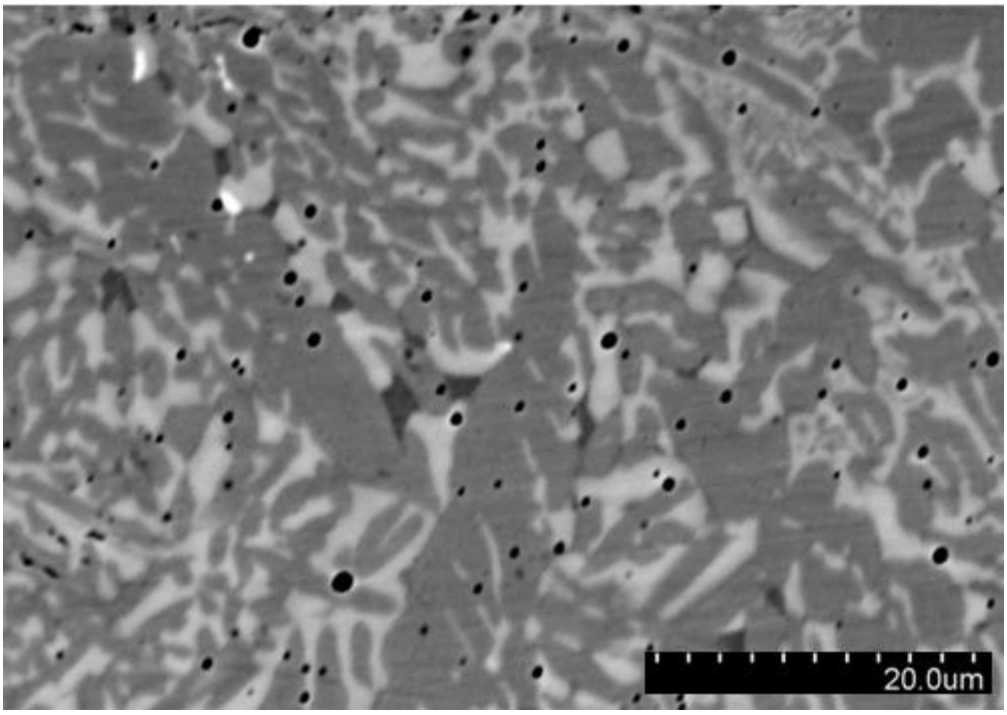

Figure 5.9 *SEM micrograph of the heat treated weld metal (850°C, 3 hours)*

The following micrograph (Figure 5.10) shows the microstructure of the heat affected zone of the specimen heat treated at 900°C. The figures shows clearly the increase of the ferrite phase compared to the weld metal, σ have a slightly developed morphology compared to the elongated precipitates in the weld zone, the formation of sigma phase in DSS is described by the decomposition of δ ferrite through an eutectoid transformation.

This reaction may consume totally the ferrite phase of the steel. After the nucleation process, a sigma phase particle grows into the adjacent δ ferrite grains, developing a phase richer in chromium and molybdenum. However, in view of the microstructure of the matrix phases, the less dense δ ferrite would also facilitate solute atoms to diffuse for the formation of σ phase from the δ ferrite region.

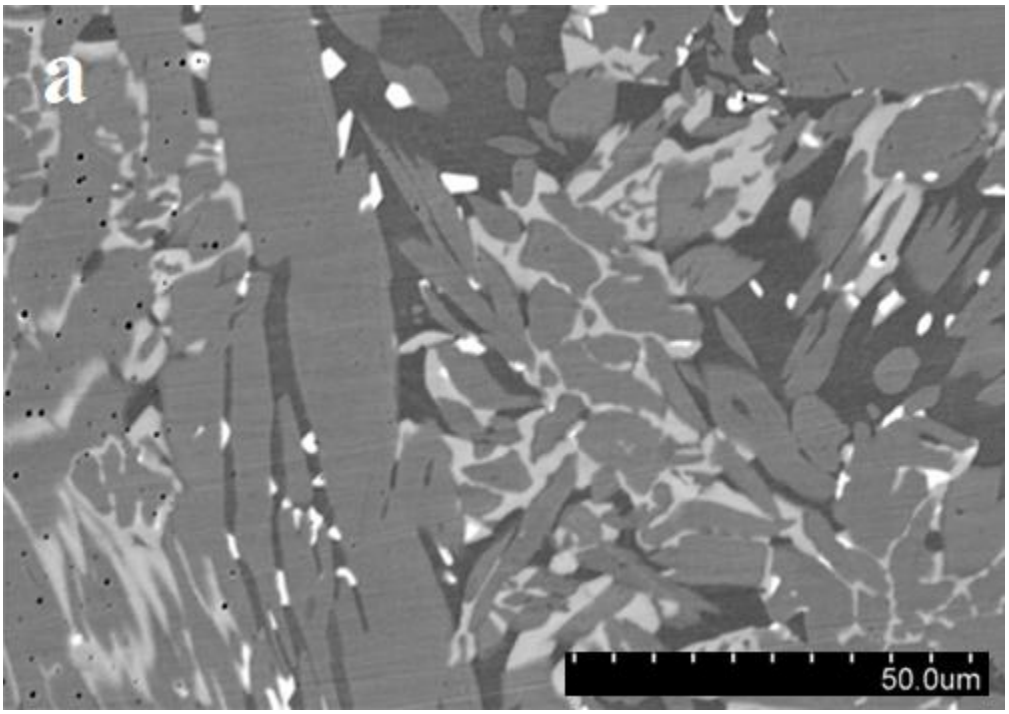

Figure 5.10a *Heat affected zone for the specimen heat treated at 850°C for 3 hours*

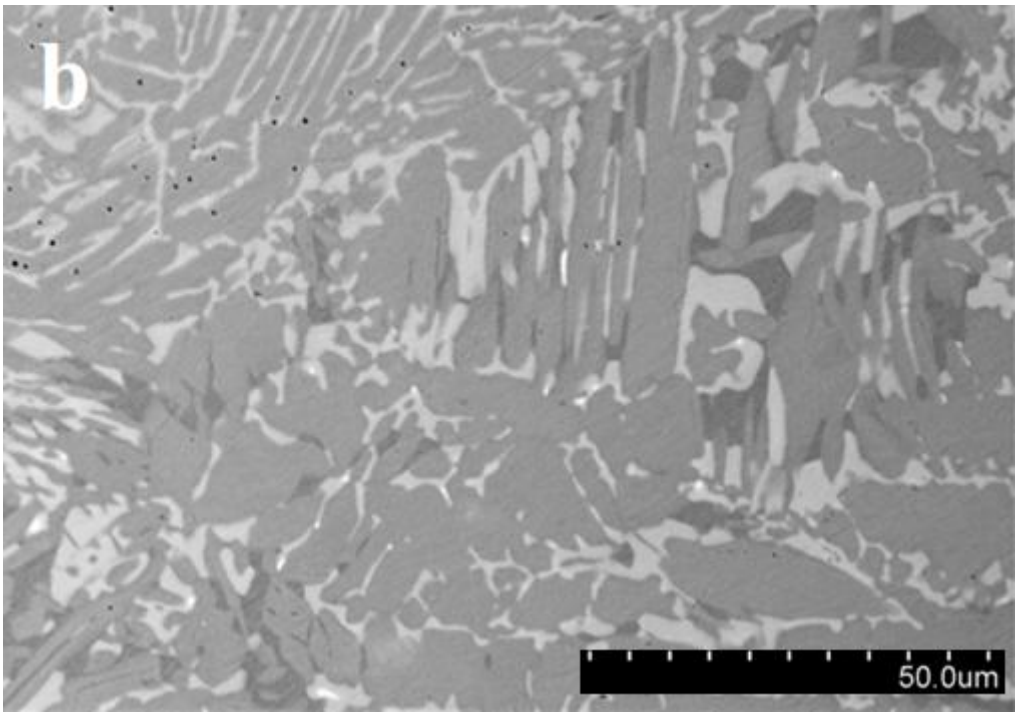

Figure 5.10b *Heat affected zone for the specimen heat treated at 850°C for 6 hours*

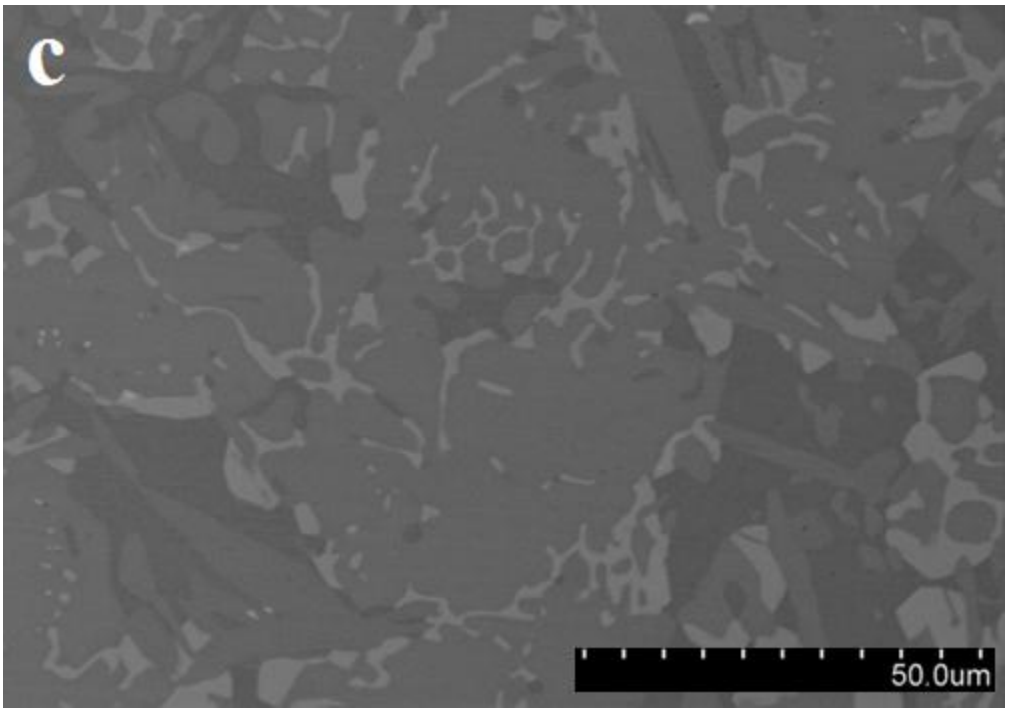

Figure 5.10c *Heat affected zone for the specimen heat treated at 900°C* for 3 hours

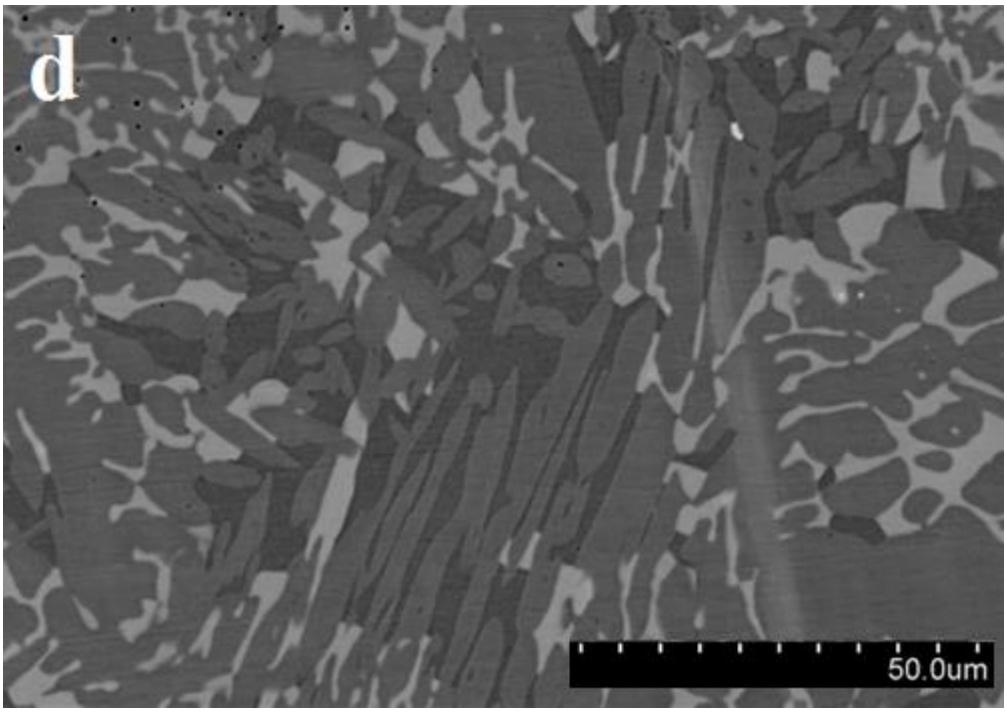

Figure 5.10d *Heat affected zone for the specimen heat treated at 900°C for 6 hours*

Figure 5.11 presents the volume fractions of sigma phase in the weld metal, HAZ and base metal respectively, the highest content of sigma appears at 850°C for 3 hours in the weld zone,

which immediately decreases in the HAZ giving a slightly increase for the base metal. The amount of sigma phase above 3 hours increases for both HAZ and base metal zones.

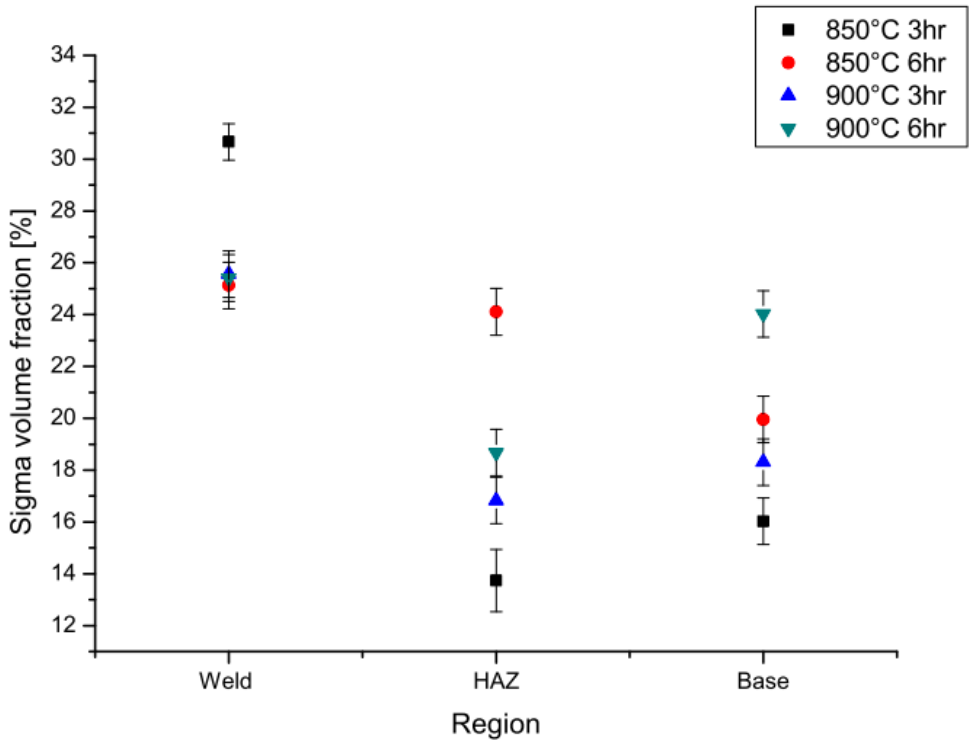

Figure 5.11 *Volume fractions of sigma phase in all specimens, lengthwise all the area*

The data of the weld metal on Figure 5.11 can be explained considering that the filler metal is more alloyed than the base one, consequently the content of sigma in that zone is the highest and formation of secondary austenite could take place. Is observable than the precipitation of sigma phase on the base metal increase at increasing the holding time and temperature, moving from the boundaries into the ferrite, embedding some small χ particles. The sigma phase grows into ferrite instead of growing into the austenite, considering that σ is rich in ferritizing elements, such as Cr, Mo and Si. Besides, the diffusion in ferrite is faster than in austenite. The σ content in the base metal confirms the fata obtained in previous research by (I. Calliari, 2010). Therefore, the σ content in HAZ is determined by the diffusion mechanism.

The mobility of the elements constituting sigma phase while the precipitation occurs, is crucial in order to known the controlling element during diffusion from the ferrite to the sigma phase. The composition of σ, easily identified on the EDX analysis, is shown on Table 5.4 for the specimens treated at 850°C and 900°C. While the Cr content only increases slightly in the ferrite, the increase of Mo is pronounced and forces the Mo to diffuse from the inwards parts of the ferrite matrix.

Table 5.4 *Chemical composition (wt. %) of σ, γ and δ ferrite as determined by EDX analysis after aging at 900°C*

Phase	**Element [wt. %]**					
	Si	**Cr**	**Mn**	**Fe**	**Ni**	**Mo**
σ	0.6	27.9	1.3	58.7	3.0	8.2
γ	0.3	21.3	1.5	67.9	6.3	2.5
δ ferrite	0.4	23.1	1.2	69.7	2.9	2.5

In the base metal, the variation of the σ phase structure trough the temperature increment can be observed on Figure 5.12 (a-d). At low temperatures (Figure 5.12 a and b) σ presents a lamellar structure within the ferrite, which is characteristic of the ferrite eutectoid transformation. A few particles of χ-phase have been detected. On the specimen heat treated at 900°C for 6 hours (Figure 5.12b), coarse particle of irregular shape, elongated sigma and lower amount of chi precipitates are shown.

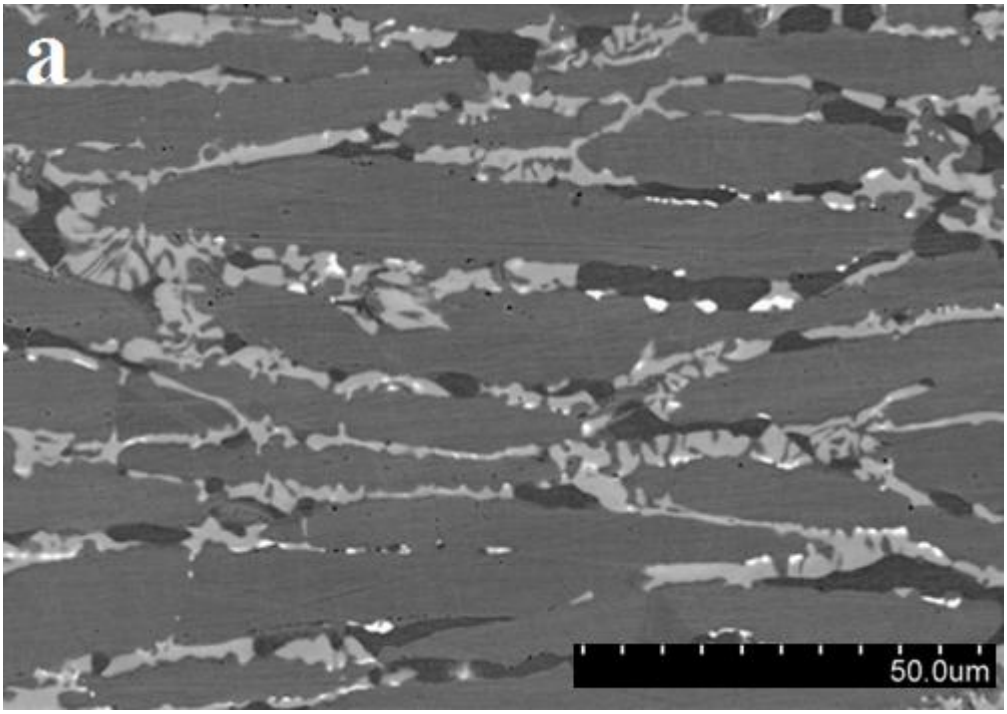

Figure 5.12a *Microstructure of SAF 2205 base metal duplex stainless steel annealed at 850°C for 3 hours*

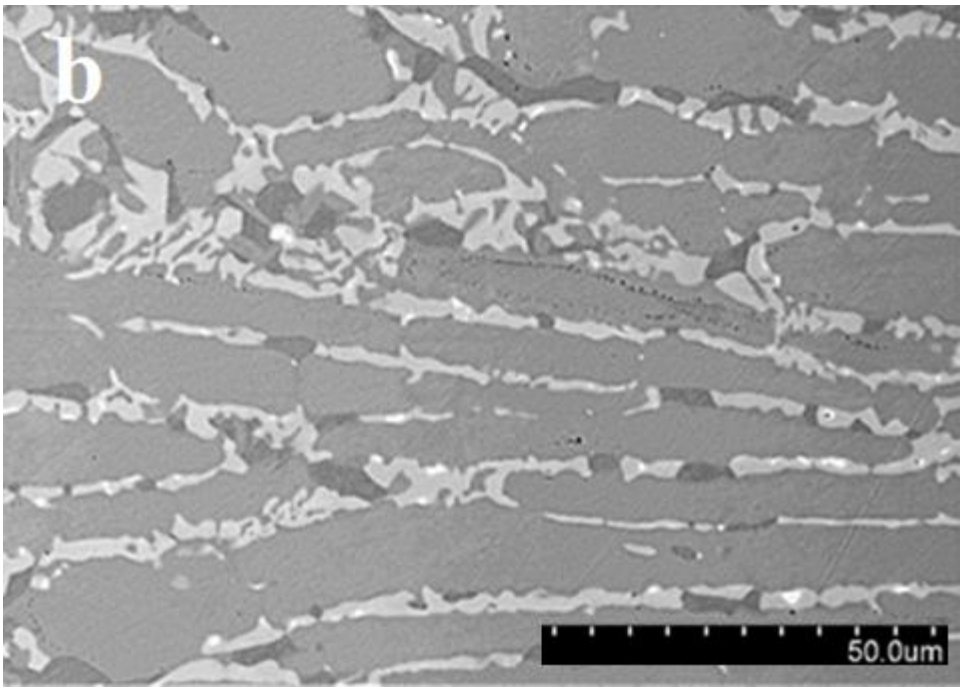

Figure 5.12b *Microstructure of SAF 2205 base metal duplex stainless steel annealed at 850°C for 6 hours*

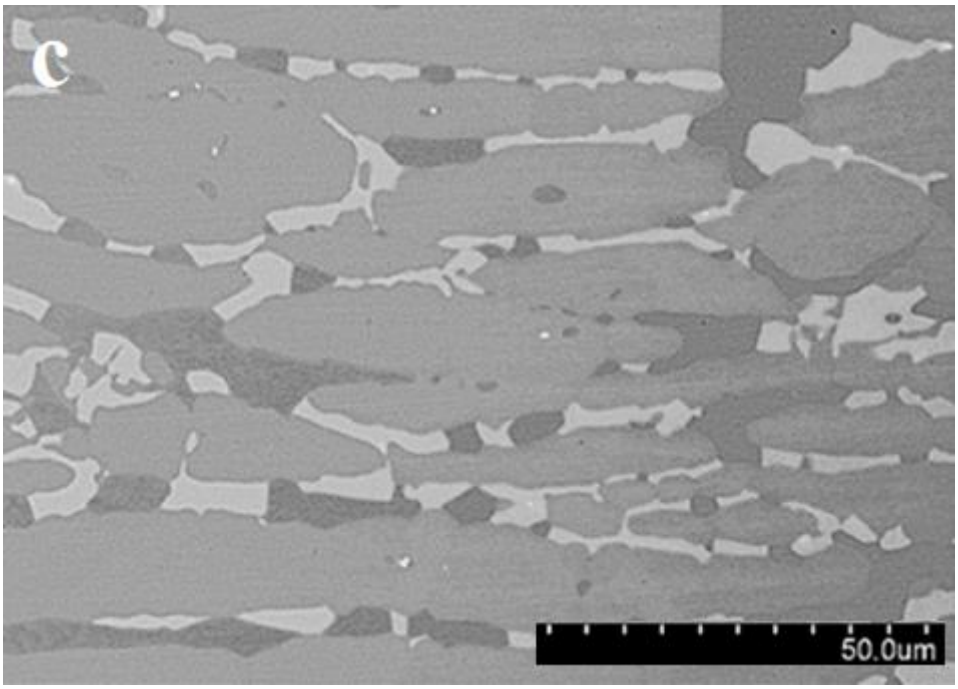

Figure 5.12c *Microstructure of SAF 2205 base metal duplex stainless steel annealed at 900°C for 3 hours*

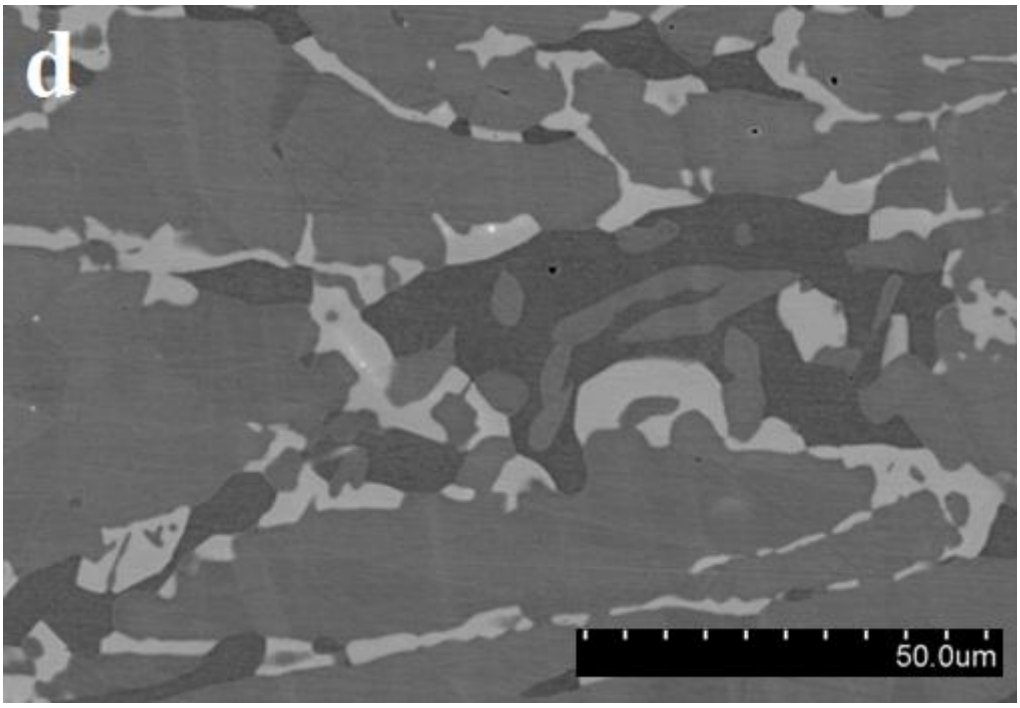

Figure 5.12d Microstructure of SAF 2205 base metal duplex stainless steel annealed at 900°C for 6 hours.

The clearly decrease of the ferrite amount after the isothermal heat treatment on the experimental results gets into the interests to develop a quantitative understanding of the δ ferrite kinetic transformation. Thermodynamic calculations with Thermo-Calc software with the steel database TCFE6 and TC-Prisma software were performed in order to study the sigma precipitation kinetic which may describe the phase transformation kinetics. The aim was to predict if the experimental results can be reproduced using available thermodynamic descriptions. However, in Appendix A the performed calculations are presented and the investigation is still in progress.

5.5 Final remarks

In order to appreciate the microstructural behavior at the high temperatures, focusing the study on the nitrides formation, besides the precipitation of sigma in SAF 2205* welded plates, different types of Cr-Ni and Cr-Mn Duplex Stainless Steels (DSS) have been subjected to isothermal heat treatments within the critical temperature range.

In the standard 2205 DSS and high-alloyed Cr-Ni DSS (2507, Zeron100 and 2510), isothermal heat treatment mainly cause the precipitation of intermetallic phases such as σ- and χ-phase, which appear after few minutes (3-5 min), while the formation of nitrides is very limited. In the 2205 grade, nitrides precipitation is rare and hardly observable, while in the high-alloyed DSS is maintained within about 1% of the volume fraction and can be accompanied by the formation of secondary austenite. Therefore, the possible reduction of the mechanical properties caused by the presence of the nitrides is totally overcome by the damage resulting from the much more harmful σ- and χ-phases, even if for small quantities of secondary phases (1-2%) and for nitrides amounts comparable to that of intermetallic, the total effect is a further deterioration of the resistance characteristics.

In the Cr-Mn DSS (2101 and 2304), as a consequence of the heat treatments, no intermetallic phases has been detected. In these cases, the microstructural damage is only represented by the precipitation of nitrides, firstly at the ferritic grain boundaries and then also at the ferrite/austenite interfaces. These steels are subject to nitrides precipitation throughout the whole testing range (600-950°C), either for shorter or longer treatment times, and the critical temperature range, at which the kinetics are favored, has been estimated around 750-850°C for both the steels.

In 2304 DSS, as a consequence of nitrides precipitation, the formation of secondary austenite has been observed, which has involved the embedding of the particles within the austenitic grains owing to a rearrangement of the grain boundaries due to diffusion mechanisms. This allows the 2304 grade to maintain a good level of toughness despite the exposure at the critical temperature range, even for long treatment times. This has not occurred in the 2101 grade, in which the nitrides remain localized at the grain boundaries, causing a deterioration of the impact toughness resistance.

In the SAF 2205* case, sigma phase nucleation occurs rather at ferrite-austenite interfaces and the growth is related to the decomposition of δ ferrite, due to the higher ferritizing content in the precipitate. The employed weld process SAW, resulted higher amounts of δ ferrite in the HAZ while in the weld metal lower amount of austenite phase was observed.

Higher sigma volume fraction is observed at 850°C heat treated specimen for 3 hours, on the weld zone, growing into the δ ferrite phase which is approximately 1% remaining phase. It was also found that higher time of heat treatment, influence the increase of volume precipitate fraction. Preeminent sigma particles also were observed after 6 hours aging.

APPENDIX A

TC-Prisma

Some of the research activity has been carried out at the Materials Science and Engineering Department at the Royal Institute of Technology in Stockholm (SE), under the supervision of the Professor Rolf Sandström.

The study was supplemented with Thermodynamic calculations with Thermo-Calc software using the steel database TCFE6 and TC-Prisma software. The goal of the calculations was to predict whether the experimental results can be reproduced using available thermodynamic descriptions and to analyze the behavior of the material under conditions experimentally studied.

The TC-PRISMA software is a general computational tool for simulating kinetics of diffusion controlled multi-particle precipitation process in multi-component and multi-phase alloy systems. Precipitation is a solid state phase transformation process, which begins with the formation of particles of a second phase from a supersaturated solid solution matrix phase that has been exploited to improve the strength and toughness of various structural alloys for centuries.

The process is thermochemically driven and fully governed by system (bulk and interface) thermodynamics and kinetics. Typically, a precipitation process has three distinctive stages: nucleation, growth, and coarsening, according to Kampmann Wagner (Numerical). However, under certain conditions, they could happen also at the same time.

With TC-PRISMA, the kinetics of concurrent nucleation, growth, and coarsening can be simulated by calculating the evolution of the probability distribution of the particle number densities, usually called particle size distribution (PSD). The simulation results can be used to understand and guide how to obtain desirable precipitates with certain PSD or to avoid undesirable precipitations during heat treatments of alloys such as aging and tempering.

TC-PRISMA relies on CALPHAD (B. Sundman, 1985) based software tools and databases to provide necessary bulk thermodynamic and kinetic data for phases in multi-component systems. The CALPHAD approach has been developed over more than 50 years and is now routinely applied to design new alloys and optimize existing materials within various metal industries, such as steel and alloys of nickel, titanium, aluminum, and magnesium.

The power of this approach is due to the adopted methodology, where free energy and atomic mobility of each phase in a multicomponent system can be modeled hierarchically from lower order systems, and model parameters are evaluated in a consistent way by considering both experimental data and ab-initio calculation results. TC-PRISMA is directly integrated with Thermo-Calc and DICTRA, which are CALPHAD based computer programs for calculating phase equilibrium and diffusion controlled phase transformation in multicomponent systems

and have a wide spectrum of accompanying thermodynamic and kinetic databases. With Thermo-Calc and DICTRA and accompanying databases, almost all fundamental phase equilibrium and phase transformation information, such as driving forces for nucleation and growth, operating tie-line under local equilibrium or para-equilibrium condition, deviation from local equilibrium at interface due to interface friction, atomic mobilities or diffusivities in the matrix phase etc., can be calculated without unnecessary and inaccurate approximations.

In addition to bulk thermodynamic and kinetic data, a few other physical properties, such as interfacial energy and volume, are needed in precipitation models implemented in TC-PRISMA. These additional physical parameters can be obtained by experiments or other estimation models or first principles calculations. As a matter of fact, volume data for steels and nickel-based alloys has already been assessed and included in TCFE6 and TCNI5 databases. It is hoped that in future interfacial energy can also be modeled in the spirit of CALPHAD method and the model parameters can be assessed by considering various kinds of experimental data with help of TC-PRISMA (Q. Chen, 2011).

A.1 Thermodynamic calculations

Stainless steel plate, hot rolled, in solution annealed and subsequently welded SAF 2205, previously reported in Chapter 5 was used as simulated experimental specimen of study.

A software package of simulation kinetics of diffusion controlled multiparticle precipitation process in multi-phase alloy systems Prisma has been employed. At 850 °C, sigma phase can be formed by three distinct mechanisms: nucleation and growth from original ferrite, eutectoid decomposition of ferrite (also forming secondary austenite) and growth from austenite after total consumption of original ferrite (Magnabosco, 2009). These three mechanisms lead to Cr depletion at the metallic matrix surrounding sigma phase, resulting in lower corrosion resistance. The fraction of sigma phase can be described by a Johnson-Mehl-Avrami (JMA) type expression, as showed in Equation A.1.

$$f = 1 - e^{(-k \cdot t^n)} \qquad \text{ec. A.1}$$

where f is the fraction of sigma phase formed (0 <f<1) after an isothermal treatment at a time period t, and k is defined by Equation A.2.

$$k = k_0 \cdot e^{\left(\frac{-Q_\sigma}{R \cdot T}\right)} \qquad \text{ec. A.2}$$

where Q_σ is the activation energy for sigma phase formation and R is the universal gas constant (8.31 $J.mol^{-1}.K^{-1}$). The exponent n can assume values between 0.5 and 2.5 for diffusion controlled growth or values from 1 to greater than 4 if phase formation occurs as discontinuous precipitation or interface controlled growth (Christian, 2002).

Several attempts in order to simulate the precipitation of sigma during the isothermal heat treatment at 850°C and 900°C for 3 and 6 hours have been performed. The system used in the program was a thermodynamic data base TCFE6, including the principals elements obtained from the initial chemical composition from the steel under study. A single temperature was provided in order to obtain the precipitation of σ phase in the SAF 2205.

After several calculations the volume fraction for precipitates were obtained, showed in Figure A.1 (a-c). However, they start forming the precipitate at lower temperatures, no precipitation occurs at higher temperatures (800-950 °C). The Figure A.1 (a-c) presents the volume fraction of sigma for the SAF 2205 at 650°C varying the interfacial energy, which must be high and is considered to occur at the δ/γ interface that is the most favorable site for precipitation of this intermetallic phase (M. Martins, 2009). Nucleation of the sigma phase may also occur at the twin boundaries in the austenitic phase and in stacking dislocations. For the precipitate, no variation was founded.

From the composition inserted in Thermo-Calc, the state diagram for the SAF 2205 * (see Chapter 5) shows the phases in equilibrium evidenced in the temperature range 700-840 °C approximately, in which the ferrite phase is fully consumed.

Therefore it was thought to use the chemical composition at 1050 ° C in the ferrite phase for determining the phase diagram and thus ensure their presence, since sigma phase is enriched of ferrite stabilizing elements.

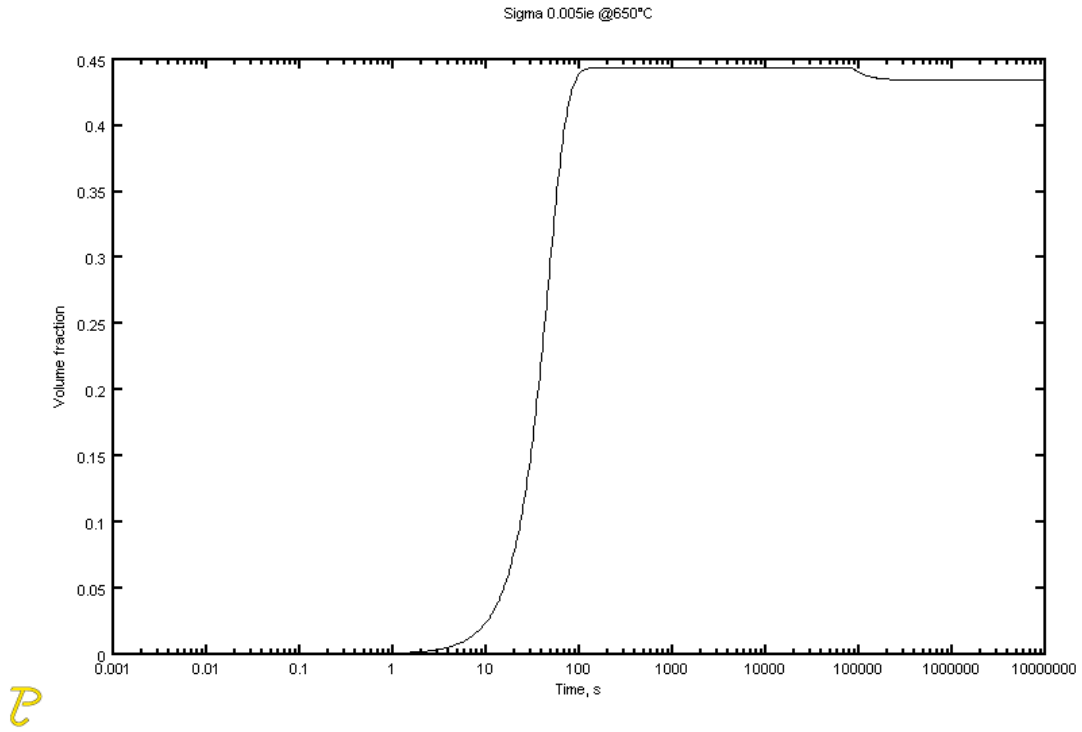

Figure A.1a *Volume fraction of sigma phase in SAF 2205 at 650°C obtained from TC-Prisma, with an interfacial energy of 0.005*

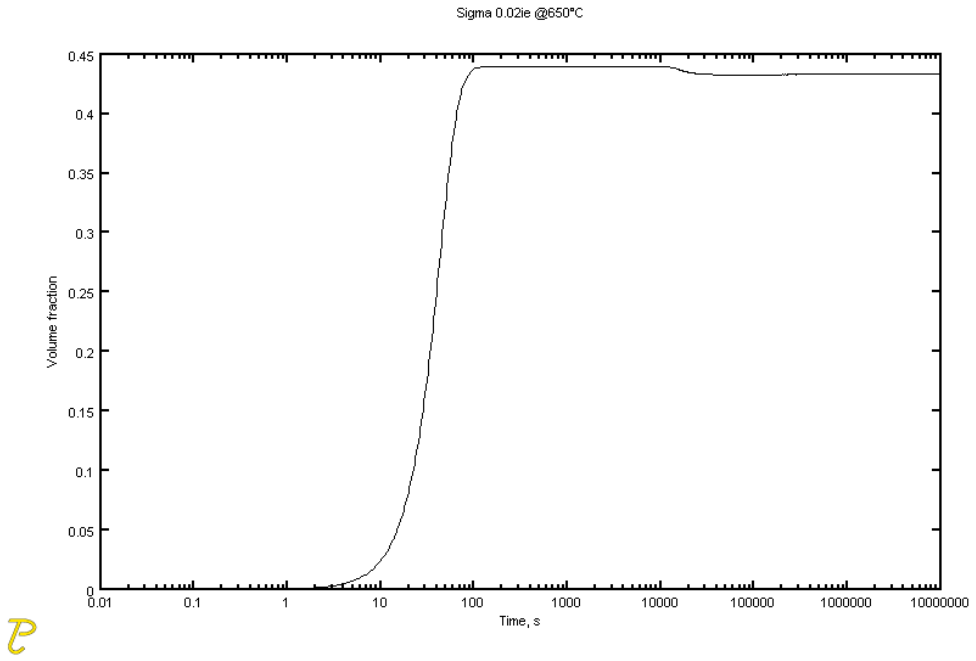

Figure A.1b *Volume fraction of sigma phase in SAF 2205 at 650°C obtained from TC-Prisma, with an interfacial energy of 0.02*

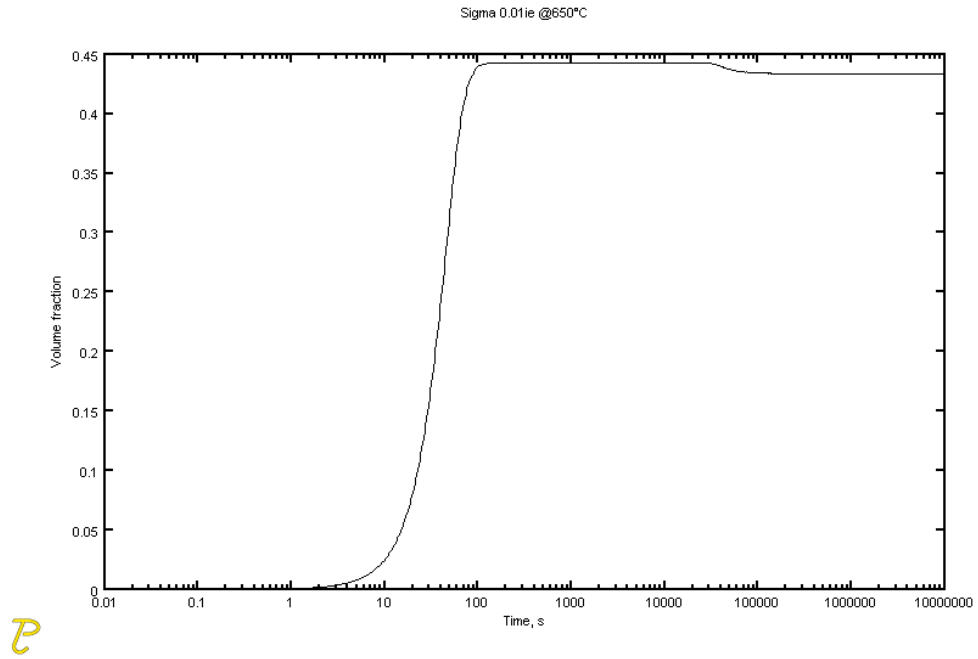

Figure A.1 *Volume fraction of sigma phase in SAF 2205 at 650°C obtained from TC-Prisma, with an interfacial energy of 0.01*

These results might seem counter-intuitive at first sight, from the viewpoint of a pure diffusional collection mechanism for precipitate growth, which experimentally the precipitation of sigma phase can occur at a temperature range between 650-950°C (Davis, 1994; N. Sathirachinda, 2010; J. Michalska, 2006), and depends on alloy level of mainly chromium and molybdenum. Finally, it is important to emphasize that this is the first version of the program, and dealing with a duplex microstructure still represents a challenge for this software.

Chapter 6

Microstructural changes on Duplex Stainless Steels after plastic deformation and heat treatment

CHAPTER 6

Microstructural changes on Duplex Stainless Steels after plastic deformation and heat treatment

Two main items are discussed in this chapter[1]: Cold work and heat treatment, process which induce microstructural transformations and became particularly arguments of interest in this research. It is well known that the properties of Duplex Stainless Steels depend strongly on the microstructure of δ/γ. The morphology, repartition and texture of both phases do not present the same mechanical behavior during deformation. These steels are subjected to precipitation of secondary phases in the temperature range 500-1000°C (σ-phase, χ-phase, nitrides) which degrade the corrosion and the mechanical properties, with a drastic drop of impact energy (from 250J to 50J), even at very low intermetallic phases contents (0.5-1%).

A broad overview of DSS is presented, subsequently a case of study using Lean Duplex 2101, Standard Duplex 2205 and Superduplex 2507 cold rolled and heat treated specimens is described. Experimental procedure is therefore descript beginning by metallography characterization of secondary phases determined by means of a Scanning Electron Microscope coupled with an Energy Dispersive X-Ray Spectroscope and different non-destructive magnetic measures in specimens.

[1] Portions of this chapter have been published in (A. F. Miranda Pérez, 2012) *et al.*, (I. Calliari, 2011) *et al*. and (I. Calliari, 2012)

6.1 Motivation

As mention in Chapter 3, the favorable combination of properties of Duplex Stainless Steels (DSS) makes this class of stainless steels widely employed in oil and gas, petrochemical, pulp and paper, pollution control, nuclear industries and, recently, DSS sheets have been introduced for tanks. Duplex grades exhibit good formability and most of their applications required relatively simple forming, such as the rolling of cylindrical sections, press forming and tank head forming by pressing or rolling.

The lower ductility of DSS compared with austenitic stainless steels must also be taken into account. Duplex grades have a minimum required elongation in most specifications of 15% to 25% in comparison with the 40% minimum elongation required for the austenitic grades. Because of their lower ductility compared with austenitic grades, for DSS it is necessary a more generous ben radius or require intermediate solution annealing in severe or complex forming.

These steels are prone to phase transformation, which may involve the both present phases (δ-ferrite and γ-austenite) as discussed in Chapter 5, in the austenitic phase may occur a diffusionless martensitic transformation induced by the cold working, as well known in the fully austenitic stainless steels (K. H. Lo, 2009; S. S. M. Tavares, 2008)

The low Ni duplex grades, characterized by a decrease of Ni which is substituted by Mn and by N, are extensively used in industrial application. Many tests have been carried out in order to study their microstructure stability after thermal treating, and the main results are the absence of σ and χ precipitation and a moderate presence of nitrides at gran boundaries. In Lean duplex the substitution of Ni by N and Mn may result in austenite phase instability therefore this tends to transform to metastable martensite. To address these concerns, a program of work was conducted to characterize the microstructure developed in cold-worked duplex grades plates as a result of damage during manufacture.

The impact toughness after solution annealing treatment is very good and after isothermal treatment the impact energy is never lower than 50 J. Furthermore, the substitution of Ni with Mn and N may induce the instability of the austenite, as suggested in previous researches, which report of a probable transformation to martensite during cold forming (J. Y. Choi, 1997). There are many factors that can influence the austenite-martensite transformation: e.g. the chemical composition, the grain size of the austenite, the temperature and the strain rate. In 25-1, the gamma-former power of Ni is partially compensated by Mb and N, but the total austenite-stabilizer effect is less than with Ni.

The deformation mode and the strain rate are other important factors. (I. Mészáros, 2005) describe that two types of martensite can be formed from metastable austenite: epsilon-hcp paramagnetic and α' bcc ferromagnetic martensite, where α' phase is more stable than ε-martensite. The diffusionless transformation from γ-phase, paramagnetic, into α' phase, strongly ferromagnetic, can be detected studying the magnetic properties of cold rolled material.

The chemical composition and the thermo-mechanical history are the most important factors in determining the kinetics and sequence of precipitation. It is well known that higher the Mo, Cr and W content, faster the precipitation occurs, but also the ferrite/austenite volume fractions and their morphology affect the process.

Since the precipitation is a diffusion process, it can be affected by the amount of the diffusivity paths and therefore by crystal disorder and dislocations density. These microstructural modifications arise during cold deformation, in relation to the degree of thickness reduction. The manufacturing process of DSSs aimed to produce sheets, as recently adopted for the fabrication of water tanks and heat exchange panels (J. Hamada, 2010), can induce several microstructural modifications as rolling textures and recrystallization during hot working and affects the formability properties.

The effects of the manufacturing conditions on the tensile properties of DSS sheet, especially elongation at RT, have been studied by few researchers, evidencing that the elongation is related to the hot-rolling texture, as well as to the annealing temperature after both hot and cold rolling (J. Hamada, 2010).

Nevertheless, the only contribution on this field is from (S. S. M. Tavares, 2005) investigation dealing with the microstructural changes produced by plastic deformation on 2205 duplex grade. On the contrary, there are no data on the mechanism and kinetic of phases precipitation in the cold rolled samples after heat treatments.

6.2 Case of study

In the present study a lean, standard and superduplex have been considered. Cold worked duplex grades have been used as downhole tubular and plates for many years. However, problems during manufacture may result in areas of the tubular exhibiting additional localized cold work.

One of the most significant factors in determining the kinetics and the sequence of precipitation in duplex grades is to have good knowledge on the chemical composition and thermo-mechanical history. At higher the Mo, Cr and W content, faster precipitation occurs, but few data on cold working, texture and deformation rate effects on such precipitation are available. In Duplex grades the metastable ferrite can decompose to a sigma phase and secondary austenite due to heat treatment, which are known as secondary phases. All the mechanical, corrosion resistance and magnetic properties are strongly influenced by this microstructural transformation.

The aim of this case of study is to analyze the mechanism and kinetic of secondary phase precipitation in cold rolled samples (from 5% to 85% thickness reduction), treated at 850°C for (10 min) and 900°C (10-30 min), water quenched. The specimens of diverse grades have been examined; morphology and composition of secondary phases have been determined by means of a Scanning Electron Microscope metallographic technique coupled with an Energy Dispersive X-Ray Spectroscope. The different magnetic properties of duplex phases are used to monitor such phase transformations; magnetics measurements have been performed to assess the amount of strain-induced martensite after cold rolling with different thickness reductions.

6.3 Experimental procedures

6.3.1 Base metal of duplex grades

The 2101 grade was received as hot rolled plates of 8 mm in thickness, solution annealed at 1050°C and water quenched. Moreover, standard duplex 2205 was received as hot rolled plate of 10mm, solution annealed at 1050°C following water quenching. The 2507 grade was received as hot rolled of 1.5 mm, solution annealed at 1100°C and water quenched. Chemical compositions are shown in Table 6.1

Table 6.1 *Chemical composition of the investigated Duplex Stainless Steels [wt. %]*

Element	C	Cr	Ni	Mo	Cu	Mn	P	S	Si	N	Fe
2101	0.028	21.72	1.13	0.15	0.32	3.41	0.026	0.01	0.78	0.13	bal.
2205	0.030	22.75	5.04	3.19	-	1.46	0.025	0.002	0.56	0.16	bal.
2507	0.015	24.8	6.89	3.83	0.23	0.83	0.023	0.001	0.24	0.27	bal.

6.3.2 Cold rolling and Heat treatment

Plastic deformation of the solution annealed materials was carried out by RT cold rolling (10-85% thickness reduction). The 2101 was examined only in rolled condition while the cold rolled 2205 and 2507 samples were heat treated in a muffle furnace at 850° for (10 min) and 900°C for (10 and 30) minutes in order to investigate the influence on cold rolling on secondary phases precipitation. A single stand reversing mill, with 130 mm diameter rolls was used. The plates were cold rolled in one direction, through many constant passes, to gradually reduce its thickness by compression. Cold rolled samples were obtained applying different thickness reductions in the range of 10-85%. Although in 2205 and 2507 steels have different precipitation kinetics, they were treated at the same temperature of 900°C (for 10 and 30 minutes), in order to compare the results in terms of atomic mobility and diffusion mechanisms, which are strongly temperature-dependent. The solution annealing temperature, the relative concentration of the elements and their partitioning affect the type of phases that will form and contribute to regulate both the activation energy for the precipitation and the flux of atoms through the different phases. Thus, the effect of the chosen temperature on the two steels will lead to different behaviors, but it is supposed that the mechanisms which regulate the diffusion process are almost the same at the same temperature.

6.3.3 Characterization techniques

The microstructural investigations were performed using a Cambridge Leica Stereoscan 440 Scanning Electron Microscope (SEM), operative in backscattered-electron mode (BSE) at 29 kV, on unetched samples. Metallographic samples were prepared with conventional grinding, polishing and etching with Beraha's etchant.

The SEM-BSE observation allows for the identification of the different phases inside the microstructure through the difference in the average atomic number: ferrite appears slightly darker than austenite while the secondary phases are brighter, owing to the greater amount of molybdenum, with the σ-phase darker than the χ-phase. The SEM was also equipped with a

Philips PV9800 Energy Dispersive X-Ray Spectroscope (EDS), which allows for a qualitative analysis of the elements inside the different phases and a quantification of them via the standardless ZAF correction. Furthermore, the amount of the secondary phases detected was estimated using image analysis software on the SEM-BSE micrographics.

6.3.4 Magnetic measurements and X-Ray Diffraction

For the identification of the phases, X-ray diffraction was performed using a Cr-Kα radiation (λ=2.2897 Å, operating at 30kV and 20mA), in step scan mode with step size of 0.025° and time per step of 5s. First magnetization curve and hysteresis loops were measured in a double-yoke DC magnet-steel tester. The predecessor equipment was firstly described by Stäblein and Steinitz. The equipment is characterized by two E-shaped soft iron yokes, opposite one another with and air-gap between each of the three pairs of transverse limbs.

The capabilities of magnetic measurements allow to a quantitative correlation between measured harmonics and mechanical properties obtained from destructive tests. Equal magnetizing windings are placed on each half of the long arms of both yokes. Hence, the equipment has a perfect symmetry. The introduction of a specimen in one gap causes an imbalanced symmetry; an additional flux is needed to complete the circuit mainly across the central air-gap, the flux in which is thus closely proportional to the magnetization (M) of the specimen. The apparatus for measuring the strength of the applied field H may be calibrated in any known field, and is found to give accurate readings of the value of H applied to the specimen (S. S. S. M. Tavares, 2006) (H. Kronmüller, 2003).

The maximum applied external field was of 210 kA/m. The present form of the measuring setup applies up-to date field sensors and data acquisition apparatus. AC measurements of the minor hysteresis loops were carried out by using a specifically designed permeameter type magnetic property analyzer, with a maximum applied external field of 2450 A/m. For each cold rolled sample the relative magnetic permeability values were derived from the resulting magnetizing curves. The coercivity (H_c) was measured by a high-accuracy Förster coercimeter (Type 1.093) equipment, based on the compensation of the own remnant magnetic field of the samples. The coercivity was measured magnetizing the samples along their rolling direction. Vickers hardness (HV) tests were also performed using a Buehler MMT-3 digital micro hardness tester. All measurements were carried out using a load of 0.5 Kg on each sample.

6.4 Results and Discussion

6.4.1 Base materials

6.4.1.1 2101 duplex grade

The as received material in the solution annealed condition is characterized by coarse grains, elongated in longitudinal direction due to the previous hot rolling. Indeed the grains are equiaxic in the transversal cross section, perpendicular to rolling direction.

Figure 6.1 shows the 2101 DSS, the austenitic grains are elongated in longitudinal direction due to the previous hot rolling (Figure 6.1 a and b) and equiaxic in the transversal cross section, perpendicular to rolling direction (Figure 6.1 c)

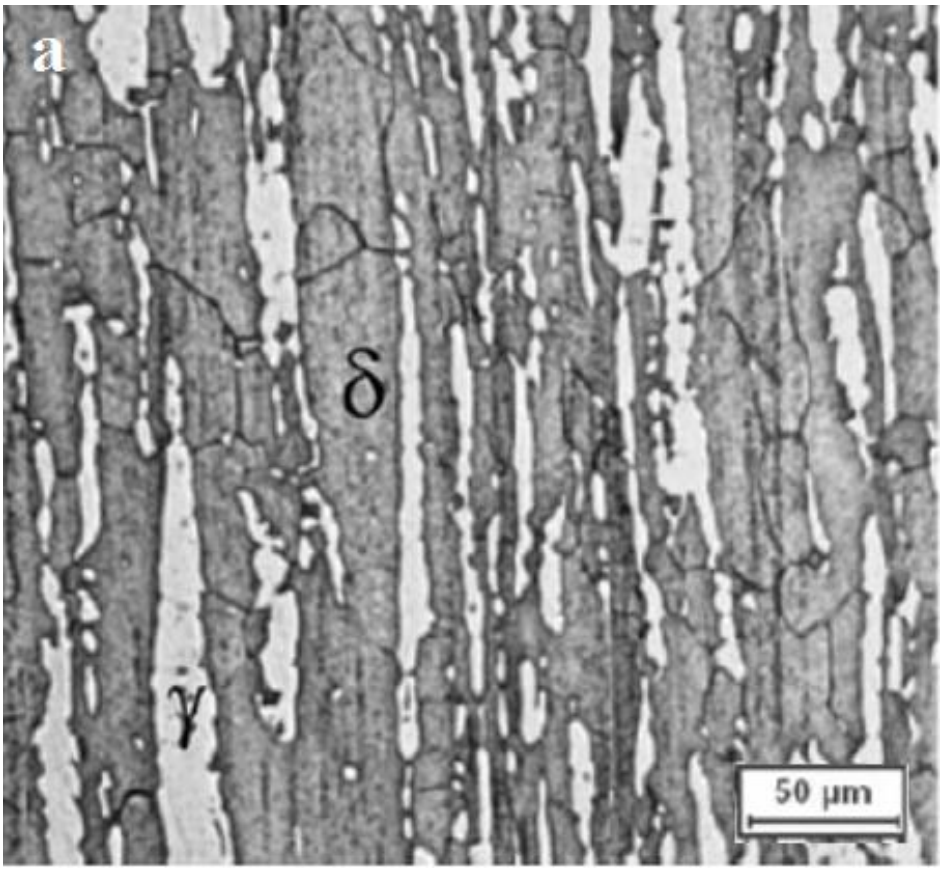

Figure 6.1 DSS 2101 a*s-received material of a Beraha's etching. a) Light optical micrograph, b) longitudinal section, SEM–BSE micrograph, c) transversal section, SEM–BSE micrograph*

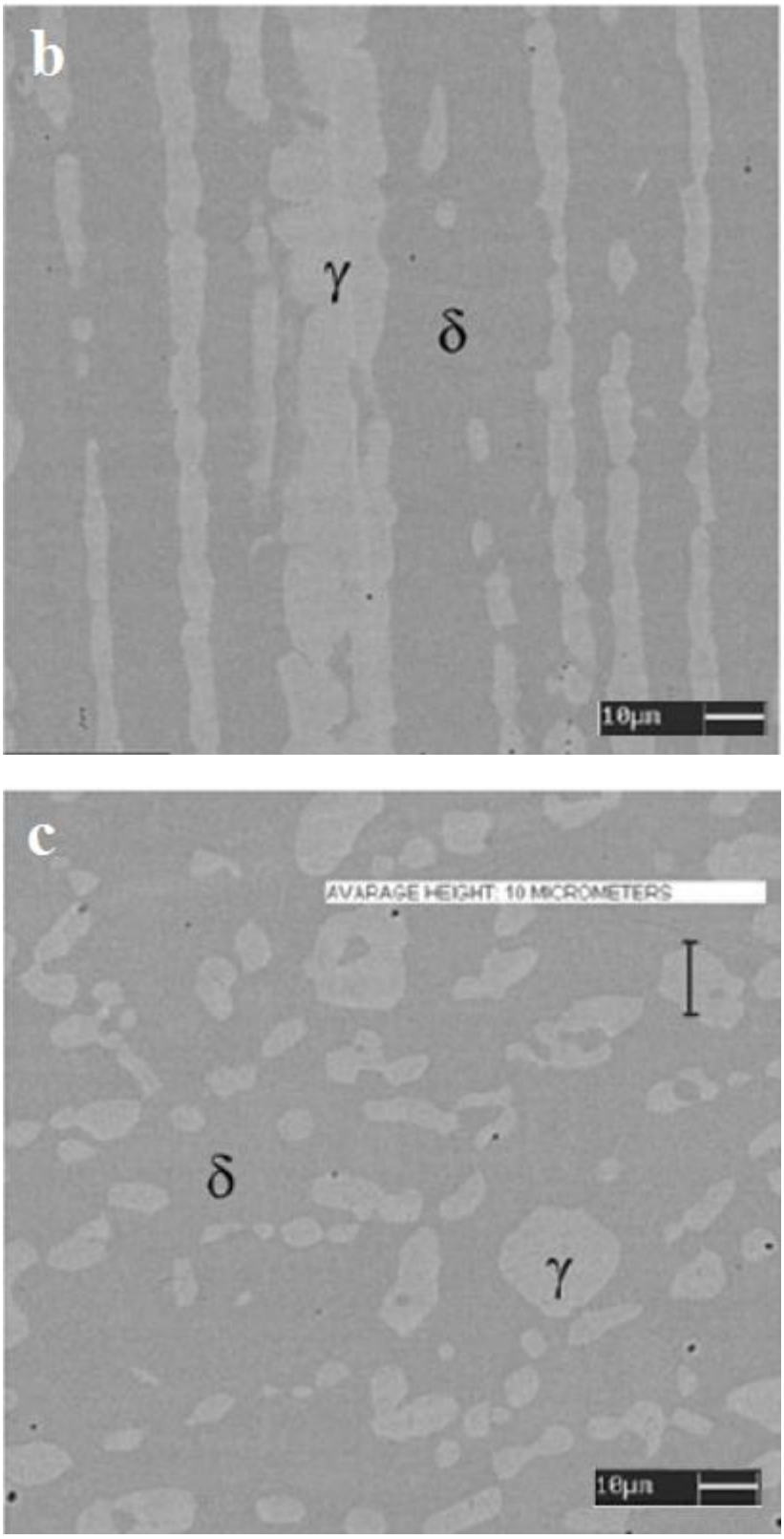

Figure 6.1 DSS 2101 a*s-received material of a Beraha's etching. a) Light optical micrograph, b) longitudinal section, SEM–BSE micrograph, c) transversal section, SEM–BSE micrograph*

6.4.1.2 2205 duplex grade

The as received material in the solution annealed condition is provided in the form of bars obtained by extrusion and consequently the microstructure consists of grains austenitic and ferritic elongated along the direction of processing by providing the typical microstructure in bands.

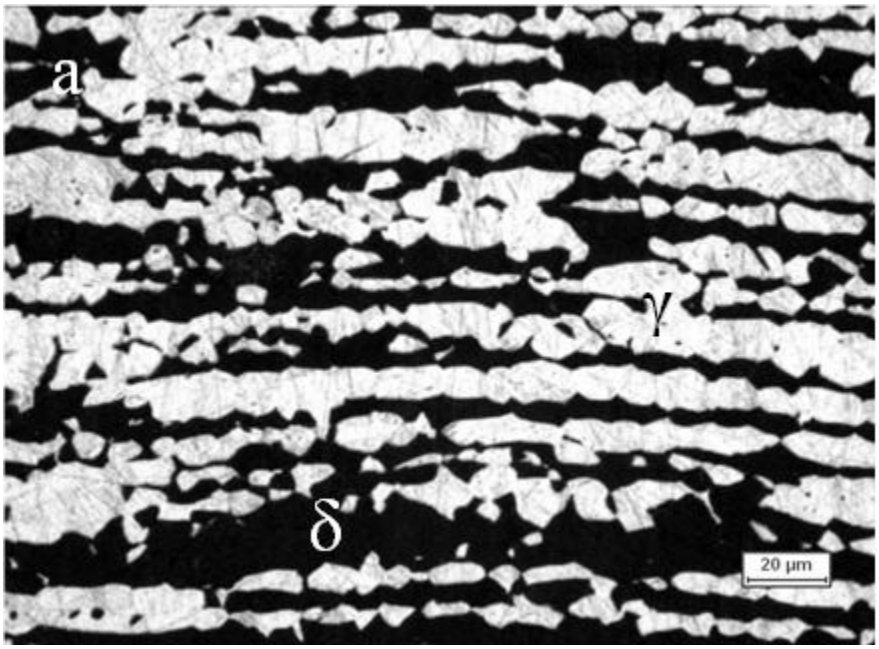

Figure 6.2 presents the longitudinal (a) and transversal (b) section respectively for the 2205 DSS, its constituted by austenitic and ferritic grains lengthen in the rolling direction.

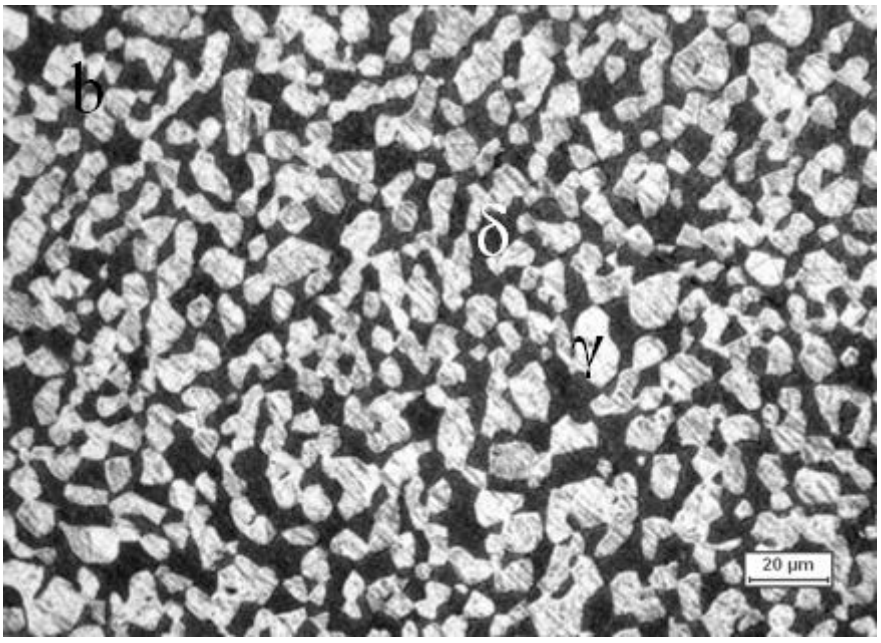

Figure 6.2 Microstructure of DSS 2205, δ= dark and γ= white; (a) longitudinal and (b) transversal section.

6.4.1.3 2507 duplex grade

In the 2507 DSS case, the material is provided in plate obtained by extrusion and, consequently, the microstructure has austenitic and ferritic elongated grains along the direction of processing by providing the typical microstructure in bands, which is shown on Figure 6.3. The underlying optical micrograph to the as received material shows the longitudinal section respect to the extrusion direction.

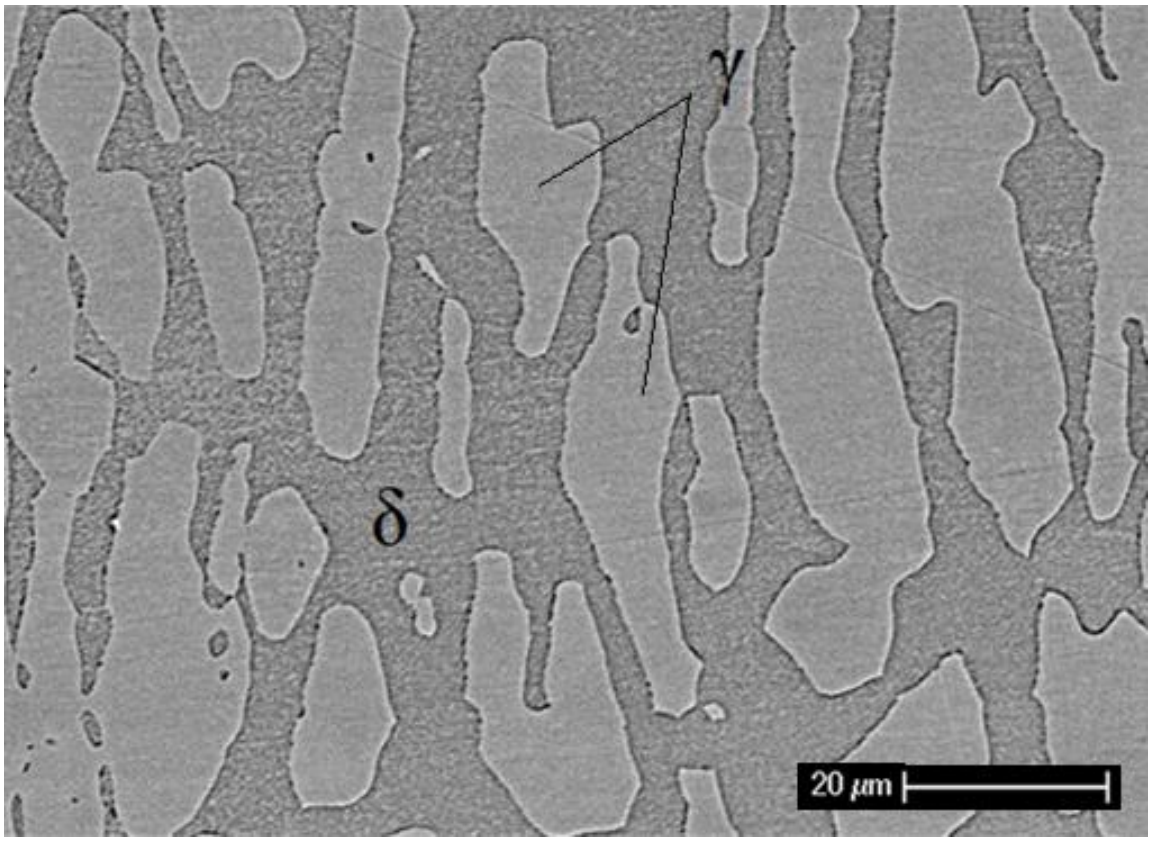

Figure 6.3 *Scanning electron micrograph at 1000x of the DSS 2507 as received material of the longitudinal section*

The phase volume fractions of the tested Duplex grades are shown in Table 6.2. Previously discussed on Chapter 3, these grades have a two-phase microstructure consisting of grains of ferritic and austenitic stainless steel, containing in their microstructure an austenitic phase as "islands" surrounded by the ferritic phase.

When Duplex Stainless Steel is melted it solidifies from the liquid phase to a completely ferritic structure. As the material cools to room temperature, about half of the ferritic grains transform to austenitic grains ("islands"). The result is a microstructure of roughly 50% austenite and 50% ferrite.

Table 6.2 *Volumetric fraction of δ-ferrite and γ-austenite phases in tested Duplex grades*

Duplex grade	**Volumetric fraction [wt. %]**	
	δ-Ferrite	**γ-Austenite**
2101	79.6	20.4
2205	51.8	48.2
2507	42.5	59.5

6.4.2 2101 cold rolled

The first effects obtained by cold rolling on both steels were a strong grain refining and changing in shape compared to the solution annealed sample microstructure as reported in (E. Ramous, 2012) In the 2101 samples the SEM-BSE and SE micrographs evidenced a microstructural modification in the austenite grains. It could be indicate a presence of a new phase with the typical platelet martensite morphology (Figure 6.4)

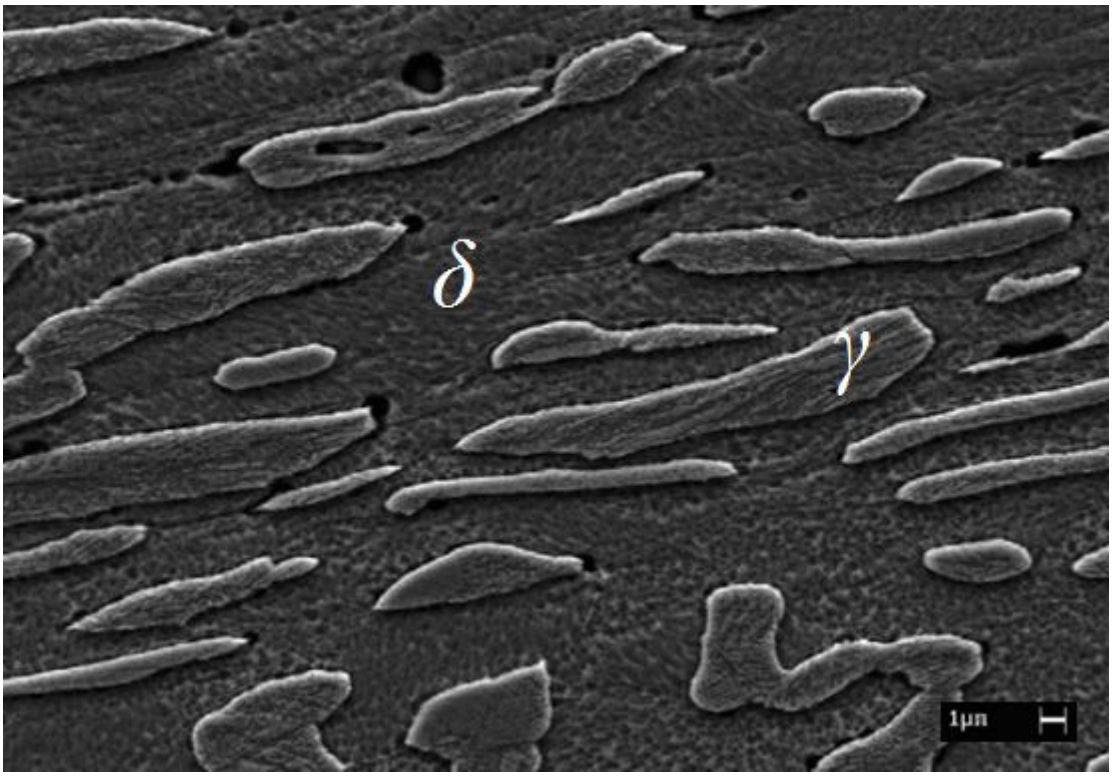

Figure 6.4 *SEM micrograph of the 2101 DSS cold rolled 80% thickness reduction with platelet in austenite grains*

The identification and quantification of martensitic phase was not possible through classical metallographic technique because the tested etchants were not able to unequivocally isolate lath martensite.

Therefore X-Ray Diffraction and magnetic measurements allowed to suggest the presence of α'–martensite. X-Ray spectrum m of the strongest deformed sample (80% Thickness Reduction) is shown in Figure 6.5.

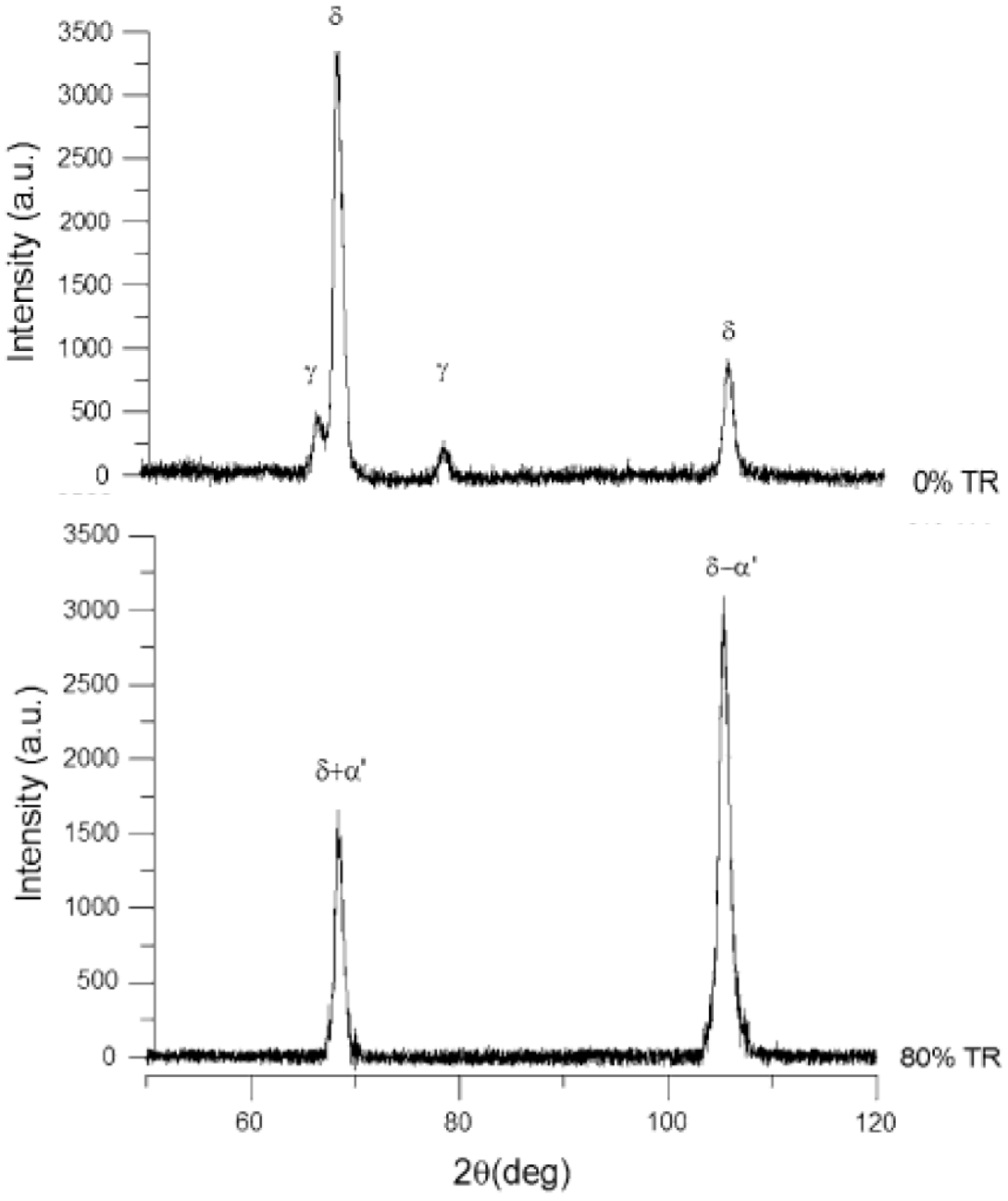

Figure 6.5 *X-Ray diffraction of the as received in the above side while the cold rolled sample down below*

It is not possible to distinguish the peaks of δ-ferrite and α-martensite because the two phases have the same crystal lattice so the same reflections. Over the detection limit, the peaks of austenite completely disappear after the maximum thickness reduction applied.

Therefore at this deformation condition all the detectable austenitic phase could be transformed into α-martensite. The saturation magnetic polarization is known to be linearly proportional with the amount of ferromagnetic phase. In the non-deformed condition only a ferromagnetic phase (δ–ferrite) was present. The saturation magnetic polarization in this case was $\mu_0 M_s$ (δ) = 0.752 T, and remained at a constant value during cold rolling.

As the material was subjected to cold deformation another ferromagnetic component was introduced in it. This could be to the appearance of α-martensite, which increased with cold deformation up to a complete detectable ferromagnetic structure made of 79.6% of ferrite, 20.4% of α-martensite and 0% of austenite.

The saturation magnetic polarization ($\mu_0 M_s$) seems to have almost the same value at the lowest cold deformation (up to 30% of thickness reduction) (Figure 6.6).

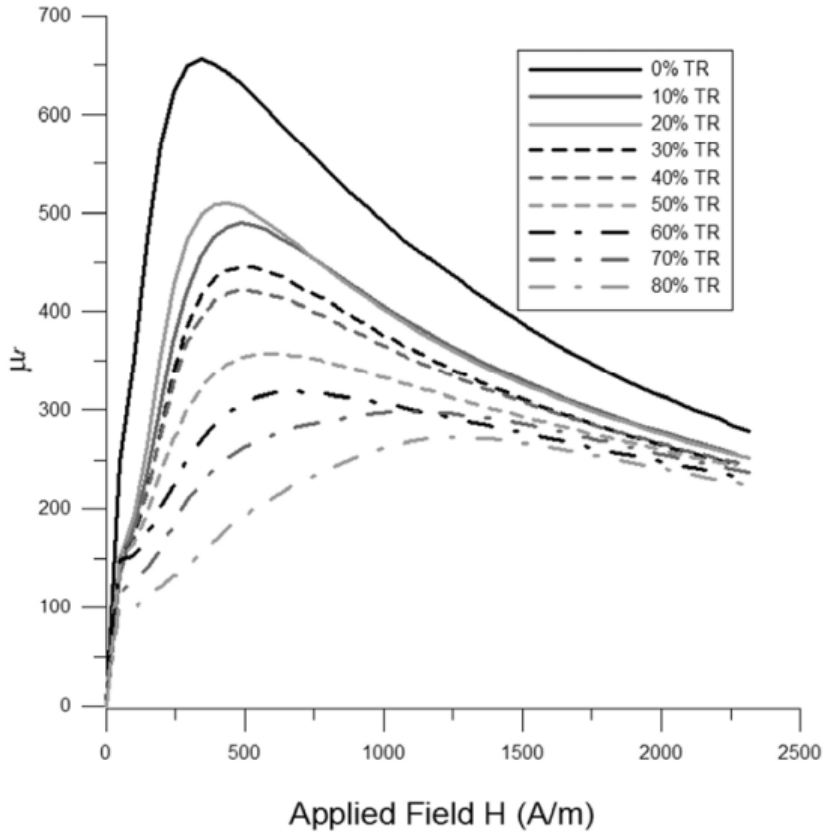

Figure 6.6 *Initial magnetization curves for each thickness reduction versus applied field*

Increasing thickness reduction at room temperature and a stronger, gradual increase in saturation magnetic polarization was highlighted. The amount of the new phase, at the moment

called α'-martensite, was calculated from the saturation induction values can be seen in Table 6.3.

Table 6.3 *New phase quantification*

Thickness Reduction [%]	0	10	20	30	40	50	60	70	80
New Phase [%]	0	0.1	0.3	1.0	7.7	8.3	12.4	16.9	20.4

Maximum relative magnetic permeability values were derived from AC normal magnetization curves (Figure 6.7). Magnetic permeability is an index of how well a material concentrates the magnetic field. The results show a relationship between the reciprocal of maximum relative magnetic permeability and the amount of the hypothesize strain induced martensite. Therefore relative magnetic permeability could be a possible parameter derived from non-destructive tests to detect martensitic transformation in the duplex stainless steel considered.

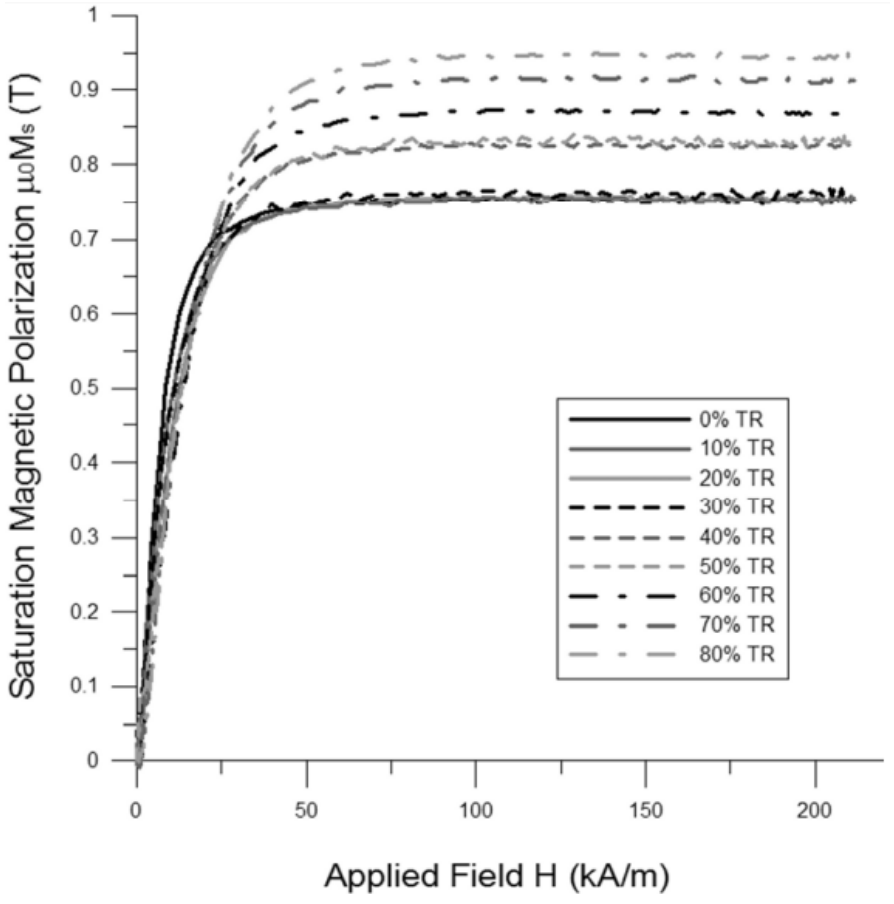

Figure 6.7 *Maximum relative magnetic permeability for each thickness reduction versus applied field*

These showed data were presented in a previously PhD thesis project (Baldo, 2010) developed in this department, which are used to demonstrate the continuation of the work presented below. The isothermal treatment after cold rolled deformation in the 2101 lean duplex grade were

performed in another work and has not been reported because no differences in transformation were founded.

6.4.3 2205 grade cold rolled and heat treated

Figure 6.8 evidence the δ-ferrite reduction that could be due to the hardening of the austenite caused for the nitrogen, which being a gammagene element promotes the formation of the phase and gives the strengthening. The low value of stacking fault energy of the austenite contributes to a greater strain hardening and the strengthening through solid solution by nitrogen. The fragmentation of the ferritic bands as well as the interconnection of the samples results more numerous, and diffuse with the deformation towards 35% to 85% of reduction.

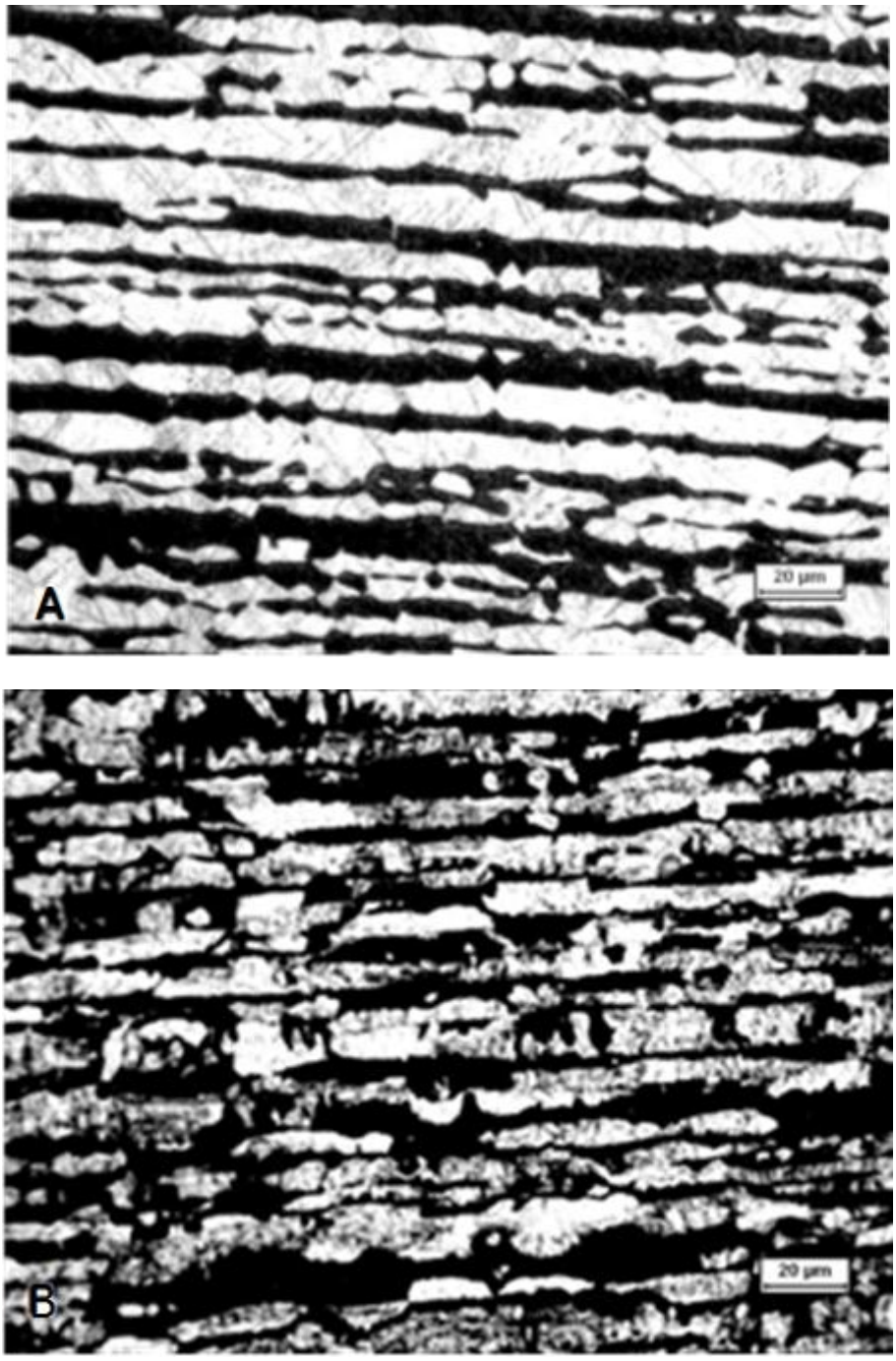

Figure 6.8 *Microstructure of cold rolled 2205 duplex stainless steel: a) 10%, b) 85% cold rolled deformation*

In a previous work (Piccolo, 2009) was noticed an austenite increment related to deformation increment, microstructural investigations evidence no martensite formation. Nevertheless, SEM, EDS and X-ray Diffraction were performed in order to confirm the previous results, which until now no martensite transformation is reveal. The investigation is currently straightforward for upcoming investigations. Forging ahead the research, the material under study was beneath cold deformation through a rolling mill.

The rolled samples were subjected to heat treatment with the base material, in order to observe the influence of the cold rolling in the phase precipitation. It can be delighted precipitation of secondary phases of acicular form, situated along the grain boundaries of ferrite/austenite and ferrite/ferrite as well as the triple union between the two phases; that are considered χ phase.

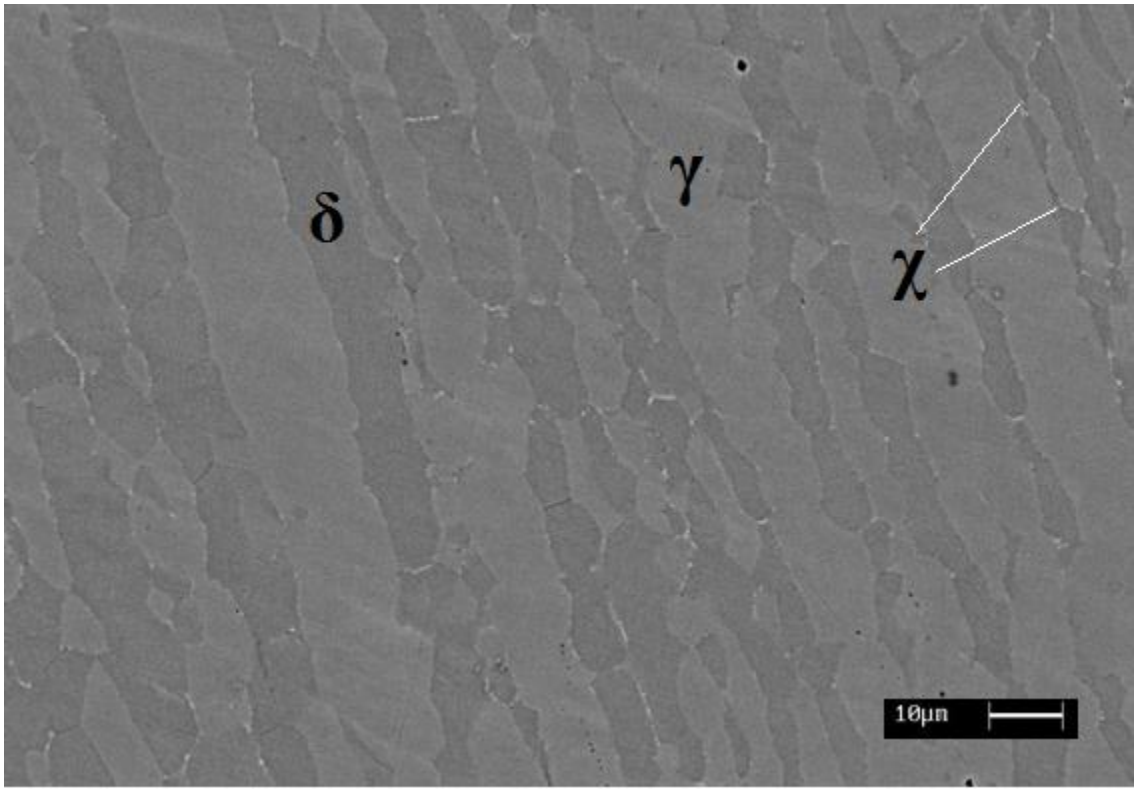

Figure 6.9 *Scanning micrograph at 2000x for deformed 15% previously treated at 850 °C (10 min) sample*

However, in Figure 6.9 the precipitation of secondary phases in terms of morphology and volume fraction for the material treated at 850°C for 10 minutes does not seems to suffer the effect of strain for the deformed samples at 5, 10, 15%.

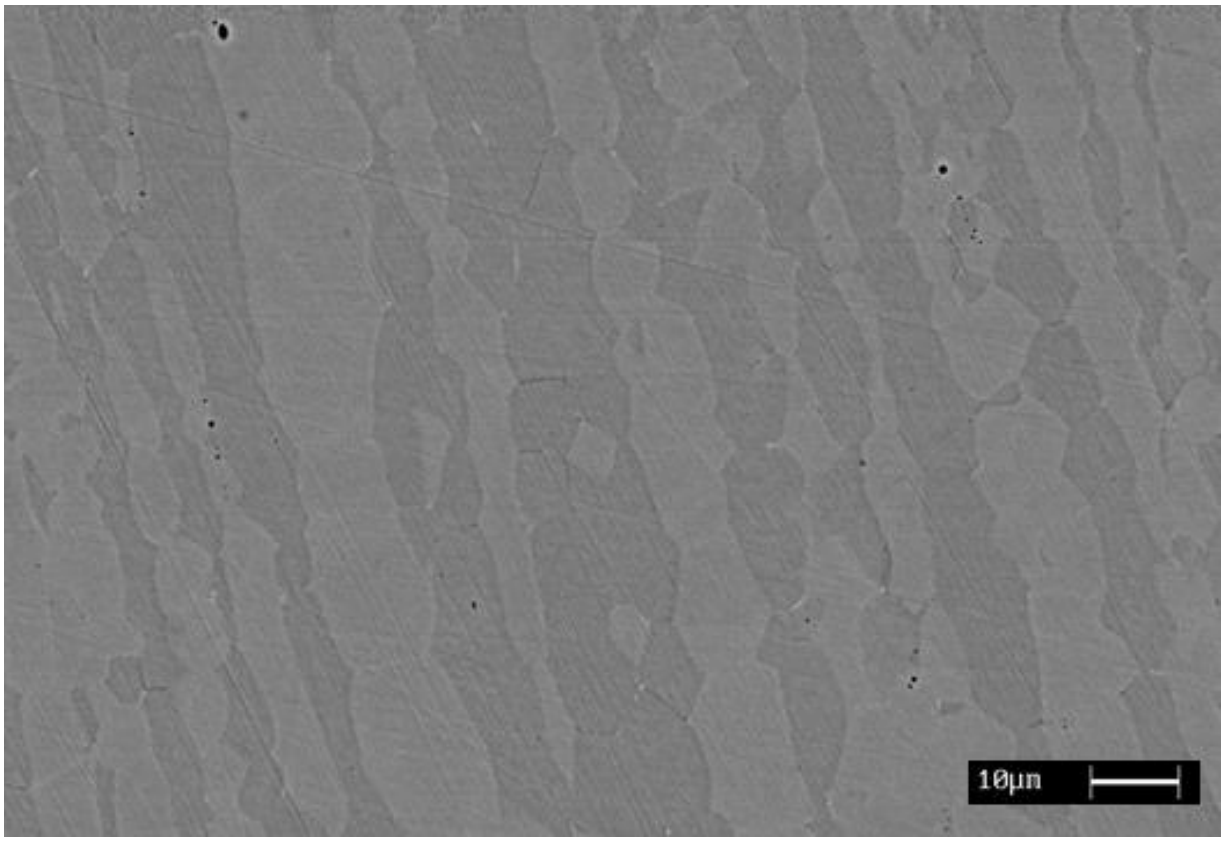

Figure 6.10 *Scanning micrograph at 2000x for deformed 10% previously treated at 900 °C (10 min) sample*

For 10 minutes of treatment seems to be unaffected in the precipitation of secondary phases, by the effect of cold rolling for the samples at lower deformations. However, it is observed that the samples deformed at 5, 10 and 15% and the as received sample at 850 °C have precipitation already for 10 minutes, for the samples heat treated at 900°C at lower thickness reductions an slighter precipitation of secondary phases is presented (Figure 6.10). This could be due to the work hardening induced by cold deformation that inhibit or promote the precipitation of secondary phases. Lower deformations inhibit the precipitation reached a certain deformation degree due to recovery. Therefore, the decrease in the density and defects is presented.

For the 10 minutes at 900°C of heat treatment, the secondary phases precipitation in the un-deformed material is very slight, it mainly consists in χ-phase (even if some σ-particles has been detected) and has been estimated around the 1% of volume fraction (Figure 6.11a).

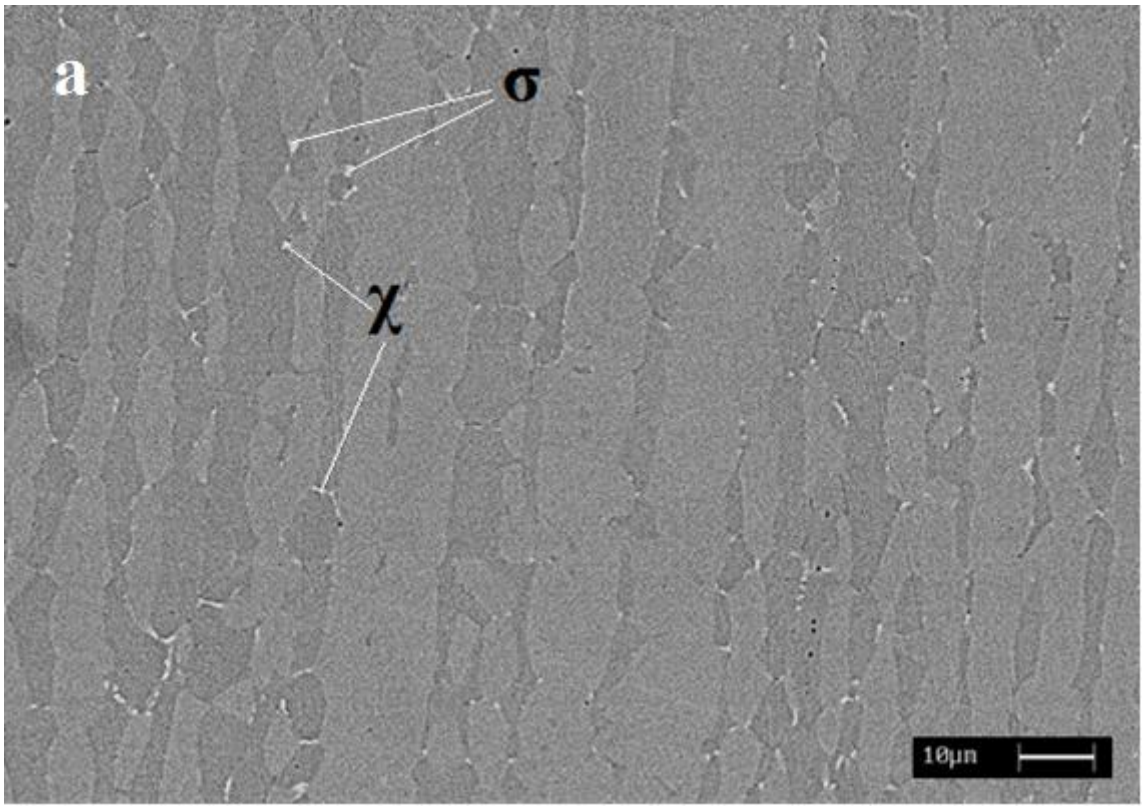

Figure 6.11 a *Secondary phases precipitation in the 2205 grade treated for 10 minutes at 900°C (SEM-BSE) undeformed material*

The plastic deformation enhances the amount and the type of the precipitating phases: as the thickness reduction increases, the χ-phase is gradually substituted by the σ-phase and, for the maximum thickness reduction; it has been almost fully replaced, reaching about the 18% of volume fraction (Figure 6.11b).

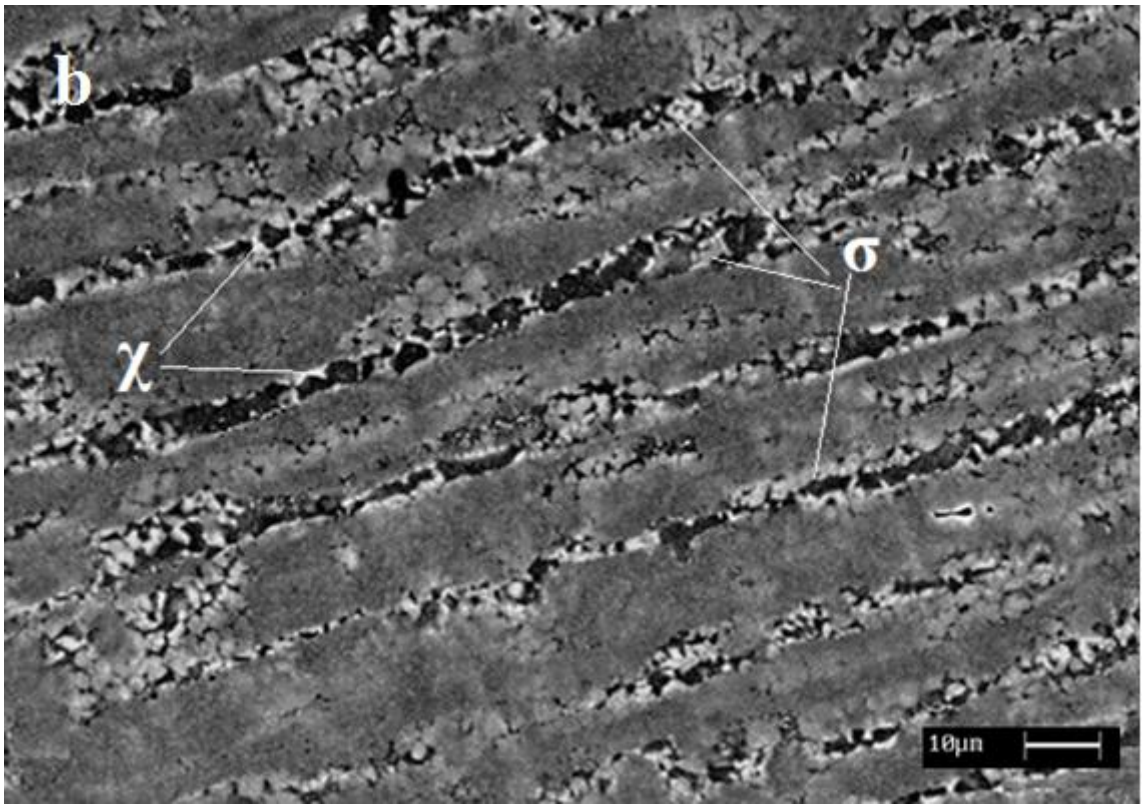

Figure 6.11 b *Secondary phases precipitation in the 2205 grade treated for 10 minutes at 900°C (SEM-BSE) with 85% of thickness reduction*

Figure 6.12 evidence the precipitation kinetics of the material treated for 10 minutes and can be described by an exponential-type law and an analysis of the SEM micrographs has shown an irregular increasing of the precipitation amount for deformation which exceeding 15%.

On the contrary, the exposure of the material for 30 minutes generates a progressive and steady increase of the precipitating phases with the increasing of the deformation and the relation between the volume fraction of secondary phases against the deformation can be considered almost linear.

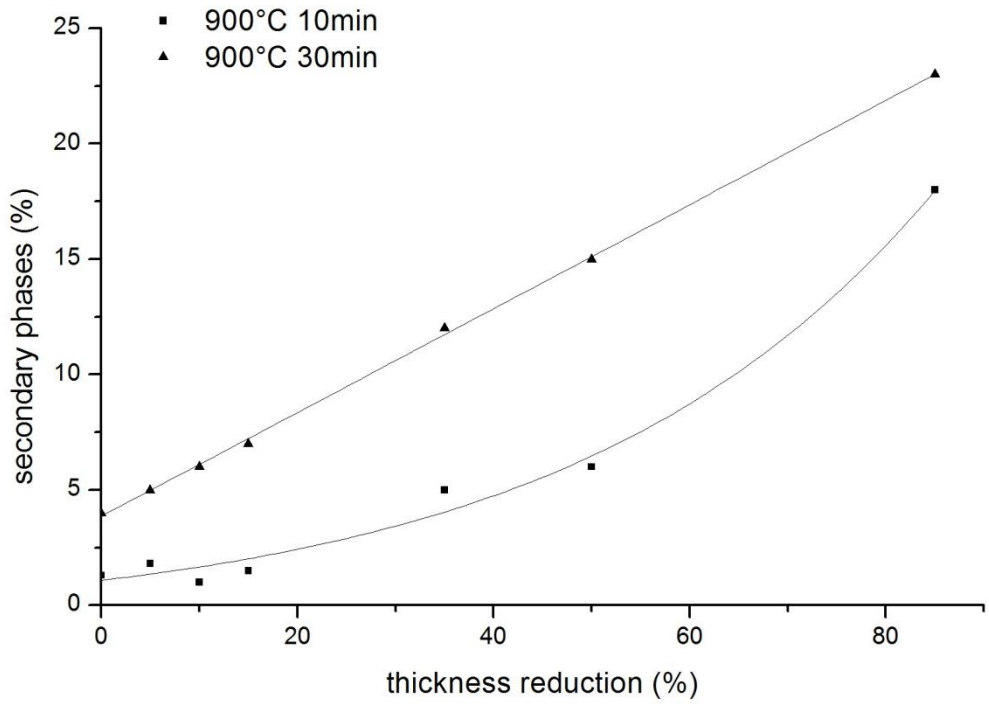

Figure 6.12 *Precipitation kinetics in the cold rolled 2205 DSS*

From the plot in Figure 6.12, the effect of the plastic deformation on the treated sample is clearly visible, especially for the shortest times. In fact, for the 10 minutes treatment, the progressive increasing of the crystal defects and the generation of micro-strain gradients of even more higher entity strongly affects the precipitation behavior.

Thus, the material passes from a slight-affected condition (in terms of secondary phases amount) for lower thickness reductions to a strongly-damaged microstructure at 85% of deformation.

This situation could be explained considering that, up to 15% of deformation, the dislocation density and the numbers of defects are not very high, even though a certain amount of surplus energy has been stored, and the distortion energy of the crystals is not sufficient to act as discriminating factor in order to reduce the time for the precipitation. On the contrary, over 35% the distortional energy stored inside the grains is enough to promote the precipitation kinetics significantly.

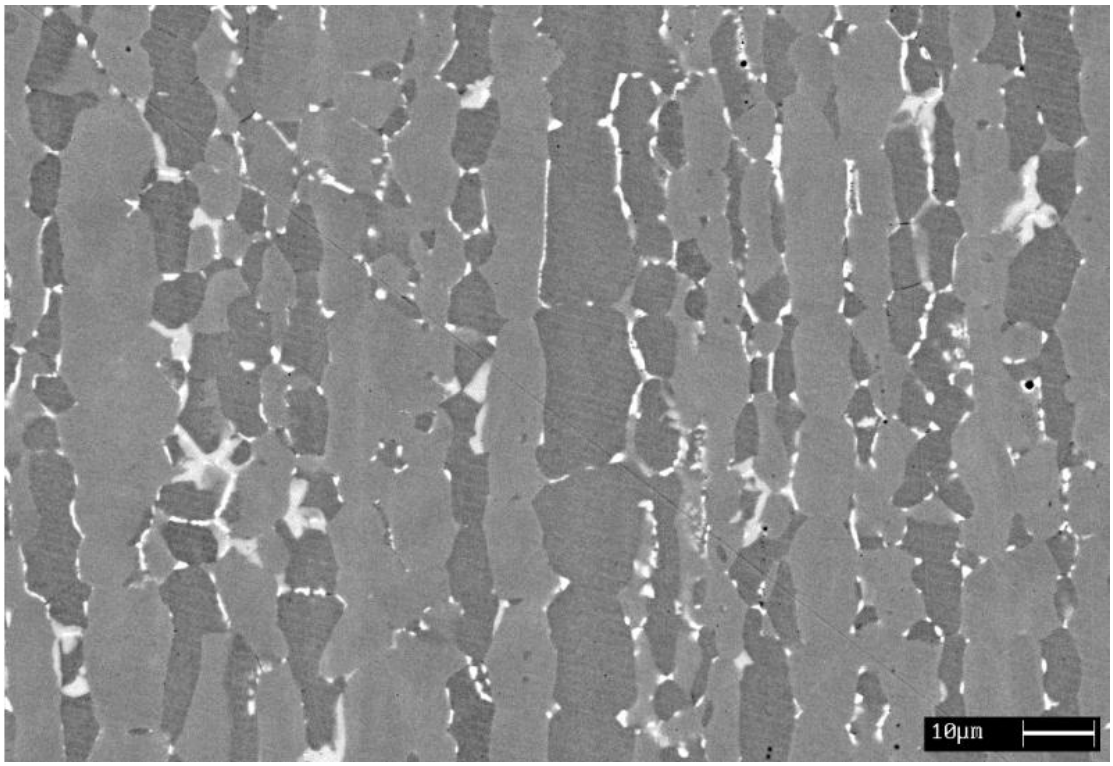

Figure 6.13 SE micrograph of the s*econdary phases precipitation*[1] *in the 2205 grade treated at 900°C for 30 minutes undeformed material*

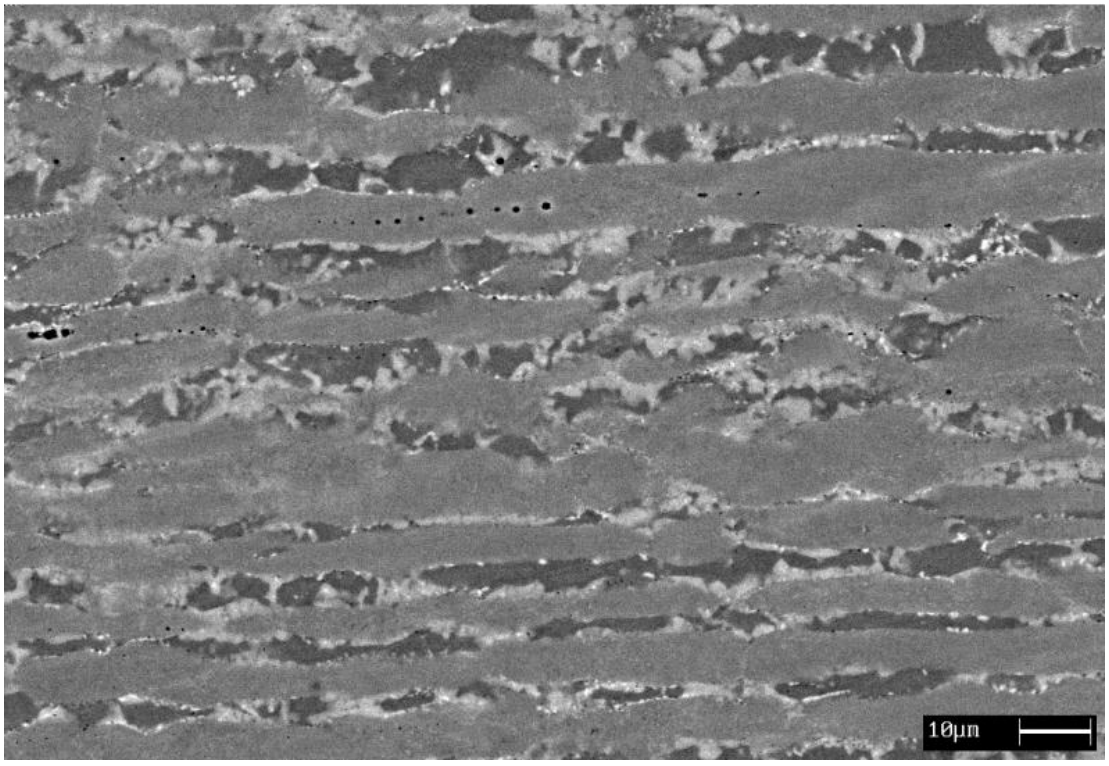

Figure 6.14 SE micrograph of the s*econdary phases precipitation*[1] *in the 2205 grade treated at 900°C for 30 minutes with 50% of thickness reduction*

1. Phases (in order of increasing brightness): ferrite (δ), austenite (γ), sigma (σ), chi (χ).

For the 30 minutes treatment the deformation also causes an increasing of the precipitation amount but without the strong drop observed in the previous case for deformations over 15%. In this case the increasing of the precipitates is more regular because the exposure time at the soaking temperature is higher, which is shown in Figure 6.14. In fact, the precipitation process is a diffusive transformation and is strongly time-dependent, thus a greater time at the treatment temperature promotes the entire diffusion process.

The EDS analysis was performed for the selected samples a, b, c and d which previously evidence a complex microstructure heat treated at 850° and 900°C; the chemical composition of the austenite and ferrite phases was measured, as well as the secondary phases presented in Table 6.4.

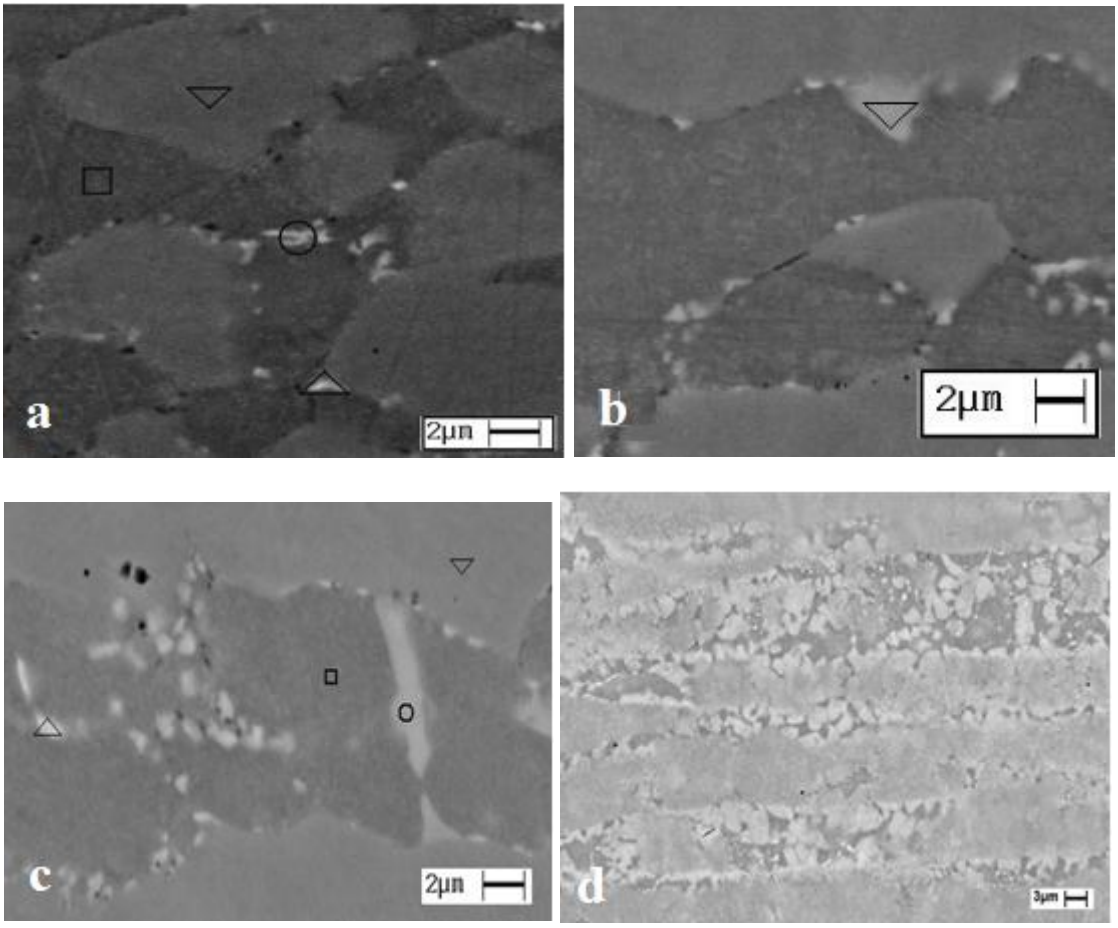

Figure 6.15 *SEM micrographs at 6000x for EDS analysis representative treated and deformed samples*

Table 6.4 *Chemical composition of evidenced secondary phases previous to cold working and isothermal treatment*

Wt. %	**Si**	**Mo**	**Cr**	**Mn**	**Fe**	**Ni**
δ	0.7	3.1	23	1.2	67.2	4.8
γ	0.6	2.6	21.9	1.3	67.3	6.2
σ	1.1	5.9	25.1	1.1	62.6	4.2
χ	0.9	7.5	23.9	1.2	62.9	3.7

In Figure 6.15, for all the samples the chemical composition outcome the EDS analysis corresponds to those for 2205 stainless steel at solubilized state (Dengo, 2002). Results more difficult to measure the secondary phases in some samples; this is caused by the small size of these precipitates that are generally smaller than the spot size of electron beam adopted for the analysis, which is approximately 1 μm. Furthermore, tiny bright precipitates can be seen in the σ phase, identified as χ phase. D sample has innumerable secondary phases, most of them were identified as χ phase, and for those larger precipitated and more contrasted, it is identified as σ phase.

6.4.4 2507 grade

6.4.4.1 2507 cold rolled *and heat treated*

In the 2507 at increasing the deformation, the grains gradually became more elongated along the rolling direction. For deformation the 65-85% thickness reduction grains, are so stretched to form almost of the bands of austenite and ferrite alternate; a similar microstructural anisotropy can be expected to lead to a corresponding anisotropy of the mechanical characteristics (see Figure 6.16 and 6.17).

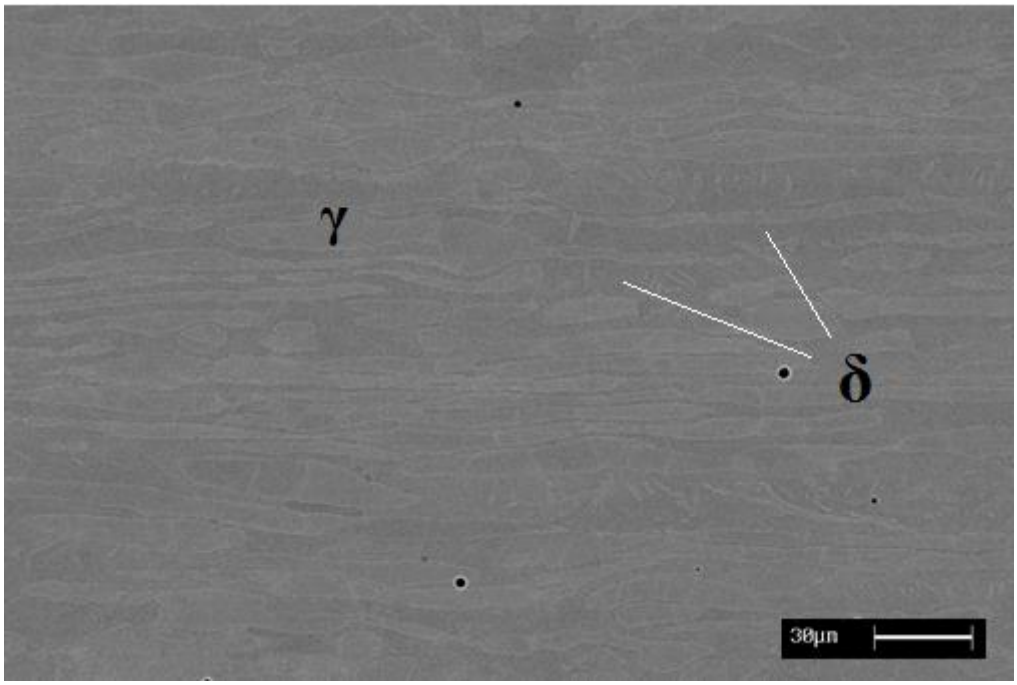

Figure 6.16 *Scanning micrograph at 1000x for deformed 10% sample*

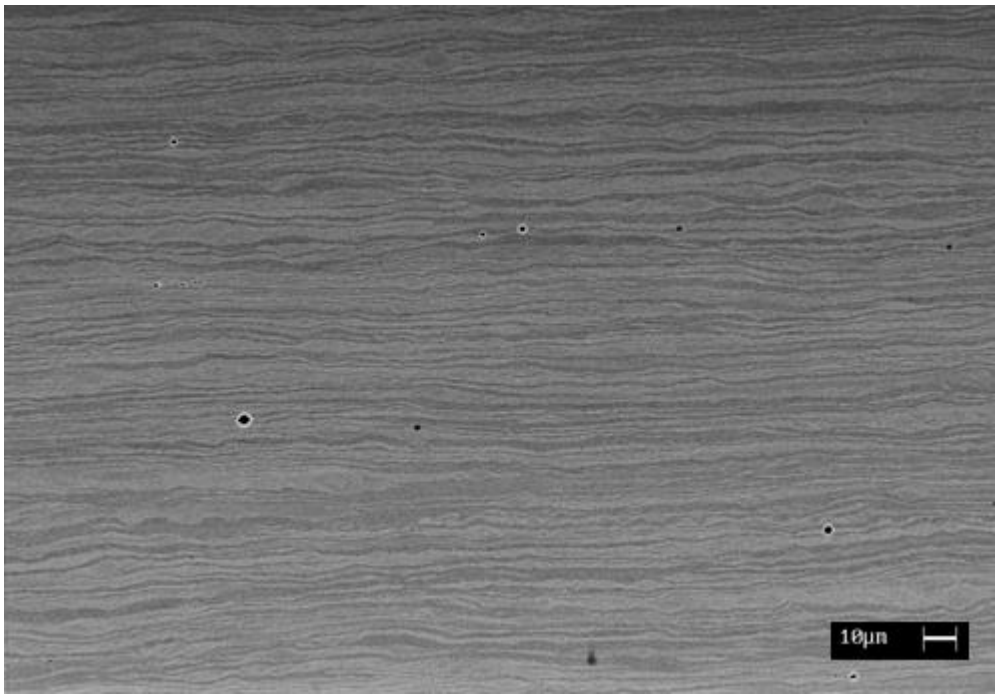

Figure 6.17 *Scanning micrograph at 1000x for deformed 85% sample*

It should be noted that the strong mechanical stress suffered by the material high-strain, does not lead to the fragmentation of the phases, which are elongated but well-defined contours. Scanning microscope analysis confirms the absence of secondary phases. From the analysis of image can deduce that the plastic deformation affects slightly on the percentage of ferrite detected, which decrease.

The austenite phase is metastable at room temperature and the processes of cold rolling can cause its partial transformation to martensite. It is also true that the Nickel plays a stabilizing role of the austenite phase and contributes to contain this phenomenon (Ruffini, 2005). It is easy to understand by SEM analysis if these changes in the contrast are due to the formation of martensite phase or to the development of slip bands.

Electron microscopy could evidence the presence of martensite on the specimens highly deformed; a possible EDS analysis on martensite would not be meaningful, because it would provide unaltered results with respect to the austenite. The martensitic transformation is not a diffusive transformation but a cooperative motion of a certain number of atoms in the crystal lattice which give rise to a new phase. However, X-Ray Diffraction measurements were performed in order to clarify whether or not the presence of martensite (Figure 6.18).

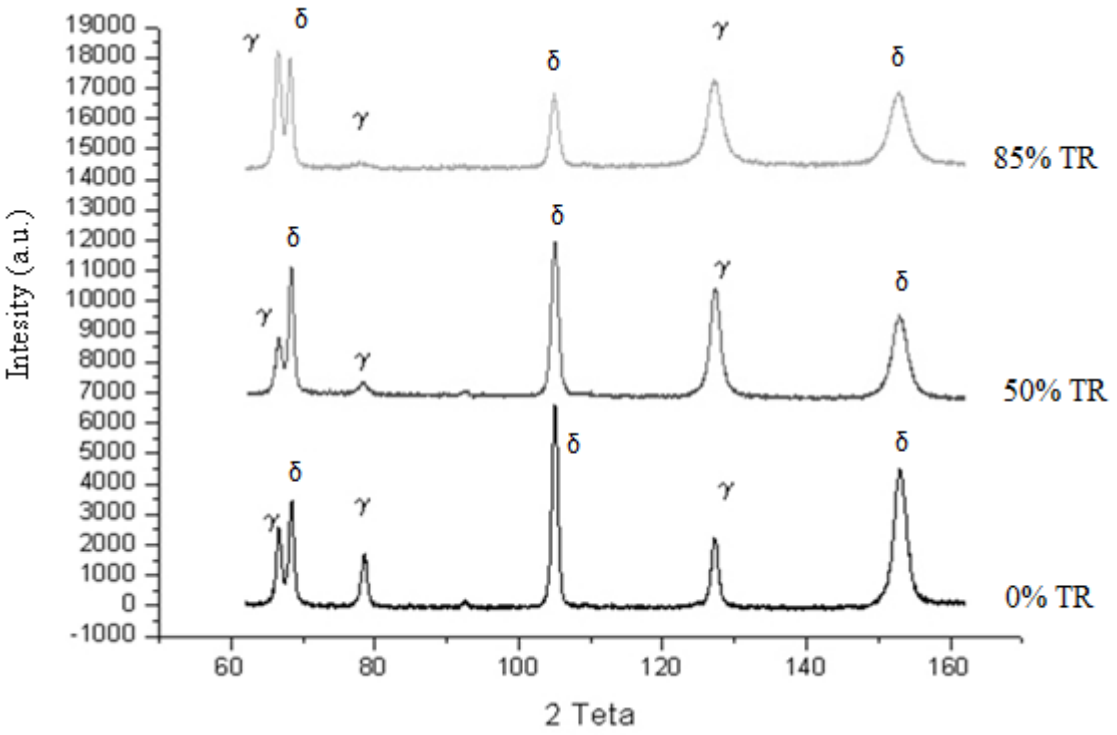

Figure 6.18 *X-Ray diffraction of the as received down below, proceeding 50% cold rolled sample finally on the top the 85% cold rolled sample*

In the low Nickel Duplex grades, show an increase in the peak of the ferrite to increase the cold deformation. This phenomenon is due to the partial transformation of austenite into martensite at higher thickness reduction. The martensitic transformation is however contained for the 2205 duplex grade due to the role, at Nickel being a stabilizer of the austenite phase.

The 2507 case is observed that, as the deformation increases, the peak of the ferrite decreases while the austenite increases. The higher nickel content into the austenite phase, contributes to the stability of the austenite phase, by inhibiting almost all its transformation to martensite.

The reduction of the peak of the ferrite is also reflected in the image analysis performed with the optical and scanning electron microscope; the percentage of ferrite therefore decrease for higher degrees of deformation. This phenomenon, concurrently with the peak increase of the austenite, can be explained by the occurrence of the formation, with a non-diffusive mechanism similar to the martensitic transformation of austenite secondary γ_2 at the expense of the δ-ferrite.

On the other hand, the magnetic tests confirm that in the cold rolled samples the amount of magnetic phase is not affected by cold rolling. Figure 6.19 presents the first magnetization for the cold rolled samples without being heat treated developed in collaboration with Budapest University of Technology and Economics (Bianchi, 2011).

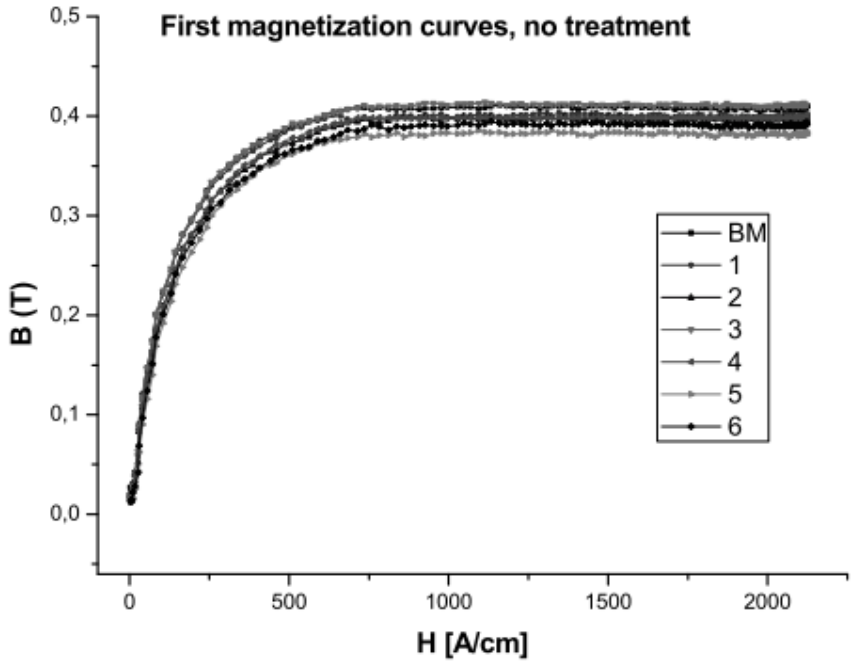

Figure 6.19 *First magnetization curves of the samples at only cold rolled state; no presence of ferromagnetic phase is observable*

Stäblein-Steinitz measurement is a closed loop DC measurement which is based on a symmetrical magnetic bridge yoke. It is able to supply an excitation field over 200˙000A/m, greater than AC measurement test. It is enough to saturate a hard magnetic material such as this SDSS. About the first magnetization curves the little shift that can be noticed is due only to the instrument (positioning of sample, noise etc.). So, this confirms again that in this steel there is no difference in the amount of ferromagnetic phase after several degrees of cold rolling. The same conclusion can be drawn watching the hysteresis loops that are exactly the same for each sample, again, all the sample reach the same value of magnetization and the little shift are only due to the device problem. Moreover, an investigation which involves the cold rolled 2507 martensitic transformation is currently carrying out in another PhD project.

6.4.4.1 2507 cold rolled *and heat treated*

For the cold rolled 2507 duplex grade after isothermal treatment, the steel exhibits a different behavior from the 2205 grade, since the soaking temperature of the treatment is critical for this steel and causes a very fast precipitation. Thus, after 10 minutes of exposure, in the base material the precipitation is around 10% of volume fraction and rapidly increases with the deformation, reaching about the equilibrium value for the 85% of deformation (Figure 6.20).

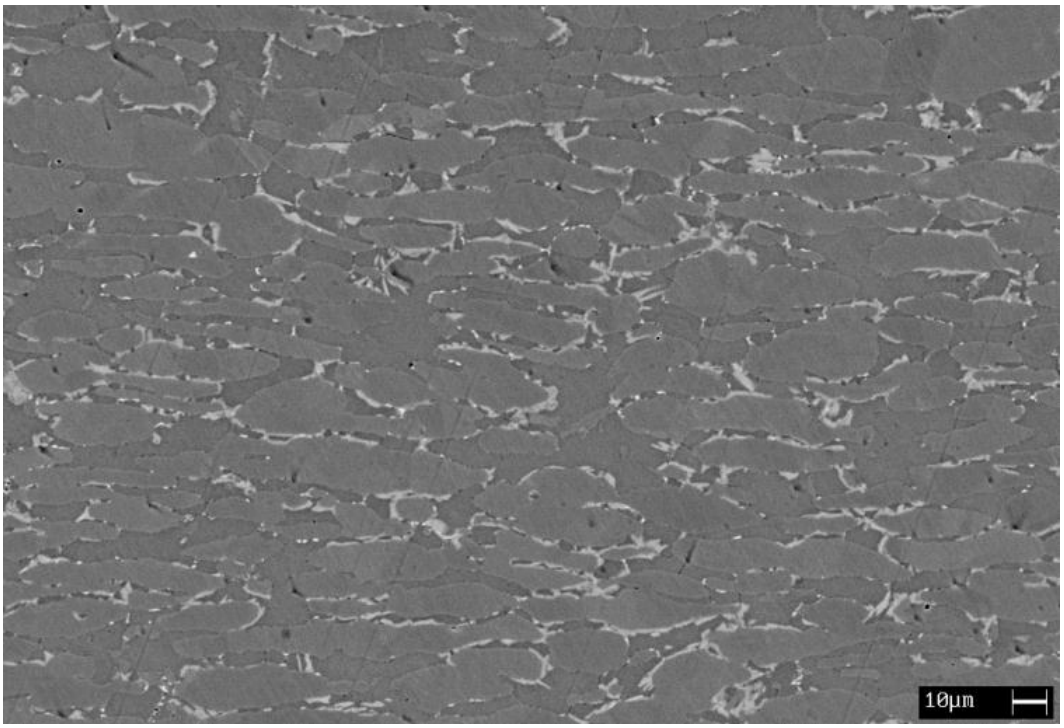

Figure 6.20a *Secondary phases precipitation[1] in the 2507 grade treated for 10 minutes (SEM-BSE): a) undeformed material and b) 65% thickness reduction.*

1 Phases (in order of increasing brightness): ferrite (δ), austenite (γ), sigma (σ), chi (χ)

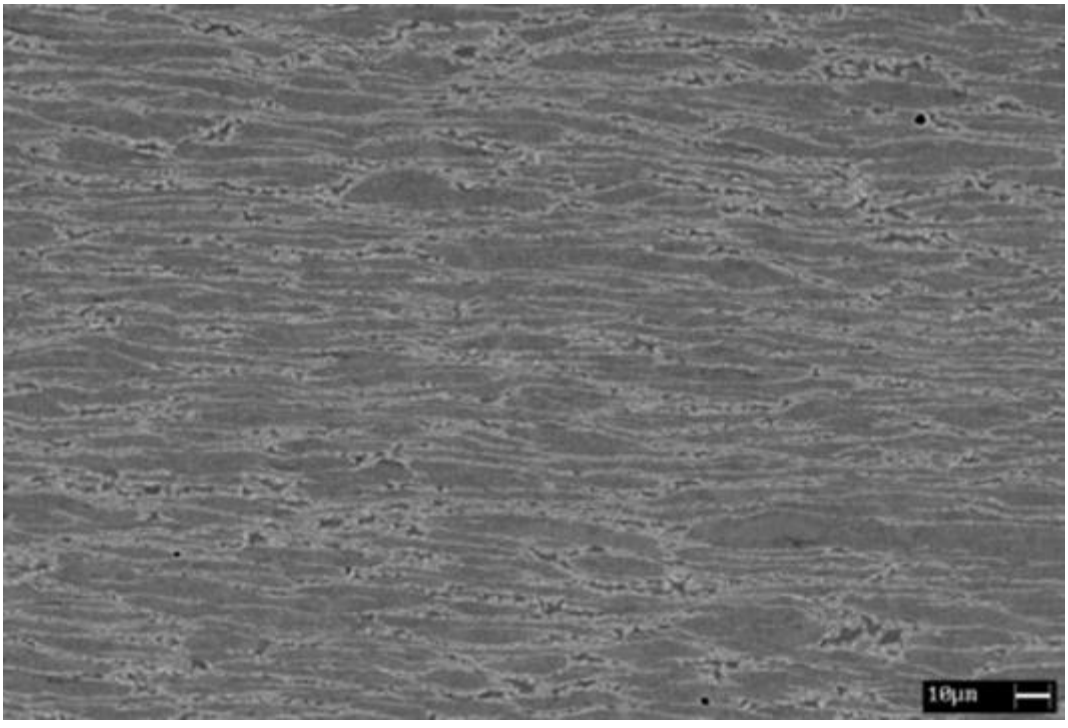

Figure 6.20b *Secondary phases precipitation[1] in the 2507 grade treated for 10 minutes (SEM-BSE) 65% thickness reduction.*

1 Phases (in order of increasing brightness): ferrite (δ), austenite (γ), sigma (σ), chi (χ)

In Figure 6.21 it is possible to appreciate the huge precipitation of sigma phase and secondary austenite, which is developed after 40 minutes of heat treatment at 900°C. The sigma phase (white particles) is mostly placed at the primitive ferrite/austenite boundary of the as received material, but also certain not negligible amount of sigma particles is observed into the austenitic grains, partitioning them. This happens at very important level from the 25% thickness reduction up to the most deformed. In that case, the partition is strong, and also due to the very fine microstructure the distinction between different grains is now very difficult.

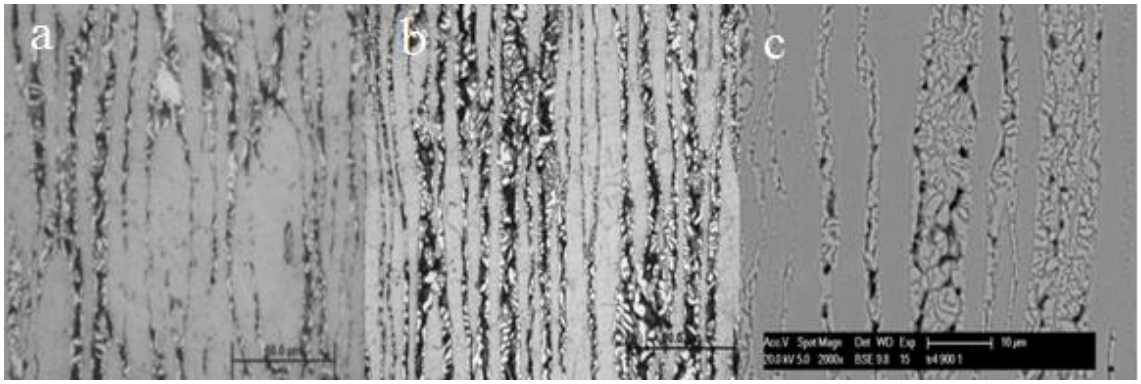

Figure 6.21 *OM micrograph, 500x Effect of heat treatment at 900°C for 40min , a) base material, b)25% TR, c) SEM micrograph, 50%TR with the partition of the austenite grains by the sigma precipitates, and the great decomposition of the ferrite*

In Figure 6.22 are plotted the results obtained in the 2507 DSS. The effect of the deformation is more pronounced for the 10 minutes treatment, while after 30 minutes the rising of the secondary phases amount with the deformation is quite slight, although the microstructural damage is wider.

However, in both cases, for the 85% of deformation the equilibrium volume fraction of secondary phases is approximately reached and the ferrite is almost completely transformed.

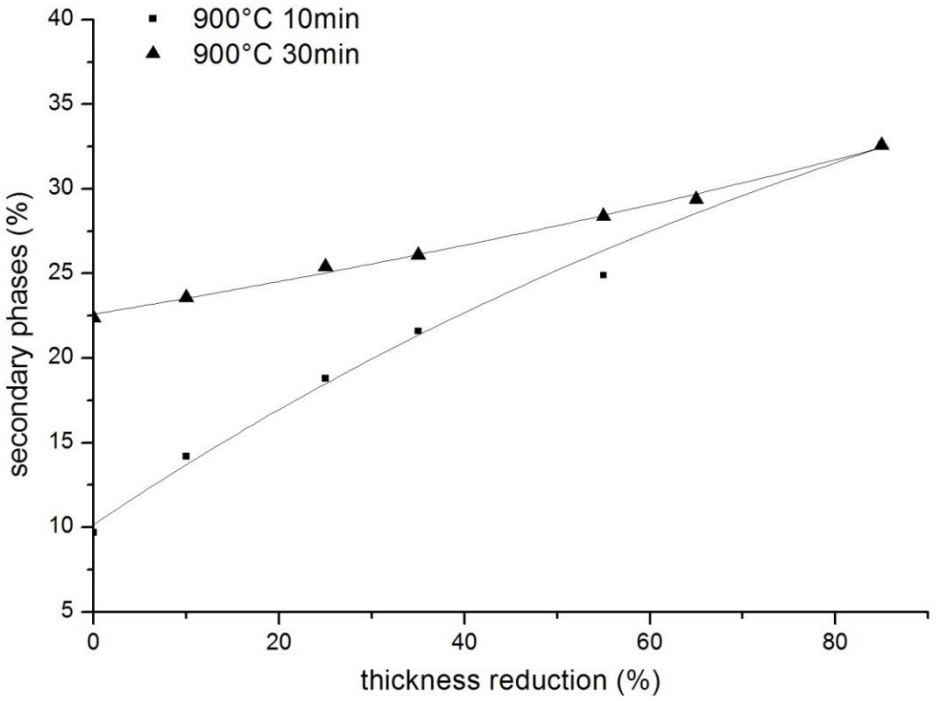

Figure 6.22 *Precipitation kinetics in the cold rolled 2507 DSS*

In the magnetic tests on the heat treated samples its decreasing of the magnetic phase is evidenced, in Figure 6.23 shows the magnetization curves of the samples after being heat treated.

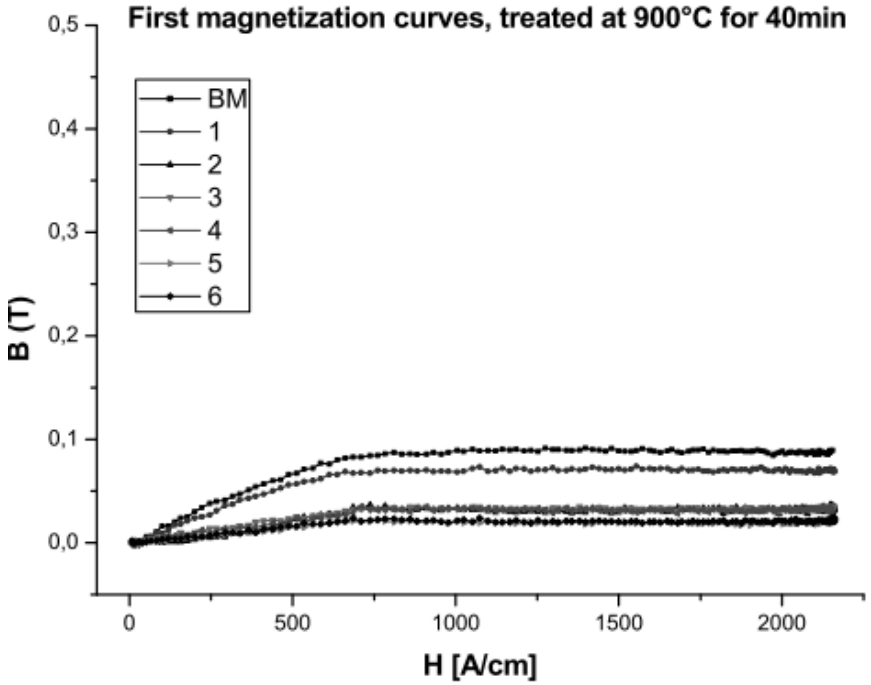

Figure 6.23 *First magnetization curves of the samples after the heat treatments. The device detect appreciable ferromagnetic phase only on the first two samples*

6.4.5 Effect of cold rolling

The cold deformed samples are characterized by a textured microstructure showing a banded structure which is gradually developed with the increasing of the deformation and the grains are elongated toward the rolling direction.

The cold rolling affects only grain's size and shape. Deformation effect is evident along longitudinal direction as stretching and thinning of austenitic and ferritic grains, and a packaging of them. The effect on the transversal direction is a crushing of austenitic and ferritic grains, while no new phases inside the austenite grains were detected by metallographic techniques and magnetic tests. The investigation on heat treated samples evidenced that the previously deformed samples have ah higher amount of secondary phases than the solution annealed ones.

During the cold deformation, the two phases exhibit a different plastic behavior and, as the thickness reduction increases, the ferrite bands are more reduced than the austenitic ones. Even though this difference in thickness between the two phases is not very pronounced at the early stages of deformation, it is evident from thickness reduction that exceeds the 50% (see Figures 6.11, 6.14 and 6.20b).

Since the solid-state phase transformation during the isothermal heat treatment involves the ferritic matrix, only the effects of the cold rolling in this phase will be discussed. The deformation induces a fragmentation of the ferritic crystal grains and a local increase of the dislocations density, leading to an increasing of the number of interfaces and defects within the matrix, which, being areas of higher energy, are to be considered as preferential sites for the precipitation of secondary phases.

6.4.6 Isothermal heat treatments and phase precipitation

For the undeformed materials the kinetics of the precipitation at these temperatures is well known: the first precipitating phase is the χ-phase in form of small particles located at the triple points and at the α/γ and α/α grain boundaries, followed by the appearance of the coarser σ-phase which grows from the boundaries toward the ferritic phase and gradually embeds the χ particles (Nilsson, 1992; I. Calliari, 2007).

The nucleation of these intermetallic compounds mainly occurs at the triple points and at the grain boundaries because of the high interfacial energy. The high distortional energy associated to these regions, which arise from the misfit between the different phases or between two crystals of the same phase, lowers the activation energy for the phase nucleation. The secondary phases formation and their growth occur by diffusion mechanisms and these regions are also high diffusivity paths, thus the initiation of the process and the phases growth are facilitated. In the examined steels, the cold rolling modifies the grains shape and therefore implies an increasing of the distortion at the interfaces making these regions even more reactive.

The plastic deformation makes the interfaces more prone to the nucleation of new phases by giving to the whole structure a surplus of internal energy, which promotes the entire process (nucleation and growth). After cold rolling, the χ-phase formation is also favored, due to the low misfit between the crystal structures of such phases and the ferrite, especially in correspondence

of the dislocations, since both phases are BCC. Moreover, the treatments were carried out below the theoretical limit value 0.75-0.8 T m (where T m is the equilibrium melting temperature), thus diffusion along grain boundaries and along dislocations becomes very important and predominate on the diffusion through the crystal lattice.

The precipitation sequence in the deformed samples is not different from that observed in the undeformed materials. The χ-phase appears always by first and is followed by the σ-phase, but the precipitation occurs also inside the ferritic grains and the kinetics of the phenomenon is modified. In fact, in the deformed samples, the nucleation sites are many more than in the undeformed material and the time during which all the process occurs is substantially reduced and depends strictly on the degree of deformation at which the material is subjected.

6.5 Final remarks

In this chapter the effect of cold rolling on the microstructures of a standard, superduplex and a low Ni duplex stainless steel has been evaluated. Moreover, an isothermal heat treatment in some grades was performed in order to observe the microstructural behavior in these types of steels.

The Lean Duplex 2101 presents a strong grain refining and hardness with increasing cold deformation. Magnetics test for this duplex grade were performed, which the data confirm that the $\gamma \rightarrow \alpha'$ transformation could take place after cold rolling from 20% thickness reduction

It was revealed a strict relation between microstructure and magnetic properties. Besides a strong dependence between coercivity and the new phase, may be α'- martensite, content has been highlighted.

The SAF 2507 does not present any α' martensite phase presence after each rate of plastic deformation. This result is validated by the two different magnetic tests very sensible to any variation of amount of ferromagnetic phase.

In the samples deformed at 50% and 85% was found at the SEM into the austenite grains, stripes and bands brighter than the neighbor, however after EDS analysis no differences in composition was found.

The steel under study were a 2205 and 2507 DSSs, cold rolled at various degrees of deformation (5-85%) and isothermally heat treated at 900°C for 10 and 30 minutes. The cold deformation modifies the microstructure, increasing the crystals disorder. As expected, the number of defects and interfaces are higher than in the undeformed materials and the grains are even more fragmented as the thickness reduction proceeds. This gives to the entire microstructure a surplus of internal energy, in terms of distortional energy of the interfaces and strain gradients at the local level, making the ferritic phase more prone to phase transformation. Grain boundaries and dislocations must be consider as high diffusivity paths and thus an increasing of them and of their interfacial energy promote the diffusional processes as the phase transformation.

The plastic deformation at room temperature significantly reduces the precipitation kinetics and the material could be substantially damaged, even for short soaking time at the critical temperature. Thus, after any degrees of cold deformation a further solution annealing treatment is recommended, in order to allow for the relaxation of the microstructure and the reduction of the internal defects.

The precipitation of sigma phase is enhanced by the plastic deformation, magnetic tests found that in the sample cold rolled at 50%, 65% and 85% the ferrite is almost totally disappeared to give $\sigma+\gamma_2$

It seems that the eutectic decomposition of ferrite does not give sigma phase and austenite in the same percent, but it depends on the strain rate. This is confirmed also by the decrease in Mo in the sigma phase. Magnetic tests demonstrate the possibility to find a quantitative correlation between measured harmonics and metallurgical data in lean duplex and superduplex stainless steels.

CONCLUSIONS

Acknowledging the importance on the solid state transformations brings technological benefits as a result from the study of those transformations, moving towards a continuous improvement. As presented in previous chapters, Advanced Steels widely and commonly materials in the world. This Thesis has shown two different types of Advanced Steels, Dual Phase and Duplex Stainless Steels.

In Dual Phase steels case, a galvanized DP600 Dual Phase welded by Cold Metal Transfer process was experimentally tested in order to study the interfacial microstructures and intermetallic formation and their mechanical tests performance. The microstructure of Heat Affected Zone was constituted with coarse grains, followed by a fine bainitic and ferritic grains. However, approaching the seam weld the microstructure is markedly martensitic. An intermetallic compound layer was formed, with 3 μm thickness and others where the layer is inhomogeneous with a maximum thickness of 40 μm whose composition are $Fe_{7,\ 26}$-$Cu_{0,\ 34}$-Si and $Fe_{3,\ 48}$-$Cu_{0,\ 52}$-Si.

Varying the speed in brazing, affects the width of HAZ that decreases at the increasing of the welding rate, but the size and amount of martensite phase in this area increases. Besides, affects the thickness of the inhomogeneous intermetallic zones, where these areas are smaller when the process is quicker. Moreover, at the increasing of the welding rate, the copper concentration in the intermetallic layer decreases due to the shorter diffusion time. Additionally, the fractographic study of the samples failed after shear tensile revealed an embrittlement effect of the intermetallic layer. Finally, CMT technique is suitable for joining dual phase galvanized steel, since favorable results were obtained with the higher heat input due to the increasing of the mechanical strength of the joint.

In the Duplex Stainless Steels phase transformations case, experimental steels grades were subjected to precipitation of secondary phases in the temperature range 500-1000°C, besides in some grades cold rolled process was applied in order to study the microstructural behavior during deformation.

Lean Duplex grades present nitrides precipitation, at the ferritic grain boundaries and δ/γ interfaces. Either shorter or longer treatment times no precipitation of intermetallic phase as σ or χ were highlighted. Especially for 2304 DSS, secondary austenite has been observed, which has involved the embedding of the particles within the austenitic grains owing to a rearrangement of the grain boundaries due to diffusion mechanisms. This transformation allows this grade to maintain a good level of toughness even for long treatment times.

The plastic deformed 2101 lean duplex grade has a strong grain refining and hardness with increasing cold deformation and from the magnetic tests was confirmed that γ→α' transformation could take place after cold rolling from 20% thickness reduction

The standard SAF 2205 precipitation of σ and χ phase is caused due to isothermal heat treatment. However, nitrides precipitation is rare and hardly observable. After welding this grade resulted higher amounts of δ ferrite in the HAZ while in the weld metal lower amount of

austenite phase was highlighted. Sigma phase nucleation occurs at δ/γ interfaces and the growth is related to the decomposition of δ ferrite, due to the higher ferritizing content in the precipitate. Precipitation of sigma reaches higher amounts at 850°C, which is the critical temperature. However, at higher time of heat treatment the volume precipitate fraction increases.

On the contrary, for the plastic deformed microstructural previously investigations evidence no martensite formation and no precipitation of secondary phases occurs. The plastic deformation after heat treatment enhances the amount and the type of the precipitating phases as the thickness reduction increases.

For the 2507, Zeron100 and 2510 grades, isothermal heat treatment cause the precipitation of σ and χ phase and the formation of nitrides is very limited, besides the formation of secondary austenite is detected too.

For the high-alloyed, 2507 was revealed a modified microstructure after cold deformation, which increase the crystals disorders making the ferritic phase more prone to phase transformation. However, at room temperature reduced the precipitation kinetics even for short treatment time at the critical temperature. Additionally, sigma phase precipitation is enhanced by the plastic deformation, resulting the ferrite phase almost totally disappeared at high reductions thickness.

REFERENCES

A. Das S. Sivaprasad, M. Ghosh, P. C. Chakraborti and S. Tarafder [Journal] // Materials Science and Engineering . - 2008. - p. 283.

A. F. Miranda Pérez I. Calliari, E. Ramous, M. Breda Trattamenti di ricottura dell'acciaio inossidabile duplex 2205 dopo deformazione plastica [Journal]. - Padova : La Metallurgia Italiana, 2012. - 5. ISSN: 0026-0843

A. F. Miranda Pérez I. Calliari, K. Brunelli, F. A. Reyes Valdés, G. T. Pérez Medina Analysis of the microstructure and mechanical properties of Dual Phase steel under the effects of different brazing rates [Conference] // XX International Materials Research Congress . - Cancún : MRS Proceedings, 2012. - Vol. 1381.

A. Fanica B. Bonnefois, J. C. Gagnepain Welding Duplex Stainless Steels: Recent Improvements [Conference] // 7th Duplex 2007 International Conference and Expo. - Grado : Associazione Italiana di Metallurgia, 2007.

A. J. Ramirez J. C. Lippold, S. D. Brandi The relationship between chromium nitride and secondary austenite precipitation in DSS [Journal] // Metallurgical and Materials Transactions A. - 2003. - Vol. 34. - pp. 1575-1597.

A. J. Strutt G. W. Lorimer [Conference] // Duplex Stainless Steel '86. - The Hague : [s.n.], 1986. - p. 310.

A. Weisbrodt M. Brummer, B. Hadler, B. Wolbank, E. A. Werner Influence of temperature cold deformation and a constant mechanical load on the microstructural stability of a nitrogen alloyed duplex stainless steel [Journal] // Materials Science and Engineering A. - 2006. - Vol. A416. - pp. 1-10.

AB Outokumpu Stainless Duplex Stainless Steels Datasheet [Report]. - Avesta : Avesta Research Center.

Alfonsson E. Lean Duplex: The first decade of service experience [Conference] // Duplex World Stainless Steels. - Beaune : [s.n.], 2010.

Alvarez I. Duplex Stainless Steels: Brieg History and Some Recent Alloys [Journal] // Recent Patent on Mechanical Engineering. - 2008. - pp. 51-57.

Ardo A. J. De Niobium in Modern Steels [Journal] // International Materials Reviews. - 2003. - pp. 371-402.

Armas I. Alvarez Duplex Stainless Steels: Brief History and Some Recent Alloys [Journal] // Recent Patents on Mechanical Engineering . - 2008. - pp. 51-57.

Ashwin Pandit Murugaiyan Amirthalingam, A.Saha Podder, A.Halder, D.Bhattacharjee, S.Chandra, R.K.Ray Strain induced precipitation of complex carbo-nitrides in Nb-V and Ti-V microalloyed steels [Journal] // Scripta Materialia. - 2005. - Vol. 53. - pp. 1309–1314.

ASM Metalworking: Sheet Forming [Book Section] // ASM Handbook. - [s.l.] : ASM International , 1993.

ASTM ASTM A480 [Report] : Producer Datasheet. - 1996.

Avesta Polarit Duplex Stainless Steels Guideline [Report] : Datasheet. - Avesta : [s.n.], 2001.

B. Josefsson J. O. Nilsson and A. Wilson Phase transformations in Duplex Steels and the relation between continuos cooling and isothermal heat treatment [Conference] // Duplex Stainless Steels 91'. - Les Ulis : [s.n.], 1991. - p. 67.

B. Josefsson J. O. Nilsson, A. Wilson Phase transformations in Duplex Steels and the relation between continuous cooling and isothermal heat treatment [Conference] // Duplex Stainless Steels '91. - Beaune : [s.n.], 1991. - pp. 67-78.

B. K. Show R. Veerababu and R. Balamuralikrishan [Journal] // Material Science and Engineering. - 2010. - p. 1595.

B. Sundman B. Jansson, J. O. Anderson The Thermo-Calc databank system [Journal] // CALPHAD. - 1985. - Vol. 9. - pp. 153-190.

Baddoo N. R. Stainless steel in construction: a review of research, applications, challenges and opportunities [Journal] // Journal of Constructional Steel Research . - 2008. - 64. - pp. 1199-206.

Bain E. C. [Journal] // Transactions AIME. - 1924. - p. 25.

Baldo S. Innovative Steels for Structural and Corrosion Resistance Applications // PhD Thesis. - Padova : Università degli Studi di Padova, 2010. - p. 153.

Bergstrom D. S. Benchmarking of Duplex Stainless Steels versus Conventional Stainless Steel Grades [Conference] // 7th Duplex 2007 Interantional Conference and Expo. - Grado : Associazione Italiana di Metallurgia , 2007.

Bianchi M. Effects of cold rolling on phase precipitation and phase transformation in a 2507 SDSS // Thesis. - Padova : Università degli Studi di Padova, 2011.

C. Bopper A. Schram Precipitation and transformation behavior of Superduplex cast alloys [Conference] // Duplex Stainless Steels '94. - Glasgow : Cambridge TWI, 1994. - Vol. 74.

C. V. Roscoe K. J. Gradwell, G. W. Lorimer [Journal] // Institute of Metals Book. - 1984. - p. 563.

C. X. Huang G. Yang, Y. L. Gao, S. D. Wu and S. X. Li [Journal] // Journal of Materials Research . - 2007. - p. 724.

Calliari I. Investigation of secondary phase effect on 2205 DSS fracture toughness [Journal]. - [s.l.] : Material Science and Technology , 2010. - 81-86 : Vol. 26.

Calliari I. Precipitation of secondary phases in Superduplex Stainless Steel Zeron 100 isothermally aged [Journal] // Materials Science and Technology. - 2010.

Cannon C. New use of Dual Phase Steels in the 2007 Saturn Aura Body Structure [Conference] // Great Designs Steel Seminar. - Livonia : [s.n.], 2011.

Chapetti M. D. Fatigue crack propagation behavior in ultra-fine grained low carbon steel [Journal] // International Journal of Fatigue. - 2005. - pp. 235-243.

Charles J. Composition and Properties of Duplex Stainless Steels [Journal] // Welding World. - 1995. - pp. 43-54.

Charles J. Duplex Stainless Steels: A review after DSS'07 held in Grado [Journal] // Steel Research International. - 2008. - Vol. 79. - pp. 455-465.

Charles J. Superduplex stainless steels: structure and properties [Conference] // 3er International Conference on Duplex Steels. - Beaune : Les Ulis Cedex, 1991. - pp. 151-168.

Chen T. H. Effects of solution treatment and continuous cooling on σ-phase precipitation in a 2205 Duplex Stainless Steel [Journal] // Materials Science and Engineering . - 2001. - pp. 28-41.

Christian J. W. The theory of transformation in metals and alloys. Part 1 [Book]. - Oxford : Elsevier, 2002. - Vol. 3 ed. : pp. 538-546.

D. S. Bergstrom J. J. Dunn, J. F. Grub and W.A. Pratt W. A: US20036551420B1 [Journal]. - 2003.

Davis J. R. Stainless Steels [Book]. - Ohio : ASM International , 1994.

Dengo S. Precipitazione di fase secondarie durante raffreddamenti controllati nell'acciaio duplex SAF 2205 [Book]. - Padova : Università degli Studi di Padova. DIMEG, 2002.

E. C. Bain W. E. Griffith Transactions AIME [Journal]. - 1927. - p. 166.

E. Keehan L. Karlsson, H. O. Andren, H. K. D. H. Bhadeshia [Journal]. - [s.l.] : Welding Journal, 2006.

E. Ramous M. Breda, A. F. Miranda Pérez, J. C. Cardenas, R. Bertelli Gli azoturi negli acciai inossidabili Duplex [Conference] // 34 Convegno Nazionale . - Trento : Associazione Italiana di Metallurgia, 2012.

E. V. Pereloma I. B. Timokhina, K. F. Russell and M. K. Miller [Journal] // Scripta Materialia. - 2006. - p. 471.

E.J. Petit Y. Grosbety, S. Aden-Ali, J. Gilgert, Z. Azari Microstructure of the coating and mechanical properties of galvanized [Journal] // Surface & Coatings Technology. - 2010. - Vol. 205. - pp. 2404–2411.

G. B. Holloway J. C. M. Farrar Welding consumables of duplex and superduplex stainless steels optimizing properties after heat treatment [Conference] // Duplex Stainless Steels '91. - Beaune : Les Editions de Physique, 1991. - Vol. 571.

Gardner L. The use of stainless steel in structures [Journal]. - [s.l.] : Progress in Structural Engineering and Materials, 2005. - 2 : Vol. 7. - pp. 45-55.

Groenewoud K. Applications of Ferritic-Austenitic Stainless Steels in oil and gas production [Conference] // U. K. National Corrosion Conference. - 1982. - pp. 151-158.

Gunn R. N. Duplex Stainless Steels: Microstructure, properties and applications [Journal] // Abington Publishing. - 1997.

H. D. Solomon T. M. Devine Influence of microstructure on the mechanical properties and localized corrosion of a Duplex Stainless Steels [Book Section] // Optimization of processing, properties and service performance through microstructural control / book auth. Halle Abrams G. N. Maniar, D. A. Nail and H. D. Solomon. - [s.l.] : American Society for Testing and Materials, 1979.

H. Kronmüller M. Fahnle Micromagnetism and the microstructure of ferromagnetic solids [Book]. - England : Cambridge University Press , 2003.

H. Sieurin R. Sandström Austenite reformation in the heat-affected zone of duplex stainless steel 2205 [Journal] // Materials Science and Engineering: A. - [s.l.] : ELSEVIER, 2006. - Issues 1–2 : Vol. 418. - pp. 250-256.

H. T. Zhang J. C. Feng, P. He [Journal]. - [s.l.] : Materials Science and Technology, 2008. - 11 : Vol. 24. - p. 1347.

Hall J. Evolution of Advanced High Strength Steels in Automotive Applications [Conference] // Great Designs Steels Seminar. - Livonia : [s.n.], 2011.

Hertzman S. Influence of spinoidal decomposition on impact strength of Stainless Steel 2377 Duplex Stainless Steel Weldments [Report]. - Stockholm : Internal Report, Swedish Institute for Metals Research, 1998.

Holtzer J. [Journal] // Brevets Francais. - 1953. - p. 803.

I. Alternberger B. Scholtes, U. Martin and H. Oettel [Journal] // Materials Science and Engineering . - 1999.

I. Calliari A. F. Miranda Pérez, G.Tortoreto, I. Meszaros Magnetic and metallographic investigation of phase transformations in Duplex Stainless Steels [Conference] // 8th International Workshop on Progress in Analytical Chemistry & Materials Characterisation in the Steel and Metal Industries. - Luxembourg : CETAS 2011, 2011.

I. Calliari G. Straffelini, E. Ramous Investigation of secondary phase effect on 2205 DSS fracture toughness [Journal]. - [s.l.] : Material Science and Technology, 2010. - 81-86 : Vol. 26.

I. Calliari M. Breda, A. F. Miranda Pérez, E. Ramous, R. Bertelli Phase transformation induced by heat treatment in cold rolled Duplex Stainless Steels [Conference] // International Conference & Exhibition on Analysis & Testing of Metallurgical Process & Materials. - Beijing : CCATM’2012, 2012.

I. Calliari M. Dabalà, E. Ramous, G. Straffelini New Lean Duplex Stainless Steel for structural applications [Journal] // Materials Science Forum. - 2009. - Vols. 604-605. - pp. 419-426.

I. Calliari M. Pellizzari and E. Ramous Precipitation of secondary phases in superduplex stainless Steels Zeron100 isothermally aged [Journal] // Materials Science and Technology. - 2011. - Vol. 27. - pp. 928-932.

I. Calliari M. Pellizzari, E. Ramous The phase stability in Cr-Ni and Cr-Mn duplex stainless steels [Journal]. - [s.l.] : Journal of Material Science, 2011. - 21 : Vol. 46. - pp. 6916-6924.

I. Calliari M. Zanesco, E. Ramous, P. Bassani Effects of Isothermal Ageing and Continuous Cooling after Solubilization in a Duplex Stainless Steel [Journal] // Journal of Materials Engineering and Performance. - [s.l.] : ASM International, 2007. - Vol. 16. - pp. 109-112.

I. Calliari P. Bassani, K. Brunelli and E. Ramous Effect of continuous cooling on secondary phases precipitation in a SDSS Zeron100 [Journal] // Journal of Materials Engineering and Performance. - in press.

I. Mészáros J. Prohászka Magnetic investigation of the effect of α'-martensite on the properties of Austenitic Stainless Steel [Journal]. - [s.l.] : Journal of Materials Processing Technology, 2005. - Vol. 161. - pp. 162-168.

I. Rampin M. Piazza, S. Baldo, A. F. Miranda Pérez, K. Brunelli, I. Calliari, F. A. Reyes Valdés The effect of braze-welding speed on the microstructure and mechanical properties of a Dual Phase Steel [Conference] // Super-High Strength Steels International Conference. - Peschiera del Garda : Associazione Italiana di Metallurgia, 2010.

IISI Application Guidelines [Journal] // Committee on automotive applications. - 2006.

IMOA Practical Guidelines for the Fabrication of Duplex Stainless Steels [Book]. - London : International Molybdenum Association , 2009.

ISO Norma ISO 14273:2000. - 2000.

ISO Norma Italiana UNI EN ISO 6507-1. - 1999.

J. Fernández S. Illescas and J. M. Guilemany [Journal] // Materials Letters. - 2007. - p. 2389.

J. Hamada N. Ono Effect of microstructure before cold rolling on texture and formability of duplex stainless steels [Journal]. - [s.l.] : Materials Transactions, 2010. - 4 : Vol. 51. - pp. 635-643.

J. Johansson M. Oden Evolution of the residual stees state in a Duplex Stainless Steel during loading [Journal] // Acta Materialia. - 1999. - pp. 2669-2684.

J. Li Z. Ma, X. Xiao, J. Zhao, L. Jiang On the behavior of nitrogen in a low-Ni high -Mo superduplex stainless steel [Journal] // Materials and Design. - 2011. - Vol. 32. - pp. 2199-2205.

J. Michalska M. Sozańka Qualitative and quantitative analysis of σ and χ phases in 2205 duplex stainless steels [Journal] // Materials Characterization. - 2006. - Vol. 56. - pp. 355-362.

J. O. Nilsson A. Wilson Influence of isothermal phase transformations on toughness and pitting corrosion of superduplex stainless steels SAF2507 [Journal]. - [s.l.] : Materials Science and Technology, 1993. - 19. - p. 545.

J. O. Nilsson A. Wilson, B. Josefsson and T. Thorvaldsson Relationship between pitting corrosion, toughness and microstructure of isothermally heat treated Superduplex Stainless Steel [Conference] // Applications of Stainless steels. - Stockholm : [s.n.], 1992. - pp. 280-289.

J. -O. Nilsson G. Chai The physical metallurgy of duplex stainless steels [Conference] // Duplex World 2010 Conference. - Beaune : [s.n.], 2010.

J. O. Nilsson P. Kangas, T. Karlsson Mechanical Properties, Microstructural Stability and Kinetics of Sigma Phase Formation in 29Cr-6Ni-2Mo-0.38N Superduplex Stainless Steel [Journal]. - [s.l.] : Metallurgical and Materials Transactions, 2000. - Vol. 31A. - p. 35.

J. O. Nilsson P. Liu Aging at 400-600°C of submerged arc welds of 22Cr-3Mo-8Ni Duplex Stainless Steel and its effect on toughness and microstructure [Journal] // Materials Science and Technology. - 1991. - pp. 853-862.

J. O. Nilsson T. Huhtala, P. Jonsson, L. Karlsson, A. Wilson Structural stability of superduplex stainless weld metal and its dependence on tungsten and copper [Journal] // Metallurgical and Materials Transactions A. - 1996. - Vol. 27A. - pp. 2196-2208.

J. R. Shaw B. K Zuidema New high strength steels help automakers reach future goals for safety, affordability, fuel efficiency and environmental [Journal] // Society of Automotive Engineers. - 2011. - p. 3041.

J. Y. Choi W. Jin Strain induced martensite formation and its effect on strain hardening behavior in the cold draw 304 Austenitic Stainless Steel [Journal]. - [s.l.] : Scripta Materialia, 1997. - 1 : Vol. 36.

Jacobsson M. Fatigue testing of the duplex grades SAF 2304, SAF 2205 and SAF 2507 [Report]. - Sanviken : Internal Report no. 6060, Sandvik Steel , 1991.

Jin J. -Y. Choi and W. [Journal] // Scripta Materialia. - 1997. - p. 99.

K. H. Lo C. H. Shek, J. K. L. Lai Recent developments in stainless steels [Journal]. - [s.l.] : Materials Science and Engineering R, 2009. - 65. - pp. 39-104.

K. Karlsson L. Bengtsson, U. Rolander, S. Pak [Conference] // Application Stainless Steel '92. - Stockholm : The Institute of Metals, 1992. - pp. 335-344.

K. Spencer M. Veron, K. Yu-Zhang and J. D. Embury [Journal] // Materials Science and Technology. - 2009. - p. 7.

Kovieczny A. Advanced Strength Steels- Formability [Conference] // Great Designs in Steel. - Livonia : [s.n.], 2003.

L. Kaufman H. Bernstein Computer calculation of Phase Diagrams [Journal]. - New York : Academic Press, 1970.

Liljas M. 80 years with Duplex Stainless Steels, a historic review and prospect to the future [Conference] // 6th European Stainless Steel. - Helsinki : [s.n.], 2008.

M. B. Cortie E. M. L. E. M. Jackson Simulation of the precipitation of sigma phase in duplex stainless [Journal] // Metallurgical and Materials Transactions A. - 1997. - Vol. 28. - pp. 2477-2484.

M. C. Young L. W. Tsay, C. -S. Shin, S. L. I. Chan The effect of short time post-weld heat treatment on the fatigue crack growth of 2205 duplex stainless steel welds [Journal] // International Journal of Fatigue. - [s.l.] : ELSEVIER, 2007. - 12 : Vol. 29. - pp. 2155-2162.

M. Martins L. C. Casteletti Sigma phase morphologies in cast and aged super duplex [Journal] // Materials Characterization. - 2009. - Vol. 60. - pp. 792–795.

M. Murayama K. Hono [Journal] // Scripta Materialia. - 2001. - p. 701.

M. Oden J. Johansson Load sharing between austenite and ferrite in Duplex Stainless Steel during cycle loading [Journal] // Metallurgical and Materials Transactions. - 2000. - pp. 1557-1570.

Magnabosco R. Kinetics of sigma phase formation in a Duplex Stainless Steel [Journal] // Journal of Materials Research. - 2009. - 3 : Vol. 12. - pp. 321-327.

N. Sathirachinda R. Pettersson, S. Wessman, J. Pan Study of nobility of chromium nitrides in isothermally aged duplex stainless steels by using SKPFM and SEM/EDS [Journal] // Corrosion Science. - 2010. - Vol. 52. - pp. 179-186.

N.Maruyama R.Uemori, M.Sugiyama The role of niobium in the retardation of the early stage of austenite recovery in hot-deformed steels [Journal] // Material Science and Engineering. - 1998. - Vol. A250. - pp. 2-7.

Nilsson J. O. Super Duplex Stainless Steels [Journal]. - [s.l.] : Materials Science and Technology, 1992. - 8 : Vol. 8. - pp. 685-700.

Nishiyama Z. [Journal] // Sci. Rep. Tohoku Imp. Univ.. - 1934. - p. 638.

P. D. Southwick R. W. K. Honeycombe Decomposition of ferrite to austenite in 26% Cr-5% Ni Stainless Steels [Journal] // Metal Science. - 1980. - pp. 253-261.

P. Johansson M. Liljas [Journal] // Corrosion Management and Application Engineering. - 2001. - Vol. 24(24).

P. Johansson M. Liljas A new lean duplex stainless steel for construction purposes [Conference] // 4th European Stainless Steels Science and Market Congress. - Paris : [s.n.], 2002.

Piccolo E. Tesi di Laurea // Caratterizzazione microstructturale dell'acciaio duplex SAF 2205 deformato a fredo. - Padova : Università degli Studi di Padova, 2009. - p. 50.

Pickering F. B. Physical Metallurgy and the Design of Steels [Journal] // Science Publishers. - 1960.

Prohászka I. Mészáros and J. Magnetic investigation of the effect of α'-martensite [Journal] // Journal of Materials Processing Technology. - 2005. - pp. 162-168.

Q. Chen H.-J. Jou, G. Sterner TC-Prisma User Guide's and Examples [Manual]. - Stockholm : Thermo-Calc Software AB, October 5, 2011. - Vol. Version 1.0.

R. B. Hutchings A. Turnbull, A. T. May Measurement of hydrogen transport in a duplex stainless steel [Journal]. - [s.l.] : Scr. Metal. Mater , 1991. - 2647-2662 : Vol. 25.

R. Badji M. Bouabdallah, B. Bacroix, C. Kaloun, B. Belkessa, H. Maza Phase transformation and mechanical behavior in annealed 2205 duplex stainless steel welds [Journal] // Materials Characterization. - 2008. - 4 : Vol. 59. - pp. 447-453.

R. W. K. Honeycombe P. D. Southwick, Precipitation of M23C6 at austenite/ferrite interfaces in Duplex Stainless Steels [Journal] // Metals Science. - 1982. - pp. 475-481.

S. Floreen H. W. Hayden The influence of austenite and ferrite on the mechanical properties of two-phase stainless steels having microduplex structure [Journal]. - [s.l.] : Transactions of American Society for Metals , 1968. - 489-499 : Vol. 61.

S. Floreen H. W. HAYDEN The influence of austenite and ferrite on the mechanical properties of two-phase stainless steels having microduplex structure [Journal] // Transactions of American Society for Metals. - 1968. - Vol. 61. - pp. 489-499.

S. Hertzman C. Hounglu Kinetics of Intermetallic Phase Formation in Duplex Stainless Steel and Their Influence on Corrosion Resistance [Report] : Report IM-2689. - Stockholm : [s.n.].

S. Hetzman W. Roberts, M. Lindenmo Microstructure and properties of nitrogen alloyed duplex stainless steel after welding treatments [Conference] // Duplex Stainless Steels 86'. - The Hague : Nederlands Institutuut voor Lastechniek, 1986. - pp. 257-261.

S. P. Bhat M. E. Fine Fatigue crack nucleation in iron and high strength low alloy steel [Journal] // Material Science and Engineering. - 2001. - pp. 90-96.

S. P. Bhat M. E. Fine Fatigue crack nucleation in iron and high strength low alloy steel [Journal]. - [s.l.] : Material Science and Engineering , 2001. - 90-96 : Vol. A314.

S. S. M. Tavares J. M. Neto, M. R. Da Silva Magnetic properties and α' martensite quantification in an AISI 301LN stainless steel deformed by cold rolling [Journal]. - [s.l.] : Materials Characterization, 2008. - 7 : Vol. 59. - pp. 901-904.

S. S. M. Tavares V. F. Terra, J. M. Pardal, M. P. Cindra Fonseca Influence of the microstructure on the toughness of a duplex stainless steels UNS S31803 [Journal] // Journal of Materials Science. - 2005. - Vol. 40. - pp. 145-154.

S. S. S. M. Tavares M. R. da Silva, J. M. Pardal, H. F. G. Abreu, A. M. Gomes Microstructural changes produced by plastic deformation in the UNS S31803 duplex stainless steel [Journal]. - [s.l.] : Journal of Materials Procedding Technology, 2006. - Vol. 180. - pp. 319-322.

S. Schreiber S. Keitel, R. Winkler and P. Zak Resistance welding of high strength steels combinations [Conference] // 2nd International Super-high strength steels Conference. - Peschiera del Garda : Associazione Italiana di Metallurgia , 2010.

S. Tsuge Y. Oikawa, H. Kajimura, H. Inoue, R. Matsuhashi A new Lean Duplex Stainless Steel exhibits excellent properties under large Heat Input Welding [Conference] // 7th European Stainless Steel. - Como : Associazione Italiana di Metallurgia, 2011. - p. 46.

S. Wessman R. Pettersson, S. Hertzman On phase equilibria in Duplex Stainless Steels [Journal] // Steel Research International. - 2010. - 5 : Vol. 81. - pp. 337-346.

Sachs G.V. Kurdjumov and G. [Journal] // Z. Phys.. - 1930. - p. 325.

Schwartz M. M. Brazing [Book]. - [s.l.] : ASM International, 1987. - Vol. 1.

Senuma T. [Journal]. - [s.l.] : ISIJ Internatioanl, 2001. - 6 : Vol. 41.

Sieurin H. Fracture toughness properties of duplex stainless steels. - 2006 : Doctoral Thesis, KTH, 2006.

Smuk O. Microstructure and Properties of Modern P/M Super Duplex Stainless Steels. - Stockholm : Doctoral Thesis, KTH, 2004.

Soulignac P. Celebrating the 70 years of Duplex Stainless Steels in Europe [Conference] // Duplex Stainless Steels 2010. - Beaune : [s.n.], 2010. - p. Paper IV.

Stickler B. Weiss and R. Phase instabilities during high temperature exposure of 316 austenitic stainless steel [Journal] // Metallurgical Transactions. - 1972. - pp. 851-866.

T. H. Chen K. L. Weng, J. R. Yang [Journal] // Materials Science and Engineering . - 2002. - pp. 259-270.

T. R. Parayil D. S. Bergstrom Characterization of Duplex Stainless Steels [Conference] // 7th European Stainless Steels Conference. - Como : Associazione Italiana di Metallurgia, 2011. - Vol. 76.

T. Thorvaldsson H. Eriksson, H. Kutka, A. Salwen Influence of microstructure on mechanical properties of a Duplex Stainless Steel [Conference] // Stainless Steels '84. - London : The Institute of Metals, 1985. - pp. 101-105.

Talonen J. Effect of strain-induced α'-martensite transformation on mechanical properties of metastable austenitic stainless steels [Report] : Doctoral Thesis. - 2007.

Tuomi A. Increased usage of Duplex materials in manufacturing of pulping equipment [Journal] // Duplex America. - 2000. - p. 401.

V. Olden C. Thaulow, R. Johnsen Modelling of hydrogen diffusion and hydrogen induced cracking in supermartensitic and duplex stainless steels [Journal] // Materials and Design . - 2008. - 10 : Vol. 29. - pp. 1934-1948.

Vogt J. B. Fatigue properties of high nitrogen steels [Journal] // Materials Processing Technology. - 2001. - pp. 364-369.

Y. -J. Kim L. S. Chumbley, B. Gleeson Determination of Isothermal Transformation Diagrams for Sigma-Phase formation in Cast Duplex Stainless Steels [Journal] // Metallurgical and Materials Transactions A. - 2004. - Vol. 35. - pp. 3377-3386.

Y. Maehara N. Fujino, T. Kunitake Effects of plastic deformation and thermal history on sigma phase precipitation in Duplex Stainless Steels [Journal] // Transactions of The Iron and Steel Institute of Japan . - 1983. - pp. 247-255.

Y. S. Ahn M. Kim, B. H. Jeong Effect of aging treatments and microstructural evolution on corrosion resistance of tungsten substituted 2205 Duplex Stainless Steel [Journal] // Materials Science and Technology. - 2002. - 18. - p. 383.

Y. Zhi-shui L. Rui-Feng, Q. Kai [Journal]. - [s.l.] : Trans. Nonferrous Met. Soc. China, 2006. - Vol. 16.

Z. Xiaodong M. Zhaohui, W. Li Current Status of Advanced High Strength Steels of Automaking its Development in Baosteel [Conference] // Steel Research China Seminar. - Harbin : [s.n.], 2011.